Identificación de nuevas proteínas que interaccionan con CtIP: Implicación de PRMT5 y CCAR2 en la resección del ADN

Ana López Saavedra

Tesis Doctoral

Universidad de Sevilla

2017

Identificación de nuevas proteínas que interaccionan con CtIP: Implicación de PRMT5 y CCAR2 en la resección del ADN

Trabajo realizado en el Departamento de Genética, Facultad de Biología, y en el Centro Andaluz de Biología Molecular y Medicina Regenerativa (CABIMER), de la Universidad de Sevilla, para optar al grado de Doctor en Biología Molecular y Biomedicina, por la licenciada Ana López Saavedra.

Sevilla, Abril de 2017

El director de la tesis,

Pablo Huertas Sánchez

El tutor de la tesis,

Andrés Aguilera López

La doctoranda,

Ana López Saavedra

Tengo mucho que agradeceros…

Pablo, gracias por darme la oportunidad de ser tu "primera" doctoranda y confiar en mi para ayudarte a ir dando forma al grupo. Muchas gracias por los ratos de charla y por enseñarme tantísimas cosas, no sólo en el terreno profesional. Gracias por no dudar en ponerte la bata y echarme una mano cuando lo he necesitado, aunque fuese para controlar el timer, hacer geles de gradiente o cortar las bandas que darían sentido a todo lo demás. Y, sobre todo, gracias por ayudarme a buscar soluciones y por tener una actitud optimista cuando a mi me ha faltado.

Gracias a todos vosotros, mis compis, mi familia cabimérica, mis amigos. Muchas gracias porque, de un modo u otro, habéis aportado vuestro granito de arena particular en esta tesis; ya sea ayudándome en momentos complicados o con "macroexperimentos", enseñándome técnicas nuevas, compartiendo conmigo vuestra sabiduría, con palabras de ánimo para llegar al final del día, con una sonrisa por los pasillos, con un abrazo consolador cuando hacía falta o con una simple cervecita los viernes o una conversación a horas tardías que demuestran que no sólo hemos sido compañeros. Todos ya formáis parte de mi vida y sé que a muchos os voy a seguir teniendo muy presentes en ella. Buhbu, Pack, qué haría sin vosotras y sin nuestras charlas?

Y, por supuesto, gracias a mi familia y a mis amigos que, a pesar de no pertenecer a este mundo de la investigación, habéis aceptado/soportado mis horarios de trabajo, habéis intentado entender en qué consistía mi tesis, os habéis preocupado por "mis celulitas" y me habéis transmitido mucha energía positiva y todo vuestro cariño y apoyo.

Gracias de verdad porque sin todos vosotros no hubiera sido posible.

Lo recordaré siempre, que una tesis no se olvida.

I did this work thanks to receiving a FPI fellowship from the Spanish Ministry of Science and Innovation and this project was funded by project grants from the Spanish Government (SAF2010-14877 and SAF2013-43255-P) and a Starting Grant from the European Research Council (DSBRECA).

TABLE OF CONTENTS

INDEX OF FIGURES

INDEX OF TABLES

ABBREVIATIONS

alt-NHEJ	Alternative non-homologous end-joining
BFP	Blue fluorescent protein
BIR	Break-induced replication
BSA	Bovine serum albumin
CDK	Cyclin-dependent kinase
CHX	Cycloheximide
CPT	Camptothecin
D-loop	Displacement loop
DDR	DNA damage response
DMEM	Dulbecco's Modified Eagle Medium
DMSO	Dimethyl sulfoxide
DNA-PKcs	DNA-dependent protein kinase catalytic subunit
DSB	Double-strand break
EDTA	Ethylenediaminetetraacetic acid
FT	Flowthrough
GFP	Green Fluorescent Protein
HBS	HEPES buffered saline
HDR	Homology-directed repair
HR	Homologous recombination
IF	Immunofluorescence
IP	Immunoprecipitation
IR	Ionizing radiation
MMEJ	Microhomology-mediated end-joining
MOI	Multiplicity of infection
MRN	MRE11A- RAD50-NBS1
NHEJ	Non-homologous end-joining
PARP	Poly-(ADP-ribose) polymerase
PBS	Phosphate buffered saline
PIKK	Phosphatidylinositol 3-kinase-like protein kinase
PLA	Proximity Ligation Assay

PVDF	Polyvinylidene difluoride
RFP	Red Fluorescent Protein
ROS	Reactive oxygen species
SDS	Sodium dodecyl sulphate
SDSA	Synthesis-dependent strand annealing
SMART	Single-Molecule Analysis of Resection Tracks
SSA	Single-strand annealing
SSB	Single-strand break
ssDNA	Single-stranded DNA
SSR	SeeSaw Reporter
TAP	Tandem Affinity Purification
TdT	Terminal deoxynucleotidyl transferase
UV	Ultraviolet light
VP16	Etoposide
WB	Western blotting

INTRODUCTION

1. The challenge of coping with DNA damage

Each of the cells that compose our organism has to cope daily with thousands of lesions on its DNA. These damages on the DNA are generated either spontaneously by endogenous factors derived from cellular metabolism or by contact with several environmental agents (Ciccia & Elledge, 2010). Such insults can take a wide diversity of forms, and might alter the sequence and/or the structure of the DNA. In the worst-case scenario, these disturbances could even generate breaks, which can affect one or both strands of the DNA (figure I1).

Naturally occurring DNA alterations are generated spontaneously during several physiological processes. Examples of this are DNA mismatches occasionally introduced during DNA synthesis, replication forks that face a damaged template, or DNA strands breaks caused by abortive topoisomerase I and topoisomerase II activity (Kunkel & Bebenek, 2000). In addition, by-products of normal cellular metabolism constitute a permanent enemy to DNA integrity from within. These include reactive oxygen species (ROS), such as superoxide anions, hydroxyl radicals and hydrogen peroxide, derived from oxidative respiration and lipid peroxidation. ROS, together with reactive nitrogen species, can lead to the formation of DNA adducts that impair base-pairing and/or block DNA replication and transcription, cause base loss, DNA single-strand breaks (SSBs), or even double-strand breaks (DSBs), the most cytotoxic lesion on the DNA (see below) (Finkel & Holbrook, 2000; Valko *et al*., 2006). There are also other spontaneous reactions intrinsic to the chemical nature of the DNA, such as interconversion between DNA bases caused by deamination, loss of DNA bases following DNA depurination, and modification of DNA bases by alkylation (Lindahl, 1993; De Bont & van Larebeke, 2004).

Otherwise, the most pervasive exogenous DNA-damaging agent is the ultraviolet light (UV) part of the solar spectrum that it is not absorbed by the ozone layer. The residual UV-A and UV-B radiation in strong sunlight can induce thousands of lesions, normally pyrimidine dimers or 6-4 photoproducts, per cell per hour of exposure (Cadet *et al*., 1997). Ionizing radiation (IR) derived from cosmic radiation, X-rays and gamma rays, also produces different types of DNA damage, including DNA double-strand breaks. IR can also come from radioactive

compounds used clinically to diagnose and treat different diseases, including the exposure to natural or man-made radioisotopes during cancer radiotherapy. Moreover, radioactive decay of naturally occurring radioactive compounds is harmful for the cells and contributes to cancer appearance (Ward, 1988). Besides these physical agents, genotoxic chemicals are other environmental sources of DNA damage that cause alterations in DNA structure. Radiomimetic drugs used in cancer chemotherapy can generate a variety of DNA lesions, such as attachment of alkyl groups to DNA bases by alkylating agents like methyl methanesulfonate and temozolomide, or introduction of covalent links between bases of the same DNA strand (intrastrand crosslinks) or of different DNA strands (interstrand crosslinks) by crosslinking agents like mitomycin C, cisplatin, psoralen or nitrogen mustard (Ciccia & Elledge, 2010). In addition, the topoisomerase poisons camptothecin (CPT) and etoposide (VP16) inhibit topoisomerase I or II and induce the formation of single-strand or double-strand breaks, respectively. These chemical compounds target the topoisomerase-DNA complexes and stabilize the cleavage complexes, preventing DNA religation and triggering the breaks (Hsiang *et al*., 1985; Fortune & Osheroff, 2000). Within this category, genotoxic compounds derived from cigarette smoke, which cause a wide variety of aromatic DNA adducts and oxidative damage, are the most prevalent cancer-causing chemicals (Phillips *et al*., 1988).

Altogether, it has been estimated that every cell in our body might face more than 10^5 spontaneous DNA lesions per day (Hoeijmakers, 2009) that should be repaired in a way that is compatible with cell survival and fitness. To minimize the impact of such burden of DNA lesions, cells have developed several mechanisms to detect the damaged DNA, signal its presence and promote its repair. If the DNA lesions are not repaired or are repaired improperly, they lead to DNA mutations or chromosome aberrations that contribute to genome instability. Although generally harmful both for the cell and the organism, these alterations also generate genetic variation thus driving evolution at the molecular level. Nevertheless, genome instability is strongly associated with human inherited diseases, premature aging and predisposition to several types of cancer (Aguilera & Gómez-González, 2008).

Because of the huge diversity of damages generated on the DNA, cells have evolved several and largely distinct DNA repair pathways to maintain genomic integrity in response to each of those specific threats. Figure I1 shows different examples of DNA lesions induced by several endogenous or exogenous agents, and the main DNA repair mechanism involved in each case.

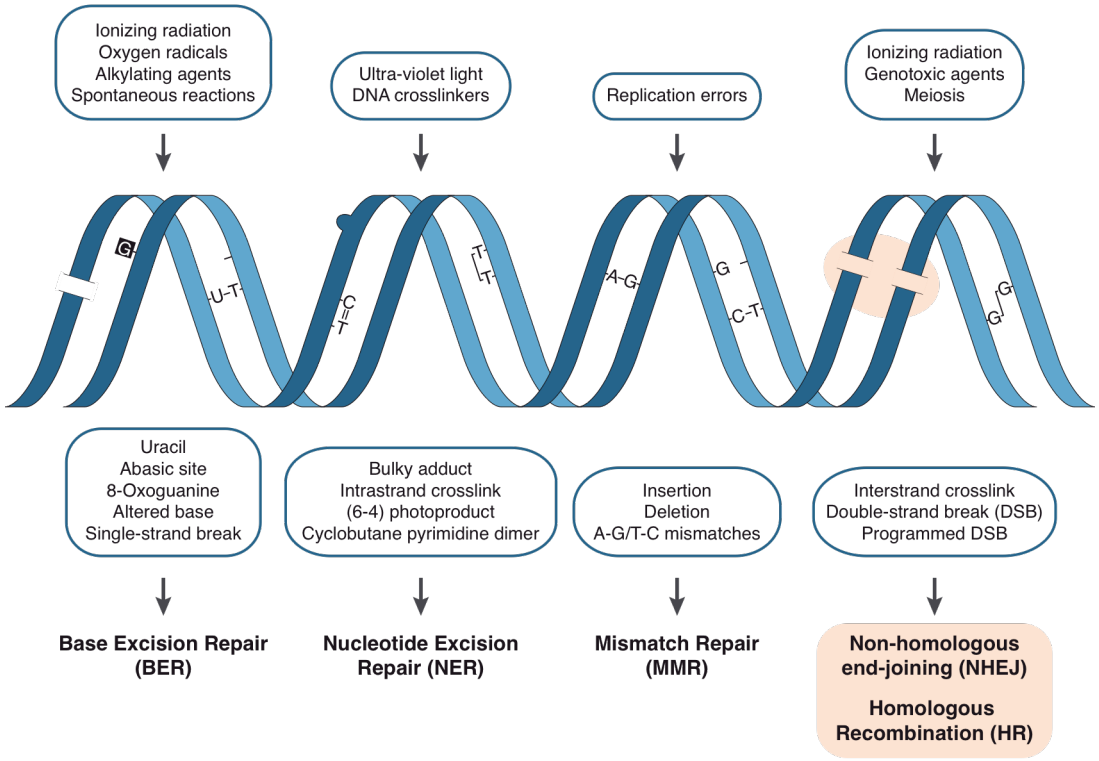

Figure I1. Sources and types of DNA damage and their associated DNA repair pathways. DNA is constantly challenged by either exogenous agents and/or endogenous sources derived from cellular metabolism (examples of these are indicated above the DNA double helix), leading to different damages that can affect one or both DNA strands. Representative damages are shown in the DNA cartoon and are listed below it. Each modification requires specific machinery for repair. The main repair pathways for each group of DNA lesions are represented at the bottom of the figure. In this thesis, we focus on the repair of DNA double-strand breaks, highlighted in light orange in the figure. (Modified from Genois *et al.*, 2014; Hoeijmakers, 2001)

Most of the agents that trigger DNA damage usually affect only one of the DNA strands, and generate a wide variety of alterations. Although there are specific repair mechanisms to counteract the different lesions that disturb only one strand, BER (Base Excision Repair), NER (Nucleotide Excision Repair) and MMR (Mismatch Repair) (figure I1) basically share the same processes. The

damage is first recognized by specific proteins and then excised from the wrong strand, generating single-stranded DNA (ssDNA) that is repaired by the action of the DNA polymerases, using the undamaged strand as a template (Hoeijmakers, 2009).

However, if the damage affects simultaneously both strands, there is not an intact, undamaged, template to copy from. For that reason, DSBs are the most difficult to repair and the more cytotoxic form of DNA damage. One single unrepaired DSB is enough to either kill or induce a terminal arrest of any cell. Thus, the repair of DSBs is carried out by more complex repair mechanisms (figure I1) (Khanna & Jackson, 2001; Ciccia & Elledge, 2010). Moreover, the response for these types of lesions requires the controlled action of multiple proteins and the coordination with a wide range of cellular events, which are modulated and altered for an accurate repair. This network of cellular pathways is collectively known as the DNA damage response (DDR) (Jackson & Bartek, 2009; Ciccia & Elledge, 2010).

2. DNA damage response

As stated above, DSBs not only activate their specific repair mechanisms but also trigger a complex signalling network that encompasses many additional processes, called the DNA damage response (Jackson & Bartek, 2009; Ciccia & Elledge, 2010). One of the main features of the DDR is the control of the cell cycle, as it does slow down or arrest cell cycle progression to increase the time available for DNA repair, thereby preventing duplication and/or segregation of broken DNA. Such regulation of the cell cycle is driven by the activation of the cell cycle checkpoints before or during DNA replication (G1-S and intra-S checkpoints) and before cell division (G2-M checkpoint) (Rouse & Jackson, 2002; Jackson & Bartek, 2009). Other aspects of the DDR include changes in the chromatin structure close to the breaks, recruitment of repair factors to the damaged DNA, transcriptional induction and repression both globally and/or in the vicinity of the breaks, activation of alternative splicing and changes in the pattern of post-translational modification in thousands of proteins involved in the many processes comprising DNA repair, and, if necessary, induction of apoptosis or senescence pathways (Jackson & Bartek, 2009; Shanbhag *et al*., 2010; Polo & Jackson, 2011; Sprung *et al*., 2011; Shkreta &

Chabot, 2015). The regulation of these processes by the DDR is highly structured in space and time. It is initiated locally but then it is converted into a global cellular reaction. This response is based on signal transduction mechanisms that begin with *sensor* and *mediator* proteins that directly recognize the damage and/or chromatin alterations occurred after damage induction. Then, the *sensor* proteins, assisted by *mediators*, activate the DDR by transmitting the signal to *transducer* proteins, which in turn convey the signal to numerous downstream *effector* proteins involved on specific pathways (Harper & Elledge, 2007; Maréchal & Zou, 2013). Some of these *effectors* are also *sensors*, and hence they create a feedback loop to maintain and spread the signalling (Shiloh & Ziv, 2013). The DDR is extremely conserved in evolution in all eukaryotes (Polo & Jackson, 2011; Arcas *et al*., 2014). However, there are strong differences in the names of the proteins involved in different organisms. So, for clarity of the text, in this thesis all the proteins will be named accordingly to the human nomenclature.

One of the first *sensors* to be recruited to DNA breaks is the MRE11A-RAD50-NBS1 (MRN) complex (figure I2). Once located at DSB sites, this complex tethers and processes the broken ends (Stracker *et al*., 2004). In addition to this DNA processing activity (see below, section 4), the MRN complex controls the signalling of the DNA damage. Additional proteins are then recruited to the damage, rapidly generating a widespread accumulation of proteins that are known as nuclear foci. First, the MRN complex is responsible for the recruitment and retention of the serine/threonine protein kinase ATM (Ataxia-Telangiectasia Mutated) (figure I2). This recruitment requires the interaction of ATM with the carboxy-terminus of NBS1 (You *et al*., 2005). 53BP1 and BRCA1, among other proteins and modifications, assist in stabilizing this interaction (figure I2) (Falck *et al*., 2005; Lee *et al*., 2010). ATM is considered the main *transducer* protein in the DDR that initiates and regulates the cascade of signals upon DNA damage. The PI3K domain located in its carboxy-terminal site, places ATM within the family of phosphatidylinositol 3-kinase-like protein kinase (PIKK) family. Once activated, ATM phosphorylates *mediator* proteins that can amplify the DDR by recruitment of other ATM substrates. One example of this is the ATM-mediated phosphorylation of the MRN complex components, which contributes to the timely activation of other proteins involved in DDR and also creates a positive feedback loop that

maintains ATM activity (figure I2) (Shiloh & Ziv, 2013). ATM kinase activity also triggers local modifications in the chromatin structure. The best characterized example is the phosphorylation of serine-139 of the histone variant H2AX, named as γH2AX, on chromatin flanking DSB sites (figure I2) (Bartek & Lukas, 2007). This histone variants substitutes canonical H2A in some, but not all, nucleosomes (figure I2) (Rogakou *et al*., 1998) Phosphorylation of H2AX also contributes to the localization and retention of MDC1 to the DSB sites (figure I2). This protein also attracts more ATM to the site of breaks and activates it, allowing additional ATM-mediated phosphorylation of H2AX variants. This serves to bind additional MDC1 molecules in a repeated process that accelerates the signalling (Lou *et al*., 2006). Hence, this phosphorylation spreads along the DNA to bring about the recruitment of DDR factors and other chromatin-modifying components, amplifying DSB signalling and promoting the repair (Bartek & Lukas, 2007; Jackson & Bartek, 2009).

Figure I2. Signal transduction mechanisms comprising ATM-induced DNA damage response. When a DSB occurs (highlighted in light orange), MRN complex is located at the site of the damage, where tethers the DNA ends and promotes the recruitment of the kinase ATM. ATM phosphorylates different substrates, such as the MRN complex or serine-139 of H2AX (nucleosomes containing this histone variant are marked in dark yellow), which serves for the recruitment of MDC1 to the sites of damage. MDC1 binds ATM and facilitates further H2AX phosphorylation. This attracts additional MDC1 molecules, causing γH2AX to spread along the chromatin and amplification of DDR signalling. BRCA1 and 53BP1 are also recruited to the breaks and contribute to damage signalling by stabilizing MRN-ATM interaction, being targets of post-translational modifications, such as sumoylation, and recruiting other proteins involved in DDR. Both RIF1 and PTIP associate with phosphorylated 53BP1 to regulate DSB repair. Among all its targets, ATM phosphorylates and activates CHK2, a key checkpoint kinase that initiates a secondary cascade of signals to regulate and coordinate cellular events in response to DSB. This figure only represents the role of ATM in the DDR, but there are other kinases involved in this process, such as ATR and DNA-PKcs. Post-translational modifications are represented with circles with a letter inside: P, phosphorylation; Ub, ubiquitylation; S, sumoylation. (Modified from Shiloh, 2006)

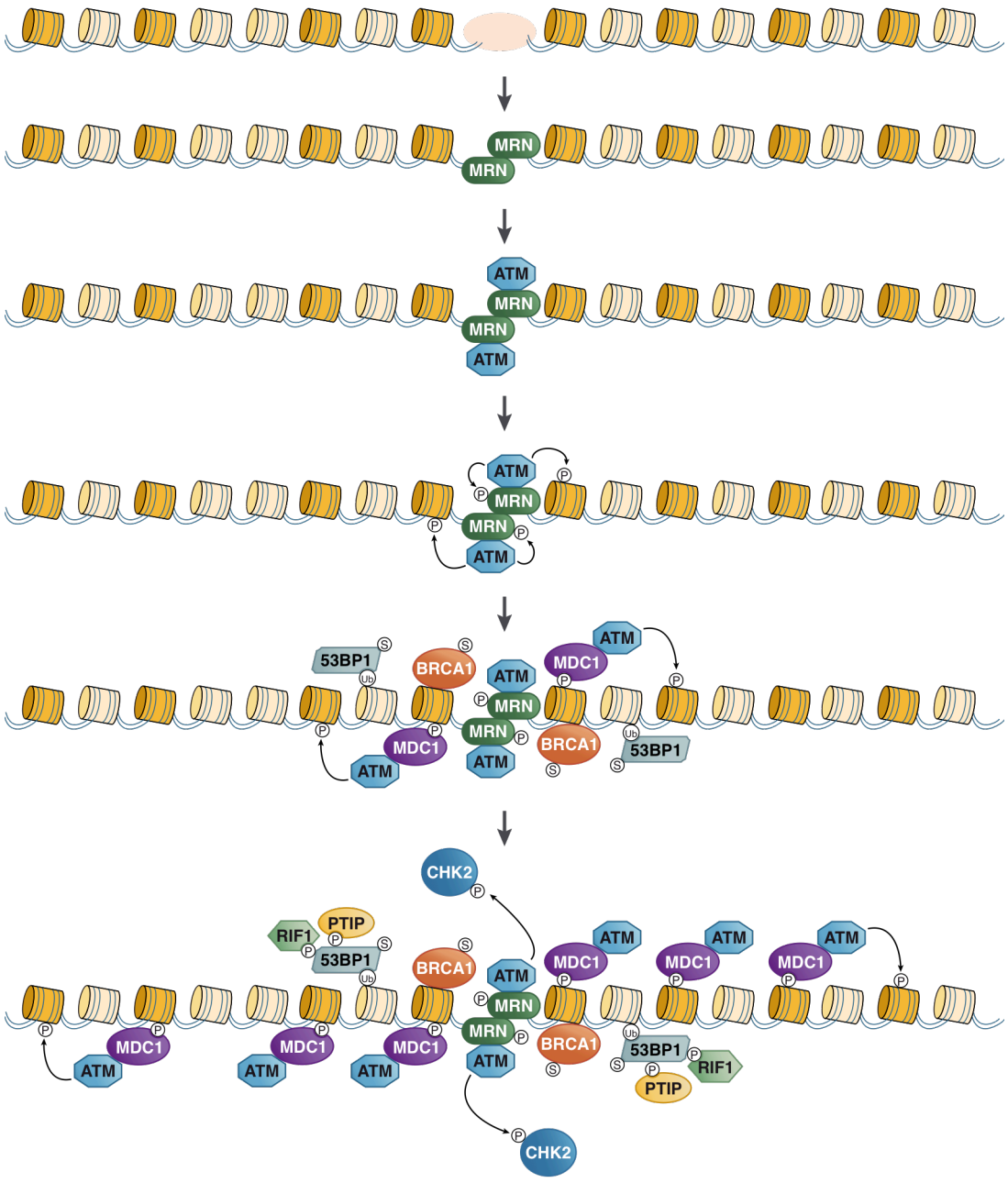

Other important *transducers* are proteins that are also members of the PIKK family, such as ATR (ATM and RAD3-related) and DNA-PKcs (DNA-dependent protein kinase catalytic subunit). Specific proteins mediate the recruitment of each of them to the site of the breaks (Falck *et al.*, 2005). Thus, ATR is recruited via its partner protein ATRIP (ATR-interacting partner), which senses RPA-coated ssDNA present at stalled replication forks or generated upon processing of DSBs (see below, section 4) (Zou & Elledge, 2003; Byun *et al.*, 2005). Full activation of ATR requires TOPBP1, which is recruited to the transition between double- and single-

stranded DNA independently of the ATR-ATRIP complex (Kumagai *et al*., 2006; Choi *et al*., 2009; Bhatti *et al*., 2011). Otherwise, the affinity of DNA-PKcs for DSBs is controlled by the presence of the DNA-end binding factor Ku70/80 heterodimer, which loads DNA-PKcs on DNA (Uematsu *et al*., 2007; Falck *et al*., 2005). These kinases, as ATM, respond to DNA damage by phosphorylating substrates involved in specific pathways. Although they play different roles in response to the breaks, there is also some degree of overlap in their targets, e. g. all three of them can phosphorylate serine-139 of H2AX, and there is even collaboration among them (Kinner *et al*., 2008; Jackson & Bartek, 2009; Shiloh & Ziv, 2013).

Despite the fact that thousands of proteins have been found to be direct targets of ATM, ATR and/or DNA-PKcs, some play more relevant roles than others in the DDR. Downstream of these proteins are two critical checkpoint kinases, CHK1 and CHK2 (figure I2). Upon activation mainly mediated by ATR or ATM phosphorylation, respectively, these proteins initiate a secondary wave of phosphorylation events to modulate the activity of other key *effectors* of the DDR and extend signalling (Bartek & Lukas, 2003). Ultimate targets of these cascades of signals include transcription factors, cell cycle regulators, the apoptotic machinery and DNA repair factors (Bartek & Lukas, 2003). Notably, induction of these kinases leads to inactivation of cyclin-dependent kinase (CDK) activity, which activates the different damage checkpoints to arrest the cell cycle or drives to programmed cell death by apoptosis (Matsuoka *et al*., 2007; Boucas *et al*., 2012).

In addition to phosphorylation, the cascade of signals that composed the DDR is accompanied by extensive induction of other post-translational modifications, which ultimately are primed by previous protein phosphorylations (Huen & Chen, 2008). These post-translational modifications comprise, among others, ubiquitylation, sumoylation, neddylation, acetylation, methylation and poly(ADP)-ribosylation, of many of the recruited proteins, including the *sensors* and *transducers* named before (Polo & Jackson, 2011; Brown & Jackson, 2015). These alterations affect also the core histones close to the breaks, generating changes in the epigenetic landscape in that region (Price & D'Andrea, 2013). Multiple proteins are simultaneously post-translationally modified by several different enzymes and play important roles in response to DNA damage. Among all, the tumour suppressor protein P53 has been shown to be CHK2- and ATM-

mediated phosphorylated, but also acetylated, sumoylated, methylated and ubiquitylated (L. Chen *et al*., 2005; Dai & Gu, 2010). These modifications lead to the stabilization and activation of its transcriptional role and to the upregulation of genes that code for proteins involved in cell cycle control, but also factors that promote programmed cell death or senescence (Huen & Chen, 2008; Shiloh & Ziv, 2013).

Once effective DNA repair has been achieved, resumption of cell cycle progression requires switching off the DDR, mainly through a well-organized process that reverts the post-translational modifications and by promoting dissociation of DDR proteins from DNA damage sites (Bartek & Lukas, 2007; Shiloh & Ziv, 2013).

3. DNA double-strand break repair pathways

As previously stated, the lack of an intact strand makes DSBs the most difficult to repair and most cytotoxic lesion on the DNA. As mentioned before, these lesions result from the contact with either exogenous agents, such as IR and certain genotoxic chemicals, or from the action of endogenous sources such as reactive oxygen species and from chemical stress on the chromosomes (Hartlerode & Scully, 2009). They can also be produced when two single-strand breaks arise in close proximity, when DNA replication forks encounter SSBs or certain other lesions or during transcription (Jackson & Bartek, 2009). In addition, DNA DSBs are generated during several specialized cellular processes, including recombination between homologous chromosomes during meiosis and developmentally regulated rearrangements, such as V(D)J recombination and class-switch recombination at the immunoglobulin heavy chain locus (Khanna & Jackson, 2001; Hartlerode & Scully, 2009). As DSBs are potentially hazardous DNA lesions, their accurate repair is essential for the successful maintenance and propagation of genetic information. Thus, in addition to the signalling through the DDR, cells have evolved a profusion of repair mechanisms to deal with them that can be roughly classified in two main categories: non-homologous end-joining (NHEJ) and homologous recombination (HR).

3.1. Non-homologous DNA end-joining

The major pathway for the repair of DSBs in mammals is NHEJ (Lieber, 2010; Radhakrishnan *et al*., 2014). It can occur throughout the cell cycle, but is of particular importance during G0 and G1 phases of mitotic cells, when is the only active repair pathway for DSBs (Rothkamm *et al*., 2003). NHEJ involves rejoining of the two DNA ends and requires one or several of the following three enzymatic activities: nuclease to remove aberrant structures at the DNA break, polymerase to fill gaps and ligase to restore the phosphodiester backbone (Lieber, 2008).

The initial step in NHEJ pathway is the binding of Ku70/Ku80 heterodimer to both ends of the broken DNA molecule (figure I3) (Downs & Jackson, 2004). Association of this complex with DNA ends may serve as a scaffold for the assembly of proteins involved in this repair mechanism (Lieber, 2008; Nick McElhinny *et al*., 2000; Yano *et al*., 2008). Thus, as mentioned in section 2, Ku-DNA complex recruits DNA-PKcs to the damaged site (figure I3). Then, Ku70/Ku80 moves inward on the DNA, allowing the contact of DNA-PKcs with the DNA and also the interaction of two DNA-PKcs molecules across the DSB to keep the broken DNA ends in close proximity (Yoo & Dynan, 1999). The interaction of DNA-PKcs with both DNA and Ku70/Ku80 leads to the activation of its serine/threonine kinase activity (Yaneva *et al*., 1997; Singleton *et al*., 1999). DNA-PKcs can phosphorylate several substrates, including proteins involved in NHEJ and even itself (Davis & Chen, 2013; Kusumoto-Matsuo *et al*., 2014). Its autophosphorylation may influence its conformation and dynamics, leaving DNA ends accessible for their repair (Jiang *et al*., 2015; Hammel *et al*., 2010; Uematsu *et al*., 2007). Besides DNA-PKcs, other specific factors, such as PAXX, XRCC4, XLF, and DNA ligase IV, are also rapidly recruited to the breaks (figure I3). These proteins bind the Ku-DNA complexes, and bridge and maintain the alignment of the DNA ends, thereby facilitating the DSB processing and stimulating ligation steps mediated by DNA ligase IV activity (Andres *et al*., 2012; Gu *et al*., 2007; Liu *et al*., 2017; Hung *et al*., 2017).

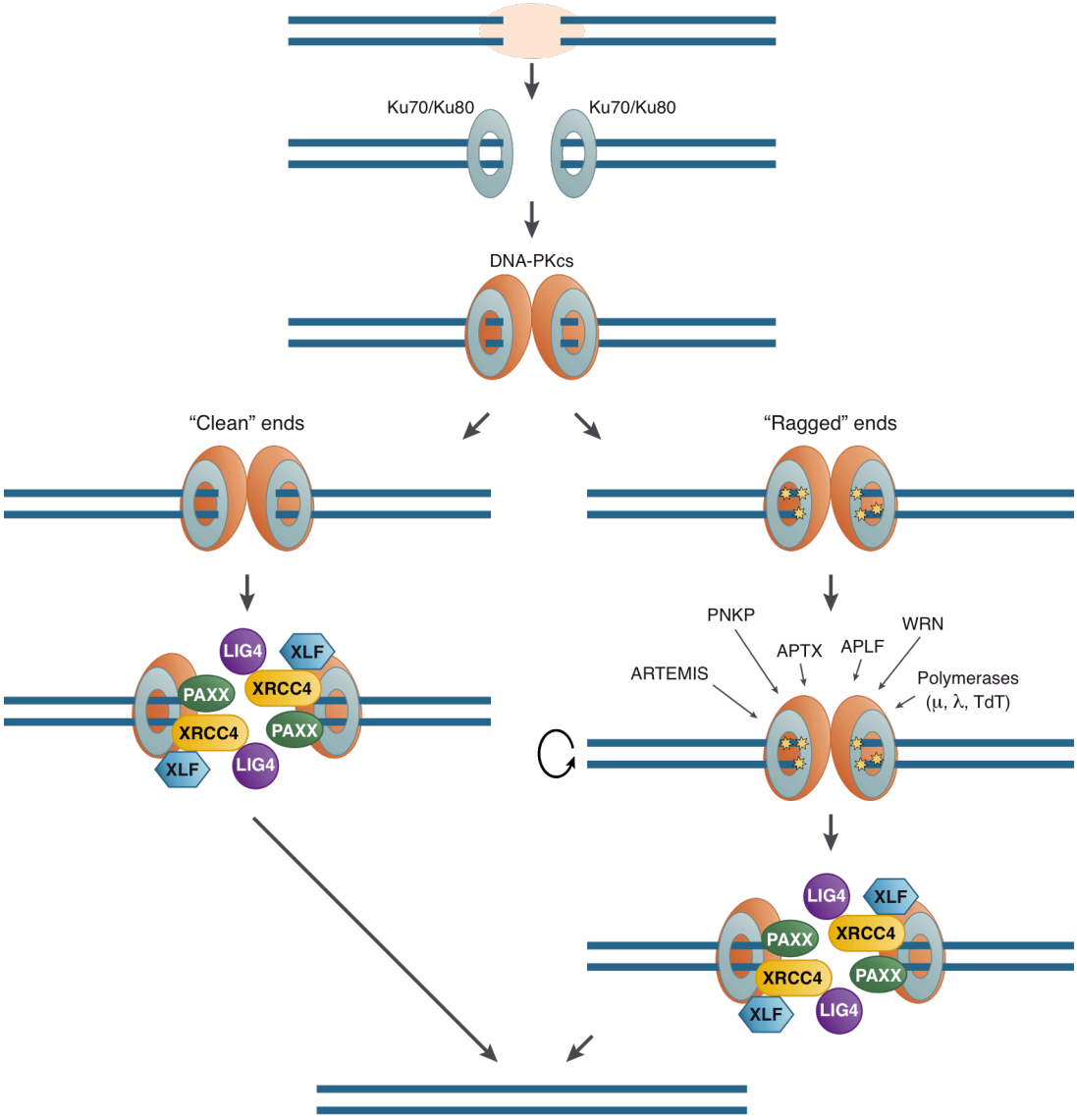

Figure I3. Mechanism for DSB repair by non-homologous end-joinig. Ku70/Ku80 heterodimer is the first to recognize and bind to the damage site (marked in light orange), acting as a scaffold for the assembly of other factors involve in this repair pathway. DNA-PKcs is then recruited and tethers both DNA ends. The different sources of DSBs result in a wide heterogeneity in the structure of the DNA ends, requiring specific enzymatic activities for their repair. For simple DSB ends also known as "clean" ends (left), the core NHEJ factors, PAXX, XRCC4, XLF and DNA ligase IV (LIG4 in the figure), are sufficient to recognize, align and ligate the broken ends. However, if the DSB ends contain complex structures or "ragged" ends (marked with stars in the figure, right), additional factors are required for its processing and repair, such as the nuclease ARTEMIS, PNKP, APTX, APLF, WRN and polymerases μ, λ and TdT. All these enzymes act iteratively and in any order until the ends are prone to be ligated (the circular arrow). The core NHEJ factors are also present during end processing (not shown in the figure for simplicity) and are required to complete the ligation and repair of the DNA molecule.

NHEJ is distinctive for the flexibility of the nuclease, polymerase and ligase activities that are used. This flexibility permits NHEJ to function on a wide range of possible substrate configurations that can arise when DSBs occur, particularly at sites of oxidative damage or ionizing radiation (Lieber, 2008). First, the heterogeneity of NHEJ arises from the many alternative ways in which the nuclease, polymerase and ligase can act during NHEJ. These enzymes act iteratively, in any order, and can function independently of one another at each of the two DNA ends being joined, leading to different results even when starting with two identical DNA ends (Lieber, 2010; Yang *et al*., 2016). In addition, DSBs can be complicated structures with a varied chemical signature at the ends. For simple DSB ends, the core NHEJ factors mentioned before are sufficient to recognize, align and ligate the broken end pairs (figure I3, left) (Waters *et al*., 2014). However, for complex DSBs that contain substantial mismatched or covalently modified DNA ends, additional factors are required to "clean" them and transform them to 5'-phosphorylated and 3'-hydroxylated tails in order to allow ligation and repair completion by NHEJ (figure I3, right) (Hartlerode & Scully, 2009; Strande *et al*., 2012). One key end-processing enzyme is ARTEMIS, which is recruited to DSBs through its direct interaction with DNA-PKcs and plays the most prominent "cleansing" role thanks to its high cleavage efficiency (figure I3, right) (Ma *et al*., 2005). Other enzymes, such as PNKP, APTX, APLF, Tyrosyl DNA phosphodiesterases and WRN, are also involved in the damage-specific end "cleaning" prior to their ligation (figure I3, right) (Waters *et al*., 2014). Moreover, some processing events may lead to creation of DNA gaps that are later filled by the specialized DNA polymerases μ, λ and terminal deoxynucleotidyl transferase (TdT) to enable break repair (figure I3, right) (Lieber, 2010; Bertocci *et al*., 2006). DNA processing during NHEJ repair generally causes deletions or insertions at the break site, being thus considered an error prone mechanism (Lieber, 2008; Lieber, 2010). However, when no processing is required classical NHEJ will be completely error free.

In the absence of one or more core components of the classical NHEJ machinery, such as Ku70/Ku80 heterodimer or DNA ligase IV, there are other DSBs repair mechanisms, collectively named as alternative non-homologous end-joining (alt-NHEJ) pathways (Lieber, 2008; Frit *et al*., 2014). Many alt-NHEJ events,

classified as microhomology-mediated end-joining (MMEJ), require the presence of other repair proteins and higher DNA end processing to exhibit terminal microhomology (5-25 nucleotides) for ligation (McVey & Lee, 2008). Thus, MMEJ share with homologous recombination some proteins, such as MRE11A and CtIP, involved in the initial step called DNA end resection (see section 4 for more details), but they do not need an extended resection or a homologous sequence to proceed (McVey & Lee, 2008; Wang & Xu, 2017). As the repair is carried out by joining the ends by base pairing at microhomology sequences, resulting in deletions at the junctions, MMEJ is inherently error-prone and a major cause of genomic instability, like chromosomal translocations and telomere fusions (McVey & Lee, 2008). However, there also exist other alt-NHEJ pathways that do not use microhomology regions for the repair (Truong *et al*., 2013).

3.2. Homologous recombination

Homologous recombination is a complex and highly regulated DSB repair mechanism. In contrast to NHEJ, HR requires the presence of a homologous sequence, preferentially the sister chromatid, as a template for the repair (San Filippo *et al*., 2008). HR comprises several recombination subpathways, each one with distinct outcomes and consequences (figure I4) (Heyer *et al*., 2010). Nonetheless, all of them share the same initial step, known as DNA end resection or DNA end processing, in which DNA breaks are processed (figure I4, i) (Huertas, 2010). As DNA end resection regulation is the main subject of this thesis, a specific section will be devoted to explain it in detail (see section 4). However, in order to understand the different recombination subpathways, DNA end resection is presented here briefly: both DNA ends are processed by degrading one strand in a 5'-3' polarity, giving rise to 3'-ssDNA overhangs. ssDNA is immediately coated by the replication protein A (RPA) complex for protection against secondary structure formation and nuclease digestion (Huertas, 2010). This resected DNA can search for, recognize and anneal to a homologous sequence elsewhere in the genome, prompting the different recombination repair mechanisms.

If the DSB is flanked by two direct sequence repeats or occurs in one of them, cells may be directed toward single-strand annealing (SSA) repair pathway

(figure I4, ii). This process consists of the annealing of the complementary single strands from each repeated sequence, which were exposed after resection (Ivanov *et al*., 1996; Krogh & Symington, 2004). This is the simplest homology-directed repair and it does not require a complex machinery to find and anneal the homologous sequence. Since the result of this repair event leads to a deletion of one of the two copies of the repeated sequence and the intervening sequence, SSA is intrinsically an error-prone process (Morrical, 2015).

Figure I4. Mechanism for DSB repair by homologous recombination. HR comprises complex and regulated processes for the repair of DSBs (highlighted in light orange). The initial step, shared by all HR subpathways, is DNA end resection. It involves the processing of DNA ends by many proteins, such as the MRN complex, CtIP, EXO1, DNA2 and BLM, generating extensive 3' ssDNA tails that are rapidly coated by RPA for protection **(i)**. The repair can be directed toward SSA if the DSB is flanked by two direct repeats (indicated in light blue). Then, the complementary single strands anneal when exposed, the excess of DNA is removed by FLAP-endonucleases, the intervening sequence and one of the repeats are deleted and the DNA molecule is ligated **(ii)**. Other HR subpathways require the formation of RAD51 nucleofilament for homology search and strand invasion. The assembly of RAD51 to ssDNA replacing RPA complex is mediated by BRCA2, PALB2 and other proteins such as RAD52 and RAD51 paralogues **(iii)**. During strand invasion, RAD51 filament promotes the annealing to the homologous sequence and the displacement of the noncomplementary strand, resulting in a D-loop formation. The homologous sequence serves as template for DNA synthesis from the 3' end of the invading strand **(iv)**. In SDSA, the D-loop structure can be dissolved after the synthesis and the invading strand is displaced and anneals with its complementary resected end. Subsequent DNA synthesis and ligation complete the repair, leading to noncrossover products **(v)**. Alternatively, the second DSB end can be captured by the annealing with the displaced strand of the D-loop to prime DNA synthesis **(vi)**. Then, D-loop can be endonucleolitically cleaved, generating crossover products **(vii)**, or the ends can be ligated after DNA synthesis, resulting in a joint molecule with two Holliday junctions **(viii)**. The resolution of this intermediate is performed by resolvases, leading to noncrossover or crossovers products if they act in the same or opposite orientation, respectively **(ix)**. Instead of being resolved, Holliday junctions can also be dissolved by a helicase-topoisomerase complex, creating noncrossover products **(x)**. Finally, if the DSB presents only one repairable end, the second-end capture fails and BIR machinery establishes a replication fork at the D-loop, potentially copying long tracts from the donor chromosome and causing loss of heterozygosity **(xi)**. (Modified from Genois *et al*., 2014)

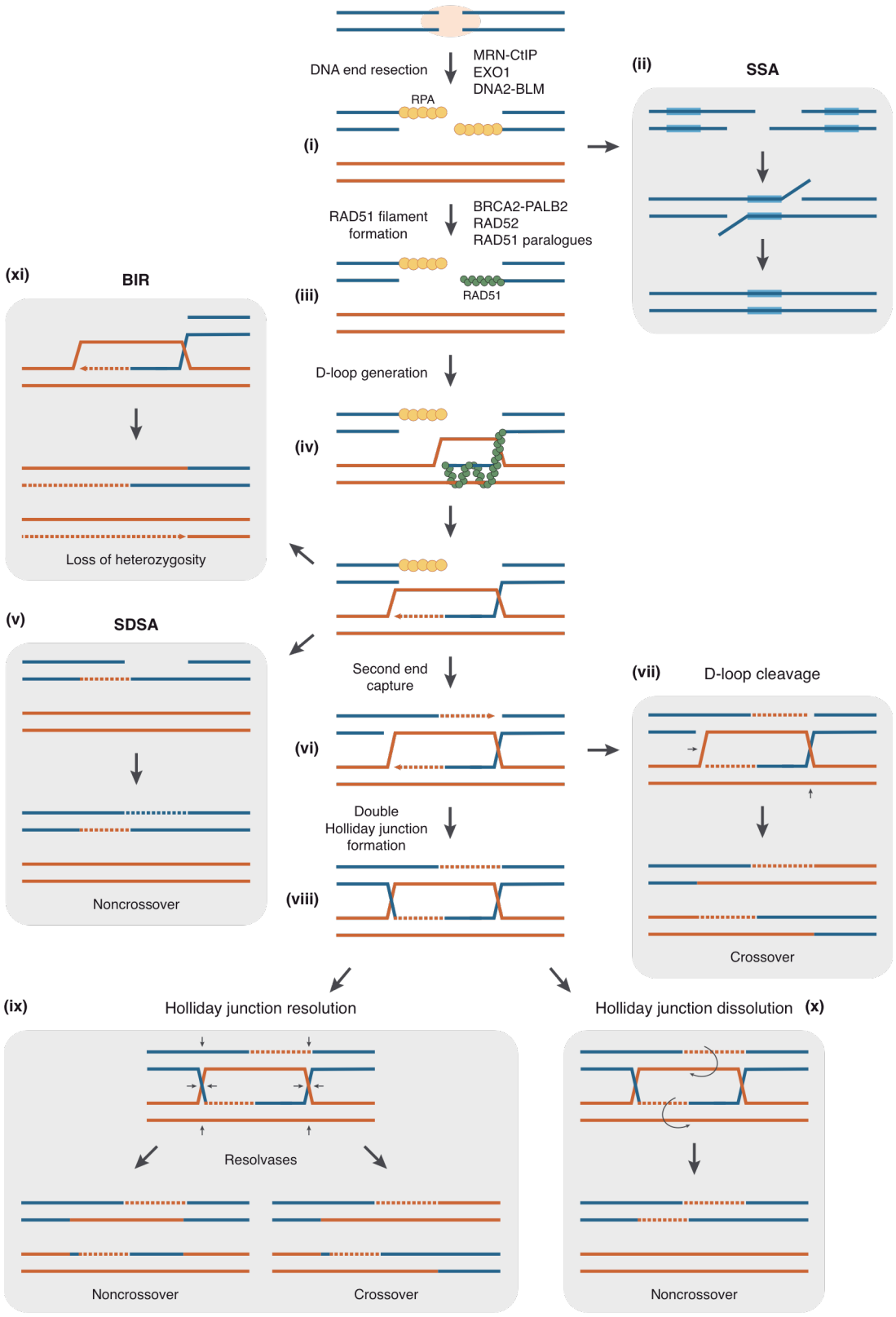
DNA end resection
MRN-CtIP
EXO1
DNA2-BLM
RPA
(i)
(ii)
SSA
RAD51 filament formation
BRCA2-PALB2
RAD52
RAD51 paralogues
(iii)
RAD51
D-loop generation
(iv)
(xi)
BIR
Loss of heterozygosity
(v)
SDSA
Noncrossover
Second end capture
(vi)
(vii)
D-loop cleavage
Crossover
Double Holliday junction formation
(viii)
(ix)
Holliday junction resolution
Resolvases
Noncrossover
Crossover
Holliday junction dissolution
(x)
Noncrossover

Otherwise, other HR subpathways require homology search and DNA strand invasion steps that depend on the formation of a RAD51 filament (figure I4, iii) (Jasin & Rothstein, 2013). Indeed, the creation of this nucleoprotein filament supresses SSA mechanism (Stark *et al*., 2004). In order to assemble the nucleofilament, RAD51 must replace RPA complex onto ssDNA. Since RPA has higher affinity for ssDNA than RAD51, mediator proteins are necessary to displace RPA complex from DNA and promote RAD51 binding (Sung *et al*., 2003; San Filippo *et al*., 2008). These mediators also promote stabilization and protection of RAD51 filament (Krejci *et al*., 2012). BRCA2, together with its partner PALB2, is one key factor that control nucleoprotein filament formation and function (figure I4, iii) (Jensen *et al*., 2010; Buisson *et al*., 2010). The recruitment of BRCA2 to DNA-damage sites is mediated by the interaction of PALB2 with BRCA1 (Zhang *et al*., 2009). Other proteins, such as RAD52 and RAD51 paralogues, act also as mediators (figure I4, iii) (Krejci *et al*., 2002; Takata *et al*., 2001; Sung & Klein, 2006). Once formed, the nucleoprotein filament searches for a homologous sequence, promotes strand invasion and the displacement of the noncomplementary strand from the duplex to generate a recombination intermediate called displacement loop (D-loop) (figure I4, iv) (Greene, 2016). The 3' end of the invading strand serves as a primer for subsequent DNA synthesis using the intact homologous sequence as a template to restore genetic material, thus extending of the D-loop structure (Daley *et al*., 2014). The extended strand invasion intermediate can be resolved in a number of different ways, leading to either noncrossover or crossover products (figure I4, v-xi) (Jasin & Rothstein, 2013).

According to the synthesis-dependent strand annealing (SDSA) model (figure I4, v), the D-loop can be disrupted after DNA synthesis from the first processed DNA end. The invading strand is then displaced from the recombination structure and anneals to its complementary sequence on the other side of the break. The repair is completed by gap-filling DNA synthesis and nick ligation, leading always to noncrossover products (Daley *et al*., 2014; Nassif *et al*., 1994).

Alternatively, the second DSB end can anneal to the displaced strand of the D-loop, in a process known as second-end capture (figure I4, vi), to prime another round of DNA synthesis (Nimonkar & Kowalczykowski, 2009). Direct processing of the resulting precursor always generates crossover products (figure I4, vii), while

ligation produces a joint molecule with two Holliday junctions (figure I4, viii) (Osman *et al*., 2003). The so-called double Holliday junction intermediate can be resolved by specialized nucleases termed resolvases. The orientation of the DNA incisions introduced by the resolvase determines whether a noncrossover or a crossover product is generated (figure I4, ix). Otherwise, these junctions can also be dissolved by a helicase-topoisomerase complex, leading in all cases to noncrossover products (figure I4, x) (Daley *et al*., 2013).

Break-induced replication (BIR) mechanism is used when the DSB presents only one repairable end, as seen at eroded uncapped telomeres or collapsed replication forks. Here, the D-loops structure is stable, but second-end capture fails either by loss or inaccessibility of the second end. Then, a replication fork is established at the D-loop, resulting in the initiation of DNA synthesis that proceeds up to the end of the donor chromosome (figure I4, xi) (Llorente *et al*., 2008; Lydeard *et al*., 2010). BIR is associated with genetic instability, including extensive loss of heterozygosity (Sakofsky *et al*., 2012).

Despite been an intrinsically error-free repair, HR must be appropriately restricted to minimize genomic instability. For example, the ideal template is the sister chromatid, thus HR is limited to S and G2 phases of the cell cycle, when the newly synthesized DNA is readily available. Indeed, the choice of the DSB repair mechanism is highly regulated in response to cell status to minimize genomic instability upon DNA breaks (Huertas, 2010). Many homologous recombination factors are cell cycle regulated, mainly by CDK-dependent phosphorylations that can promote protein recruitment to the sites of damage (Heyer *et al*., 2010; Hartlerode *et al*., 2011). Other factors and post-translational modifications lead to suppression of HR during G1 phase by regulating HR downstream steps, such as the interaction between BRCA1 and PALB2-BRCA2 complex needed for RAD51 filament formation (Orthwein *et al*., 2015). However, the best-known regulated step of the DSB repair pathway choice is DNA end resection, as it promotes break repair by HR while, at the same time, supresses NHEJ (Ferretti *et al*., 2013).

4. DNA end resection

As stated before, DNA end resection is the first step for DSB repair by homologous recombination, and is a common process for all HR subpathways. In most organisms, this mechanism of end processing is composed of two stages (Mimitou & Symington, 2008). An initial, short-range, DNA end resection is slow and involves limited 5' DNA end resection. This step is catalysed mainly by the MRN complex and CtIP (figure I5), which also promote the recruitment of proteins involved in the following step of long-range end resection (Mimitou & Symington, 2009). As mentioned in section 2, MRN complex rapidly binds to DSBs, where has a role in tethering both DNA ends to allow the repair and acts as a sensor in the DNA damage response (Stracker *et al*., 2004). MRE11A is the core component of the MRN complex and has several enzymatic activities, including endonuclease activity on ssDNA and DNA hairpin and 3'-5' exonuclease activity on double-stranded DNA (Stracker & Petrini, 2011). Since 3' overhang generation requires 5'-3' exonuclease activity, opposite to the ones exhibits by MRE11A by itself *in vitro*, the MRN complex is thought to perform the initial DNA end resection by endonucleolytic cleavage of the 5'-terminated strand away from the DNA break followed by 3'-5' digestion toward the DNA end (figure I5) (Shibata *et al*., 2014). NBS1 is an important regulator of the MRN complex since it promotes DNA binding, association with CtIP and nuclease activity of MRE11A (Trujillo *et al*., 2003; Paull & Gellert, 1999). Otherwise, RAD50 belongs to the structural maintenance of chromosomes (SMC) family, thus exert its structural function by binding DNA ends in an ATP-dependent manner and holding them in close proximity (de Jager *et al*., 2001).

CtIP, among other functions in many cellular processes (see the following section for more details), plays a key role activating this first step of DNA end resection. It interacts with the MRN complex and stimulates the endonuclease activity of MRE11A (Sartori *et al*., 2007). This function of CtIP as cofactor of MRE11A is dependent on its CDK-mediated phosphorylation of threonine-847, effectively limiting resection to S and G2 phases (Huertas & Jackson, 2009; Anand *et al*., 2016). Additionally, CtIP possess intrinsic 5' flap endonuclease activity, which has been proposed to process protein adducts at DSBs (Makharashvili *et al*.,

2014; H. Wang *et al.*, 2014). Apart from MRN complex and CtIP, proper DNA end resection requires the action of additional factors such as the tumour suppressor BRCA1 (figure I5). BRCA1 interacts physically with both CtIP and the MRN complex (Yu *et al.*, 1998; Zhong *et al.*, 1999); however, its role in regulation of DNA end resection is mainly through its binding with CtIP. This interaction depends on CDK-mediated phosphorylation of serine-327 of CtIP (Yu & Chen, 2004), and has been shown that modulates resection speed (Cruz-García *et al.*, 2014). In addition, recent studies have identified EXD2, a novel 3'-5' exonuclease that works as a cofactor of the MRN complex and is required for this initial end-processing (figure I5) (Broderick *et al.*, 2016).

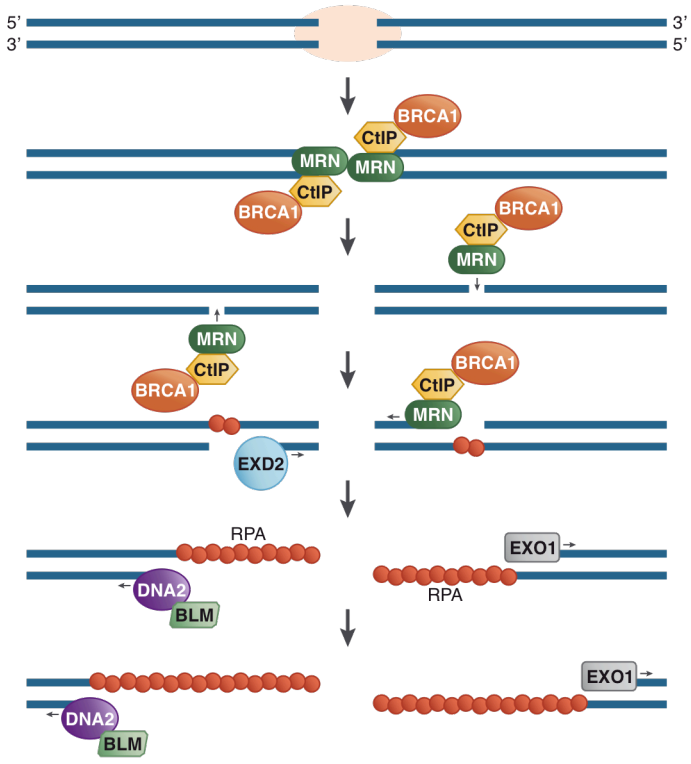

Figure I5. Mechanism of DNA end resection. DNA end resection generates 3' overhangs and is carried out in two stages. DSBs (marked in light orange) are first recognized by the MRN complex, which is responsible for the initial short-range resection through its association with CtIP. CtIP can form a complex with BRCA1 and promotes the endonuclease activity of MRN. The MRN complex generates a nick on the 5'-terminated strand and degrades it toward the end by its 3'-5' exonuclease activity. EXD2 is a 3'-5' exonuclease that can contribute to this first digestion of the DNA. The following long-range resection is performed by two redundant pathways, one mediated by the 5'-3' exonuclease EXO1 (right), and the other involving the activity of the nuclease DNA2 together with BLM helicase (left). Extensive ssDNA tails are generated as a result, which are rapidly coated by RPA complex for protection.

The endonucleolytic cleavage of the 5'-terminated DNA strand in this first step generates an entry site for the long-range resection machinery to carry out 5'-3' resection away from the DSB (Mimitou & Symington, 2008). Two redundant pathways are required for extensive resection to generate 3'-ssDNA overhangs (Nimonkar *et al*., 2011). One involves the activity of DNA2 together with BLM (figure I5). DNA2 possesses a bipolar nuclease activity that can endonucleolytically degrade ssDNA with either 3' or 5' polarity (Kim *et al.*, 2006). Thus, the helicase BLM unwinds duplex DNA by their 3'-5' helicase activity, generating ssDNA tails for incision by DNA2. RPA complex coats generated ssDNA for protection (figure I5) and serves as a control for DNA2 cleavage polarity by preventing 3'-5' ssDNA degradation (Nimonkar *et al*., 2011; Zhou *et al*., 2015). Recent studies suggest that the activity of BLM in this pathway is enhanced by the formation of the BLM-TOPOIIIa-RMI1-RMI2 complex (Sturzenegger *et al*., 2014). In addition, WRN, a BLM paralogue, has been described to act epistatically with DNA2 to promote extensive resection (Sturzenegger *et al*., 2014). The second long-range resection pathway is catalysed by the 5'-3' exonuclease EXO1, which degrades the 5'-terminated strand to generate the extensive 3'-ssDNA tail (figure I5) (Mimitou & Symington, 2009). BLM also interacts with EXO1 and *in vitro* enhances its exonuclease activity, although this function is independent of BLM helicase activity (Nimonkar *et al*., 2008). PCNA also stimulates EXO1 activity by tethering the nuclease to the damaged DNA (Chen *et al*., 2013). The ssDNA-RPA intermediate resulting from resection serves for the formation of RAD51 filament and activation of the ATR-mediated checkpoint to slow or arrest cell cycle progression (Genois *et al*., 2014).

As mentioned before, the repair pathway used to repair DSB in different conditions must be regulated in order to ensure an accurate repair. The best characterized regulatory point is the decision NHEJ versus HR, where the major restriction step is the competition between DNA end protection and DNA end resection (Symington & Gautier, 2011), mediated by the antagonistic activity of 53BP1 with its downstream effectors and BRCA1-CtIP complex. It was first described that loss of 53BP1 renders BRCA1-deficient tumours resistant to PARP1 inhibitors by restoring HR, and even increases their viability, suggesting that both proteins compete with each other to influence the DSB repair pathway choice

(Bouwman *et al*., 2010; Bunting *et al*., 2010). 53BP1 is a positive regulator of NHEJ that acts as a scaffold protein to facilitate the recruitment of factors involved in DSB protection from end resection and hence committing the repair to NHEJ. ATM-mediated phosphorylation of 53BP1 is required for the interaction with those anti-resection proteins (Symington, 2016). The key ones are RIF1 and PTIP (figure I2). Both proteins have a role in preventing end resection, although they act independently (Chapman *et al*., 2013; Escribano-Díaz *et al*., 2013; Callen *et al*., 2013). Indeed, PTIP promotes NHEJ repair by recruiting the ARTEMIS nuclease to sites of DNA damage (J. Wang *et al*., 2014), while RIF1 is required for MAD2L2 (also known as REV7) recruitment, which inhibits DNA end resection (Xu *et al*., 2015; Boersma *et al*., 2015).

Despite a pro-HR environment in S and G2 phases of the cell cycle, NHEJ machinery is also active and 53BP1 and its downstream effectors are recruited to the DSB site even then. However, the action of BRCA1-CtIP leads to the removal of 53BP1 and its partner RIF1 from DSBs to facilitate processing of DNA ends, switching the repair to HR (Chapman *et al*., 2012; Escribano-Díaz *et al*., 2013). It is not completely clear how this dual antagonistic role of 53BP1-RIF1 and BRCA1-CtIP is balanced to elicit the appropriate response in relationship with cell status. It is known that the induction of end resection in S and G2 phases requires CDK-dependent phosphorylations, such as phosphorylation of serine-327 and threonine-847 of CtIP to allow the interaction with BRCA1 and its role in resection initiation, respectively (Escribano-Díaz *et al*., 2013). Indeed, a phosphomimicking mutant of CtIP (CtIP-T847E) partially rescues the sensitivity of BRCA1-deficient cells to PARP1 inhibition, even in the presence of 53BP1, suggesting that CtIP has an important role in promoting DNA end resection and, therefore, in the control of the DSB repair pathway choice (Polato *et al*., 2014). Additionally, BRCA1 has been recently implicated directly in perturbing RIF1-53BP1 interaction by promoting dephosphorylation of 53BP1 (Isono *et al*., 2017).

5. CtIP. Functions and interactors: beyond DNA end resection

The human *CtIP* gene is located at chromosome 18q11.2, and encodes for a protein containing 897 amino acids (Fusco *et al*., 1998). Before its function in DNA end resection was discovered, CtIP (CtBP-interacting protein) was initially characterized for its role in transcription regulation, DNA replication and G2-M DNA-damage checkpoint control through its association with CtBP, RB (Retinoblastoma) and BRCA1 (Schaeper *et al*., 1998; Fusco *et al*., 1998; Wong *et al*., 1998; Yu *et al*., 1998). The first function described for CtIP was as a cofactor of the transcriptional repressor CtBP, which binds to a PLDLS motif in CtIP located between residues 490 and 494 (figure I6) (Schaeper *et al*., 1998). In addition, CtIP is involved in regulation of cell cycle progression into the S phase and DNA replication as it associates with the Retinoblastoma pocket protein family members RB1 and RBL2 through the motif LECEE (residues 153-157, figure I6), although this motif is not essential for the interaction (Fusco *et al*., 1998; Meloni *et al*., 1999). Cell cycle transition from G1 to S phase is mainly controlled by E2F and RB family members, which repress S-phase genes expression by blocking their promoters (Weintraub *et al*., 1992). CDK-mediated phosphorylations of RB during G1 phase disrupts its association with E2F factors, allowing activation of E2F-mediated transcription, thus leading to cells enter in S phase (Harbour *et al*., 1999). CtIP participates in releasing RB from the E2F-responsive promoters, acting as an activator to promote G1-S transition (P. Chen *et al*., 2005). Indeed, CtIP can promote the expression of genes essential for S-phase entry, like cyclin D1, as well as activate its own promoter owing to they are regulated by RB-E2F pathway (Liu & Lee, 2006). Other transcriptional factors also interact with CtIP, such as Ikaros (IKZF1), TRIB3 and LMO4, evidencing its role in regulating gene expression (Koipally & Georgopoulos, 2002; Xu *et al*., 2007; Sum *et al*., 2002). Other studies indicate that CtIP participates in the surveillance of ongoing DNA replication by its binding to PCNA at replication forks, thus acting in the maintenance of genomic stability (Gu & Chen, 2009). As described in the previous section, CtIP also interacts with the BRCA1 BRCT domains specifically when is CDK-mediated

phosphorylated in the residue serine-327 (figure I6) (Yu *et al.*, 1998). Besides the role in DNA repair (Cruz-García *et al.*, 2014), this interaction has been identified as necessary for G2-M checkpoint activation (Yu & Chen, 2004) and to control cell cycle progression through the regulation of P21 expression (Li *et al.*, 1999). Moreover, BRCA1 and CtIP can form a complex with the transcriptional regulator LMO4 that represses BRCA1-mediated transcriptional activation (Sum *et al.*, 2002). Most of CtIP interactors are tumour suppressors, such as RB1, BRCA1, LMO4 and Ikaros (Burkhart & Sage, 2008; Venkitaraman, 2002; Visvader *et al.*, 2001; Wang *et al.*, 1996), revealing a potential function of CtIP in tumorigenesis. Indeed, several mutations in CtIP are associated with different types of cancer (Wong *et al.*, 1998; Bilbao *et al.*, 2010; Gaymes *et al.*, 2013), as well as it was found a relationship between CtIP levels and specific breast cancer types (Soria-Bretones *et al.*, 2013; Wang *et al.*, 2016).

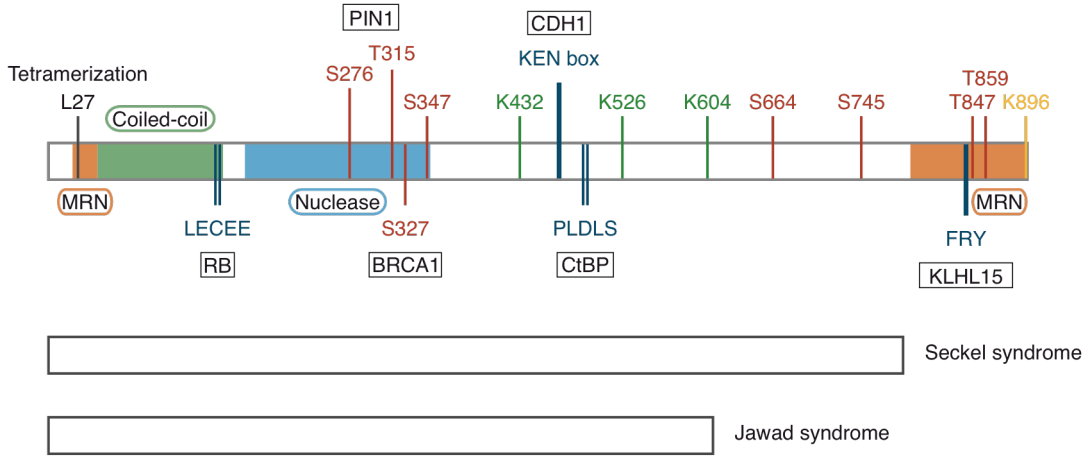

Figure I6. Scheme representing CtIP known features. CtIP interacts with the MRN complex by its amino and carboxy terminus (shown in orange). CtIP also binds RB and CtBP through its LECEE and PLDLS motifs, respectively. CDH1 and KLHL15 associate with CtIP by KEN box and FRY motifs, respectively. CDK- and ATM/ATR-dependent phosphorylations are represented in red. Phosphorylation of residue S327 mediates the interaction with BRCA1, while phosphorylation of residues S276 and T315 is responsible for the binding of PIN1. CtIP is also acetylated (marked in green) and sumoylated (marked in yellow) in different residues. Blue section depicts a nuclease domain, while green region represents a coiled-coil domain for CtIP homodimerization. In addition to homodimerization, the residue L27 mediates CtIP tetramerization. Truncated forms of CtIP corresponding to Seckel and Jawad syndromes are shown at the bottom. (Modified from Makharashvili & Paull, 2015).

As shown, CtIP interacts with multiple proteins and exerts its functions in different branches of DNA metabolism; however, it is now better known for its role in DSB repair by promoting DNA end resection together with the MRN complex (Sartori *et al*., 2007).

Functional orthologs of CtIP are found in most eukaryotic species, like Sae2 in *Saccharomyces cerevisiae* and Ctp1 in *Schizosaccharomyces pombe*, as well as in *Caenorhabditis elegans*, *Xenopus laevis*, *Arabidopsis thaliana* or mouse (You & Bailis, 2010). These proteins vary considerably in length and may have different functions compared to CtIP; however, both Sae2 and Ctp1 also interact with its corresponding MRN homolog and function together with it to promote DNA end resection for HR-mediated DSB repair (Takeda *et al*., 2007). Despite limited sequence homology, there are small conserved regions located in the amino and carboxyl terminus of CtIP. The domains needed for the interaction with the MRN complex are located in both regions, between residues 22 and 45 of the amino-terminus and the last 108 residues of the carboxy-terminal tail (figure I6) (Yuan & Chen, 2009; Sartori *et al*., 2007). A coiled-coil domain is identified near the amino-terminal region (residues 45-160, figure I6), which appears to fold back as a four helix bundle and mediates CtIP homodimerization (Dubin *et al*., 2004). CtIP self-interaction is required for its function in DNA end resection, its recruitment to DSBs on chromatin upon DNA damage, and regulation of its damage-induced phosphorylations, although it is not essential for the interaction of CtIP with BRCA1 and MRN (Wang *et al*., 2012). Recently, it was found that the actual *in vivo* structure of CtIP is a stable homotetramer that is required for its recruitment to the site of damage and its function in DSB repair (Davies *et al*., 2015). CtIP tetramerization is mediated by the residue leucine-27, which does not interfere with CtIP dimerization (Davies *et al*., 2015). In addition, a nuclease domain is also found in the amino-terminus, including residues from approximately 180 to 350 (Makharashvili *et al*., 2014). Otherwise, carboxy-terminal domain includes the CDK phosphorylation site threonine-847, previously mentioned as essential for CtIP-mediated resection initiation, which correlates with serine-267 in *S. cerevisiae* Sae2 (Huertas *et al*., 2008; Huertas & Jackson, 2009). Close to this amino acid, it was identified the also conserved residue T859 (T279 in *S. cerevisiae* Sae2), which plays a role in DNA end resection (Peterson *et al*., 2013). The importance of this

carboxy-terminal domain in CtIP function is reflected in two genetic disorders in humans, the Seckel and Jawad syndromes. Different mutations in the *CtIP* gene result in expression of carboxy-terminally truncated forms of CtIP (figure I6), leading to the defects in ATR activation and processing of DNA damage observed in these patient cells (Qvist *et al*., 2011).

CtIP is subjected to multiple post-translational modifications, including phosphorylation, ubiquitylation, acetylation and sumoylation, which control the interaction with its partners and its multiple roles in DNA metabolism (Makharashvili & Paull, 2015). Among these modifications, CtIP is extensively phosphorylated by CDK according to the cell cycle and by ATM and ATR kinases upon DNA-damage induction, thus regulating its activity (Makharashvili *et al*., 2014). The best characterized are the previously mentioned CDK-dependent phosphorylation in serine-327, which mediates CtIP and BRCA1 interaction, and threonine-847, which is essential for CtIP function in DNA end resection (figure I6) (Yu & Chen, 2004; Huertas & Jackson, 2009). Other phosphorylation sites are serine-276 and threonine-315, which mediate interaction with PIN1 and control CtIP stability (Steger *et al*., 2013); serine-347, required for CtIP nuclease activity (Makharashvili *et al*., 2014); serine-664 and serine-745, whose ATM-mediated phosphorylation abolish the dissociation of BRCA1 from CtIP and are involved in CtIP nuclease activity (Li *et al*., 2000; Makharashvili *et al*., 2014); and threonine-859, which is ATR-dependent phosphorylated in response to DSBs and is required for binding of CtIP to chromatin (Peterson *et al*., 2013) (figure I6). Otherwise, CtIP is also acetylated in lysine-432, lysine-526 and lysine-604 (figure I6), and its deacetylation mediated by SIRT6 is necessary to promote DNA end resection and homologous recombination (Kaidi *et al*., 2010). Several experiments carried out by Isabel Soria Bretones in our laboratory demonstrate that CtIP is also subjected to SUMO1- and SUMO2-mediated sumoylation. In particular, sumoylation of residue lysine-896 at the end of the carboxy-terminal domain is essential for the role of CtIP in DNA end resection (figure I6) (Soria-Bretones and Huertas, personal communication). When interaction between CtIP and BRCA1 occurs, BRCA1 catalyses CtIP ubiquitylation, which does not target CtIP for degradation and is associated with its recruitment to damaged chromatin and its function in checkpoint control (Yu *et al*., 2006).

CtIP can interact with CDH1 after mitotic exit and in late S-G2 phases after DNA damage through a conserved KEN box located between residues 467 and 469 (figure I6). CDH1, in turn, binds to and is an activator of the ubiquitin E3-ligase APC/C. Therefore, CtIP is subjected to APC/C-mediated polyubiquitylation that targets it to proteasomal degradation, leading to resection control during G1 and G2 phases (Lafranchi *et al*., 2014). Moreover, CDK-mediated phosphorylation of residues serine-276 and threonine-315 allows binding of PIN1 (figure I6), a protein responsible for mediating prolyl isomerization of the residues proline-277 and proline-316. CtIP isomerization promotes its ubiquitylation and subsequent proteasomal degradation (Steger *et al*., 2013). Recent studies have identified CUL3-KLHL15 as the possible E3 ligase responsible for driving this PIN1-dependent CtIP ubiquitylation (Ferretti *et al*., 2016). KLHL15 is a substrate-specific adaptor for Cullin3(CUL3)-based E3 ubiquitin ligases, which can interact with the FRY motif of CtIP located between residues 840 and 842 (figure I6) and conserved across vertebrates. When associates with CtIP, KLHL15 mediates CtIP ubiquitylation that promotes its proteasomal degradation (Ferretti *et al*., 2016). Thereby, PIN1, CUL3-KLHL15 and APC/C(CDH1) negatively regulate CtIP protein stability and, consequently, limit DNA end resection to facilitate HR. Indeed, extensive DNA end resection generates long ssDNA stretches that are prone to mutation cluster formation, often ascribed to cancer (Roberts *et al*., 2012; Jimeno *et al*., 2015; Chen *et al*., 2015; Kijas *et al*., 2015; Tkáč *et al*., 2016; Zong *et al*., 2016). Thus, the control of DNA end resection is essential for the maintenance of genomic stability.

In summary, CtIP seem to act as a hub that integrates different cellular and environmental cues to modulate many aspects of cell metabolism, including DNA end resection. Those signals arise in the form of either post-translational modifications, protein-protein interactions or a combination of both (such as CDK phosphorylation at serine-327 that induces BRCA1 interaction). Thus we reasoned that the identification of novel CtIP interactors might elucidate CtIP function. As CtIP is considered a tumour suppressor protein, new insights on its regulation may also reveal possible targets for cancer treatment.

OBJECTIVES

The main goal of this thesis is to get new insights into the role of CtIP in double-strand break repair and its regulation, which summarizes the following objectives:

1. Identification of novel CtIP interacting partners involved in DNA end resection.

2. Analysis of the influence of PRMT5 in promoting DNA end resection through its association with CtIP.

3. Characterization of CCAR2-CtIP interaction and their antagonistic functions in DSB repair.

RESULTS

1. Isolation of novel CtIP interacting partners

1.1. Tandem Affinity Purification followed by mass-spectrometry reveal new proteins that interact with CtIP

As mentioned in the introduction (section 5), CtIP is a multifunctional protein involved in several processes through interaction with many different partners. The aim of this work was the identification of novel CtIP interactors that could regulate its cellular roles, with an emphasis in DNA end resection. To address this objective, we set up a Tandem Affinity Purification (TAP) protocol based on two consecutive rounds of immunoprecipitation using two different tags: FLAG and GFP (Green Fluorescent Protein), to ensure maximum purity of the complexes obtained.

Thus, we transfected U2OS cells with a GFP-6XFLAG-CtIP fusion (see materials and methods chapter, section 1.5, for details) and generated stable cell lines clonally pure by isolation of several individual clones that were later selected in the presence of G418. To check whether the DNA construct was integrated and expressed, we screened for the presence of CtIP, FLAG and GFP by western blot assays with protein cell extracts from 42 clones. Figure R1 shows western blots of 3 representative clones compared with control U2OS cells (see figure R1, panels a, b and c for the different antibodies).

Several clones, like clone 40, showed no GFP-6XFLAG-CtIP (figure R1), so they were discarded. Others, such as clone 27 and clone 38, displayed ectopic tagged-CtIP expression. Although clone 27 had expression levels closer to endogenous CtIP than clone 38 (figure R1, panel a), the antibody against GFP did not detect the protein in the cell extract from this clone, probably due to a modification in the GFP (figure R1, panel c). Therefore, we selected clone 38 to carry out the TAP assay and from that point onwards we named it as GFP-6XFLAG-CtIP cell line.

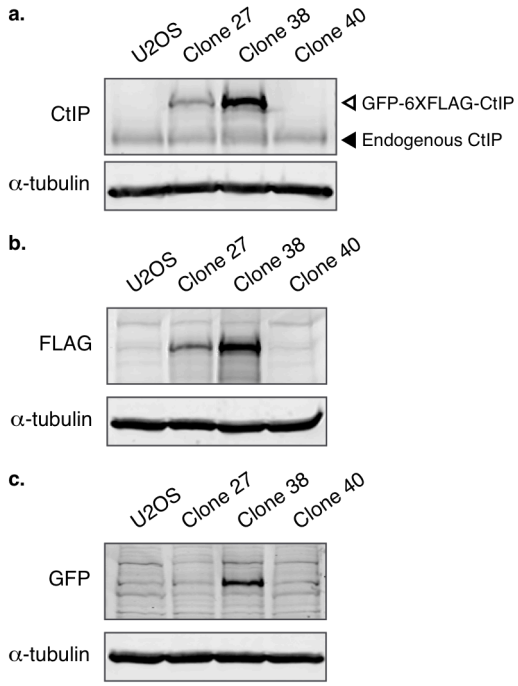

Figure R1. GFP-6XFLAG-CtIP stable cell line generation and clone selection. a, Western blot showing CtIP expression in different clones transfected with GFP-6XFLAG-CtIP plasmid and selected with G418. Protein extract from U2OS cells were used as control. Antibodies against CtIP and α-tubulin, as loading control, were used. Solid triangle indicates the position of endogenous CtIP and white triangle marks the exogenous version of the protein. **b, c,** Same as (**a**) but blotting with antibodies against FLAG or GFP, instead of CtIP, respectively.

The Tandem Affinity Purification protocol we used is detailed in the methods section and a scheme is shown in figure R2, panel a. Briefly, we planned a first step of immunoprecipitation using monoclonal anti-FLAG antibody covalently attached to agarose beads, followed by elution with an excess of 3XFLAG peptide in mild conditions to prevent dissociation of CtIP interacting proteins. This eluate would be subjected to a second step of immunoprecipitation using a magnetic resin covalently bound to an anti-GFP antibody. Finally, CtIP and its interactors would be eluted by boiling in protein loading buffer. We reasoned that such protocol would allow purification of CtIP partners with a high grade of specificity.

To set up the conditions for the TAP protocol, we had to test the buffer used for cells extracts at the different steps of immunoprecipitation and the efficiency of the elution with 3XFLAG peptide. In addition to GFP-6XFLAG-CtIP stable cell line, we used U2OS cells as control of immunoprecipitation specificity. Thus, after selecting the GFP-6XFLAG-CtIP clone, we first tested immunoprecipitation using FLAG beads with two different buffers for cell extracts and IP, followed by elution by boiling in protein loading buffer. As shown in figure R2 (panel b), the IP worked equally with both buffers, RIPA and Lysis Buffer. Then, we repeated this experiment using three times more sample than in the previous one and now eluting with 3XFLAG peptide. Again, the IP worked with both buffers and the

elution was efficient in both cases (figure R2, panel c). However, we decided from that point onwards to use Lysis Buffer as the elution and the IP process in general seemed more effective than with RIPA, with less protein loss during washes (figure R2, panel c; compare left and right panels).

Once we had set up FLAG IP and elution from FLAG beads, we performed a pilot complete experiment including U2OS cell extract as control sample and with both steps of immunoprecipitation, using Lysis Buffer during the entire process. In this occasion, part of the samples from each step of the experiment were resolved by SDS-PAGE and silver stained to test the purity of the eluate. Figure R2 (panel d, left) shows the first immunoprecipitation with anti-FLAG resin. Most of the proteins, those that do not interact with CtIP and did not bound unspecifically to the matrix, remained in the flowthrough (FT) or were washed away. After elution with 3XFLAG peptide, we could observe several bands. Albeit some of them were still unspecific, as they also appeared in the control sample, we found others that interacted specifically with CtIP (figure R2, panel d, left, see triangles). Using the second IP with anti-GFP beads we were able to purify further the eluted sample. While there were almost no bands in the control, we could still precipitate several proteins in the GFP-6XFLAG-CtIP expressing sample (figure R2, panel d, right, marked with triangles).

In parallel, we followed CtIP purification using the same immunoprecipitation approach by immunoblotting using an anti-CtIP antibody. Besides efficient GFP-6XFLAG-CtIP purification (figure R2, panel e, white triangle), we also co-immunoprecipitated endogenous CtIP (figure R2, panel e, solid triangle). As CtIP forms a stable homotetramer (Davies *et al*., 2015), this confirmed both, that the ectopic version of the protein was incorporated into natural occurring CtIP complexes and our ability to co-purify CtIP interacting proteins. However, we realized we were not able to elute all tagged protein from anti-FLAG beads with the 3XFLAG peptide, because we could still see the band for GFP-6XFLAG-CtIP when boiling the resin after elution (figure R2, panel e, FLAG Beads). To optimize the process, we added a second round of elution with the same amount of 3XFLAG peptide. Figure R2 (panel f, left) shows a western blot with samples obtained after both elutions and what was left at the anti-FLAG resin. We confirmed that we could elute some more tagged CtIP with the second elution step,

but still some protein remained bound to the resin. So, we then added a third elution step (figure R2, panel f, right). Samples collected after all three rounds of elution were combined and incubated with the anti-GFP resin to complete the experiment. Now, we ensured that almost no protein remained bound to the anti-FLAG beads, although we could not see the band for GFP-6XFLAG-CtIP in the third elution sample probably due to the dilution (figure R2, panel f, right).

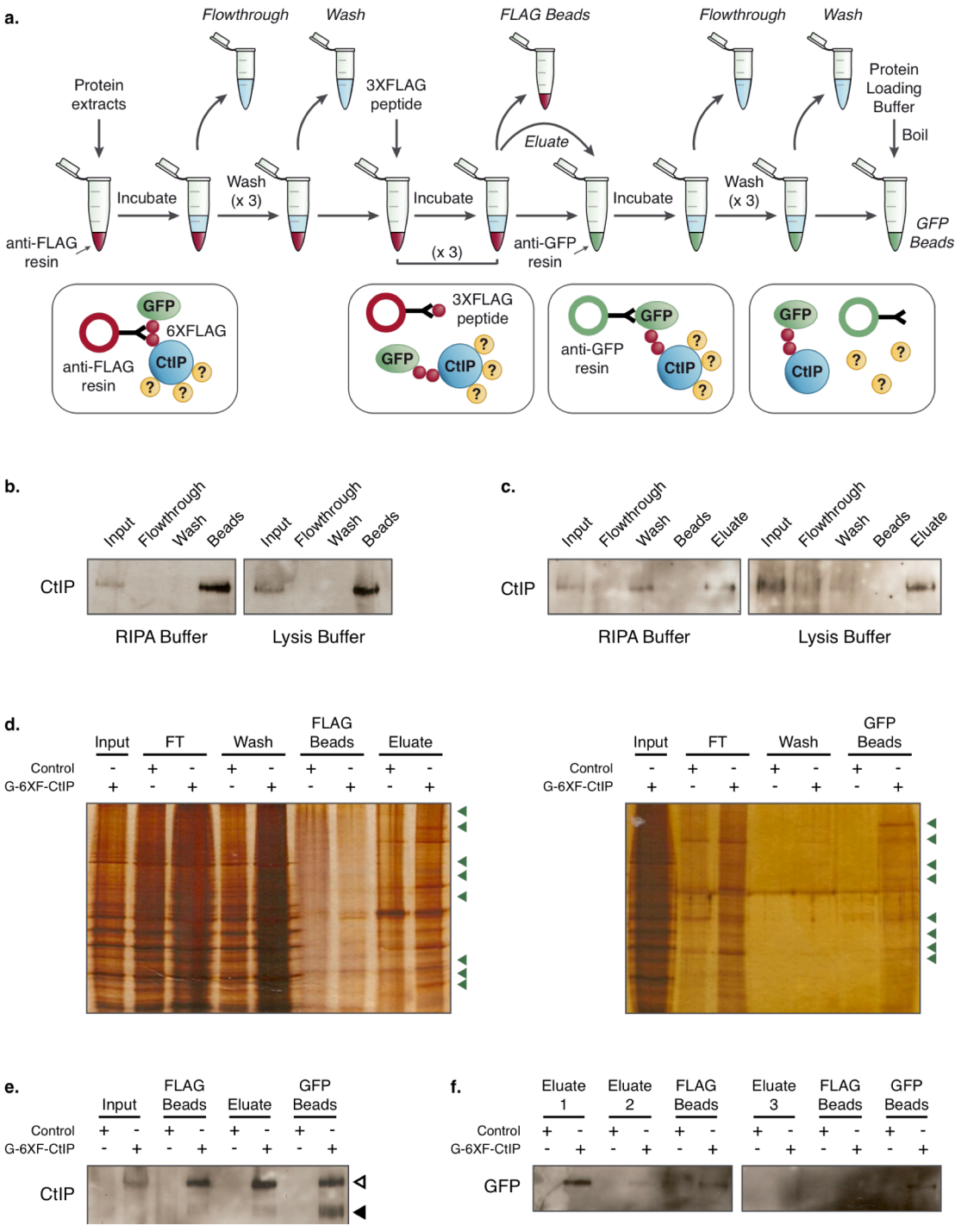

Figure R2. Setting up the conditions of the Tandem Affinity Purification protocol. a, Scheme representing TAP protocol used to identify proteins that interact with CtIP. Cartoons (bottom) show the interactions that occur in the different steps of the process. Question marks symbolize unknown CtIP partners. Other samples that were taken during the optimization process, such as flowthrough and wash of each column or the beads samples, are indicated in italics. **b,** Protein samples collected from cells harbouring GFP-6XFLAG-CtIP construct in two different buffers (RIPA and Lysis Buffers) were subjected to immunoprecipitation using anti-FLAG beads. Samples from different purification steps (input, flowthrough, wash and beads) were boiled with protein loading buffer, resolved by SDS-PAGE and immunoblotted with anti-CtIP antibody. **c,** Same as (**b**) but with an additional elution step using 3XFLAG peptide instead (eluate). Beads were boiled after elution in order to assess the elution efficiency by checking the leftover protein bound to the matrix. **d,** Protein extracts from GFP-6XFLAG-CtIP cells (G-6XF-CtIP) or control cells were used for two-step affinity purification. First, complexes were isolated using anti-FLAG beads and eluted using 3XFLAG peptide (left). Then, a second purification was carried out using anti-GFP resin. Finally, beads were boiled with protein loading buffer to elute purified proteins (right). Part of the samples collected from each step of the process were resolved by SDS-PAGE and silver stained. FT means Flowthrough. Bands that appeared specifically in the sample from GFP-6XFLAG-CtIP cells but not in the control are marked with a triangle. **e,** Same experiment as in (**d**) but the samples were immunoblotted with anti-CtIP antibody. White triangle marks the exogenous CtIP version and solid triangle the endogenous protein. **f,** Protein samples obtained as described in (**d**) and (**e**) were subjected to one (left) or two (right) additional elution steps. Purified exogenous CtIP was identified using anti-GFP antibody.

Thus, we concluded that this protocol was suitable for immunoprecipitation using both resins sequentially and that this procedure allowed purification of CtIP and other proteins that interact with it.

Once the conditions for the Tandem Affinity Purification were set up, we scaled up the protocol and proceeded with the TAP. At the end of the process, we eluted CtIP complexes bound to the anti-GFP resin by boiling with protein loading buffer. They were resolved by SDS-PAGE using a gradient gel for better resolution, followed by silver staining of the proteins. Bands that appeared specifically in the GFP-6XFLAG-CtIP but not in the U2OS control are marked in figure R3 (panel a). As CtIP functions are heavily controlled by the cell cycle machinery (Makharashvili *et al*., 2014), we wondered if it might be any difference among the bands precipitated

according to the cell cycle phase. For this purpose, we included in the experiment protein samples from GFP-6XFLAG-CtIP cells in different phases of the cell cycle after double-thymidine synchronization (figure R3, panel b; see R3 panel c for the result of the synchronization process). Strikingly, we found little or no differences in all cell cycle phases (figure R3, panel b) and in the asynchronous sample, so we could conclude that with our approach we were mainly isolating CtIP constitutive interactors.

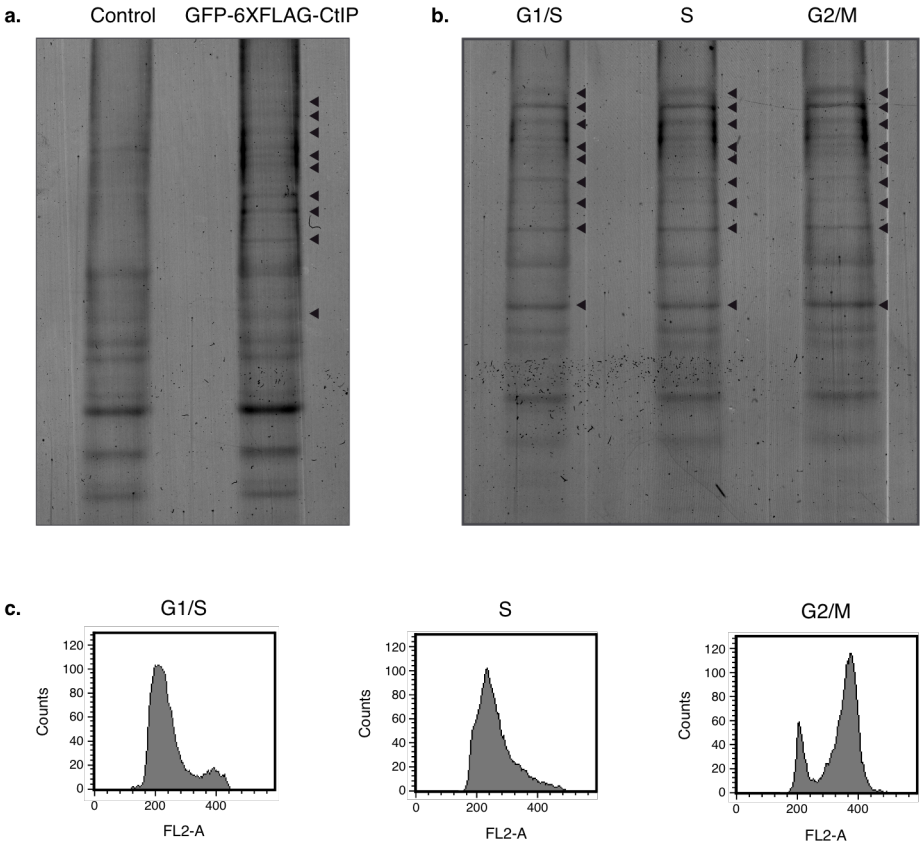

Figure R3. Isolation of new CtIP partners. a, After purification of CtIP complexes (see main text), eluates were resolved by SDS-PAGE and silver stained. Different bands corresponding to the proteins immunoprecipitated are shown. Those bands that appeared specifically in the sample from GFP-6XFLAG-CtIP cell line but not in the U2OS control, marked with a triangle, were sequenced by mass-spectrometry. **b,** Same as (**a**) but displaying the bands purified from samples of GFP-6XFLAG-CtIP cells in different phases of the cell cycle. Those bands marked with a triangle differ from the control and are the same in the three samples. **c,** Representative graphs showing the cell cycle results by flow cytometry after double-tymidine synchronization of the G1/S, S and G2/M samples used in panel (**b**).

Finally, we excised marked bands from the silver-stained gel from GFP-6XFLAG-CtIP sample (figure R3, panel a) and sent them for peptide identification by mass spectrometry. Proteins detected with a high score after purification are shown in table R1. Members of the HNRNPU family were already described as CtIP binding partners (Polo *et al*., 2012) and so validated the ability of the procedure to isolate proteins that interact with CtIP. All the other proteins detected represent new CtIP interactors.

Table R1. Proteins identified by mass spectrometry of the bands purified.

Protein	Aliases	Gene	Unique peptides
CtIP	RBBP8, RIM, COM1, SAE2, SCKL2, JWDS	RBBP8	37
SF3B1	SAP155, MDS, Hsh155, PRPF10, PRP10, SF3b155	SF3B1	34
RBM10	DXS8237E, KIAA0122, GPATCH9, GPATC9, TARPS, ZRANB5, S1-1	RBM10	31
SF3B3	SF3b130, SAP130, STAF130, KIAA0017, RSE1	SF3B3	27
SF3B2	SF3B145, SAP145, SF3b1, SF3b150, Cus1	SF3B2	26
PRMT5	HRMT1L5, SKB1Hs, JBP1, SKB1, IBP72	PRMT5	25
DHX15	DDX15, DBP1, HRH2, PRPF43, PRP43, PrPp43p	DHX15	24
SFPQ	PSF, PPP1R140, POMP100	SFPQ	23
DHX9	DDX9, RHA, NDHII, NDH2, LKP	DHX9	22
CCAR2	KIAA1967, DBC1, DBC-1, P30DBC, NET35	CCAR2	18
KIF11	EG5, KNSL1, TRIP5, MCLMR, HKSP	KIF11	15
HNRNPU	SAF-A, SAFA, P120, HNRPU, U21.1, HNRNPU-AS1	HNRNPU	14

1.2. Characterization and relevance of those new CtIP interactors in DNA end resection

The main interest of our laboratory is to understand CtIP DNA resection role. Thereby, as first characterization of the isolated proteins, we studied if they were involved in DSB processing. As mentioned in the introduction (section 4), resection of DSBs gives rise to long ssDNA tails that are immediately coated by the RPA protein complex for protection. Thus, the accumulation of RPA at the sites of the break observed by immunofluorescence using RPA antibody can be used as readout of DNA end resection (see figure R4, panel a, for examples of cells positive or negative for RPA foci). The damage-induced phosphorylation of H2AX (γH2AX) was used to visualize broken chromatin. Hence, we analysed cells depleted of the new CtIP interactors (figure R4, panel b) for RPA foci formation upon exposure of the cells to 10 Gy of ionizing radiation. SF3B3 was selected as a representative of the SF3B complex, as three different subunits were isolated interacting with CtIP. We used shRNAs against a non-target sequence and CtIP as negative and positive controls, respectively.

Figure R4. Characterization of novel CtIP interactors. a, Representative immunofluorescence micrographs of irradiated samples using anti-RPA and anti-γH2AX antibodies. Cells expressed the indicated shRNAs. White arrows mark cells considered positive for RPA foci. The rest of them are representative of cells negative for RPA foci. **b,** Representative western blots showing depletion of the different factors upon downregulation with shRNAs. In each case, a sample from a depleted culture and a control transfected with a non-target shRNA is shown upon blotting with the indicated antibodies. α-tubulin was used as loading control. **c,** Cells transduced with lentiviral particles bearing shRNAs against the indicated genes were irradiated (10 Gy). shCtIP and a non-target shRNA (shNT) were used as positive and negative controls, respectively. One hour after irradiation, cells were fixed and immunostained with anti-RPA and anti-γH2AX antibodies to observe foci formation of these proteins after damage. The number of cells that show RPA foci was scored and represented as a percentage of the total. See panel (**a**) for a representation of RPA positive cells. The graph represents the average and standard deviations of at least three independent experiments. For each replica, at least 200 cells were measured. A Student t-test was performed and one, two or three asterisk(s) denotes statistical significance at $p<0.05$, $p<0.01$ and $p<0.001$, respectively.

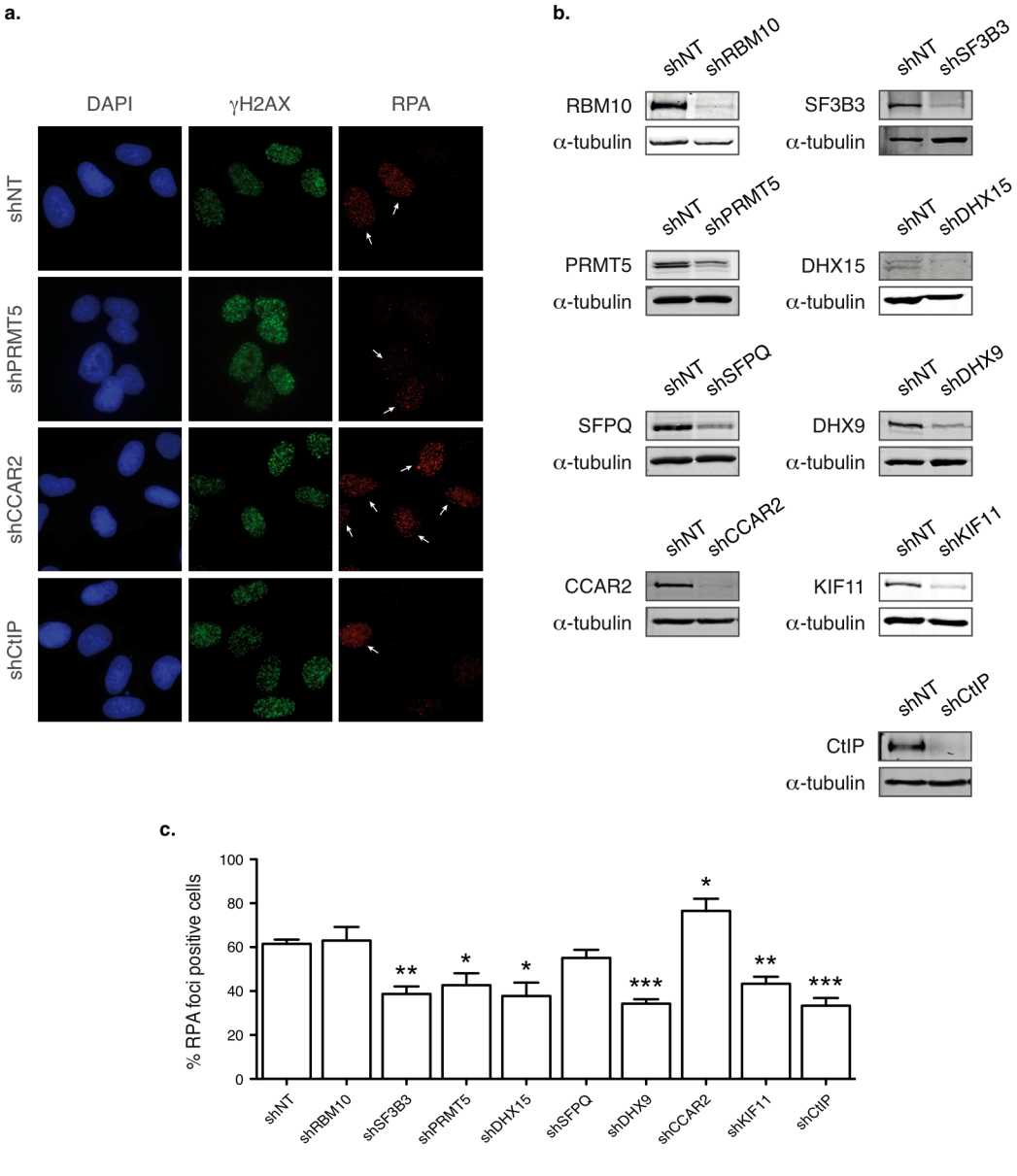

Then, we observed that depletion of any of those factors, but RBM10 and SFPQ, affect DNA end resection either by stimulating it (CCAR2) or hampering it (SF3B3, PRMT5, DHX15, DHX9 and KIF11) (figure R4, panel c). No changes were observed in γH2AX foci formation. After this initial characterization, we decided to continue exploring the role on DNA end resection of PRMT5 and CCAR2, each with opposite effects on this process (figure R4, panel c). The in-detail characterization of some other isolated new CtIP interactors has been carried out by other members of the laboratory (Prados-Carvajal, López-Saavedra *et al.*, second round of revision).

2. Symetric methylase PRMT5 interacts with CtIP and promotes DNA end resection

2.1. CtIP-PRMT5 interaction is damage-independent and it is influenced by CtIP Serine 327 phosphorylation

We first validated PRMT5 interaction with CtIP. To do so, we used anti-GFP beads and protein extracts from U2OS stably transfected with either GFP-CtIP or GFP, as negative control. We resolved the eluates by SDS-PAGE and blotted with anti-CtIP and anti-PRMT5 antibodies. As expected, we co-purified endogenous CtIP using overexpressed GFP-CtIP as a bait (figure R5, panel a, solid and white triangles). Moreover, we could co-immunoprecipitate PRMT5 specifically in the samples expressing GFP-CtIP (figure R5, panel a, marked with an arrow), confirming the interaction between both proteins. We assessed whether CtIP-PRMT5 interaction is regulated by the presence of DNA damage by performing the IP with protein cell extracts collected 1 hour after exposure to 10 Gy of ionizing radiation. As seen in figure R5 (panel a), similar levels of PRMT5 were co-immunoprecipitated in both conditions. So, we conclude that this protein interacts with CtIP in a damage independent manner.

The tumour suppressor gene *BRCA1* plays several roles in homologous recombination, including some that requires its interaction with CtIP in a CDK phosphorylation-mediated manner at serine 327 (Yu & Chen, 2004; Cruz-García *et al*., 2014). Thus, we wondered if CtIP-BRCA1 interaction might influence the binding of PRMT5 to CtIP. We repeated the immunoprecipitation using anti-GFP resin with samples collected in undamaged conditions from U2OS cells stably expressing GFP, GFP-CtIP or GFP-CtIP mutants that change the interaction with BRCA1 by either mimicking constitutive phosphorylation and hence interaction (GFP-CtIP-S327D) or abolishing said phosphorylation and the interaction (GFP-CtIP-S327A) (Cruz-García *et al*., 2014). To avoid any influence of endogenous CtIP in the interaction, we depleted it by infection with lentiviral particles harbouring shCtIP. The GFP-CtIP constructs are all shRNA resistant. Depletion efficiency of the endogenous protein could be observed when compared with U2OS extract (figure

R5, panel b, left, marked with solid triangles). Strikingly, the result of the IP showed that CtIP-PRMT5 interaction is impaired when CtIP does not interact with BRCA1 (figure R5, panel b, right, compare S327A mutant with wild-type or S327D variant). This finding suggests that: i) BRCA1 bridges the interaction between CtIP and PRMT5; ii) all three are in the same complex that is somehow destabilized by BRCA1 absence; or iii) independently of BRCA1, phosphorylation of serine 327 in CtIP is essential for PRMT5 binding.

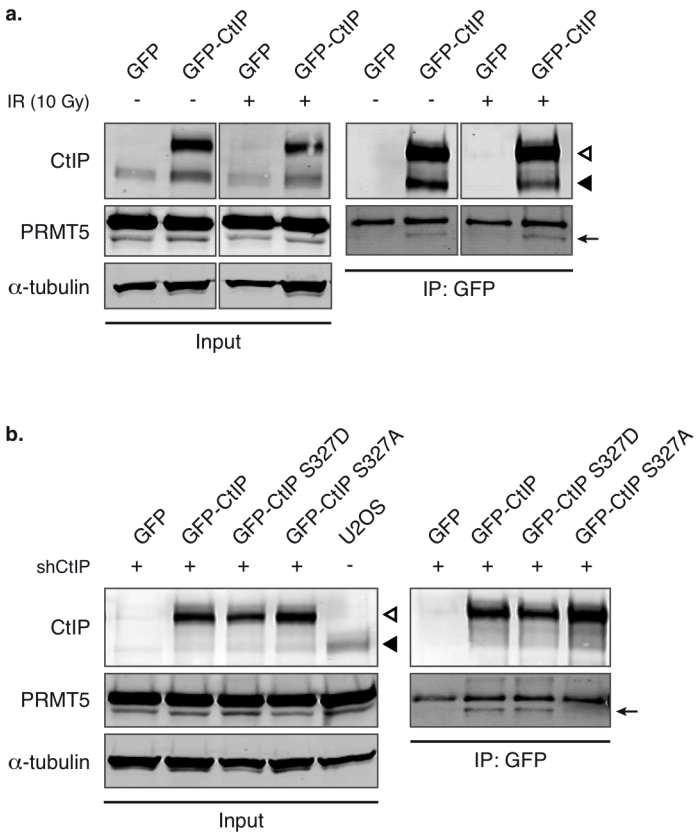

Figure R5. Validation of CtIP-PRMT5 interaction by immunoprecipitation. a, Protein extracts from U2OS stably transfected with either GFP or GFP-CtIP construct in undamaged conditions or 1 hour after 10 Gy of IR were used for immunoprecipitation using anti-GFP resin. Eluates were resolved by SDS-PAGE and blotted with antibodies that recognize the indicated proteins. White triangle marks the exogenous CtIP versions, solid triangle the endogenous CtIP and the arrow shows the band corresponding to PRMT5. **b,** Same as (**a**) but only in undamaged conditions and using protein samples from cells stably expressing GFP, GFP-CtIP or the CtIP mutant versions S327D and S327A. Cells were depleted of endogenous CtIP by transduction with lentiviral particles harbouring an shRNA against this protein. Protein extract from U2OS cells is shown in the western blot to assess depletion efficiency. Other details as in (**a**).

2.2. PRMT5 promotes DNA end resection

In agreement with the initial characterization (figure R4), we confirmed that downregulation of PRMT5 hampers DNA end resection by decreasing the number of cells that were positive for RPA foci upon induction of DNA damage with ionizing radiation (figure R6, panel a). For an example of depletion efficiency, see figure R6, panel b.

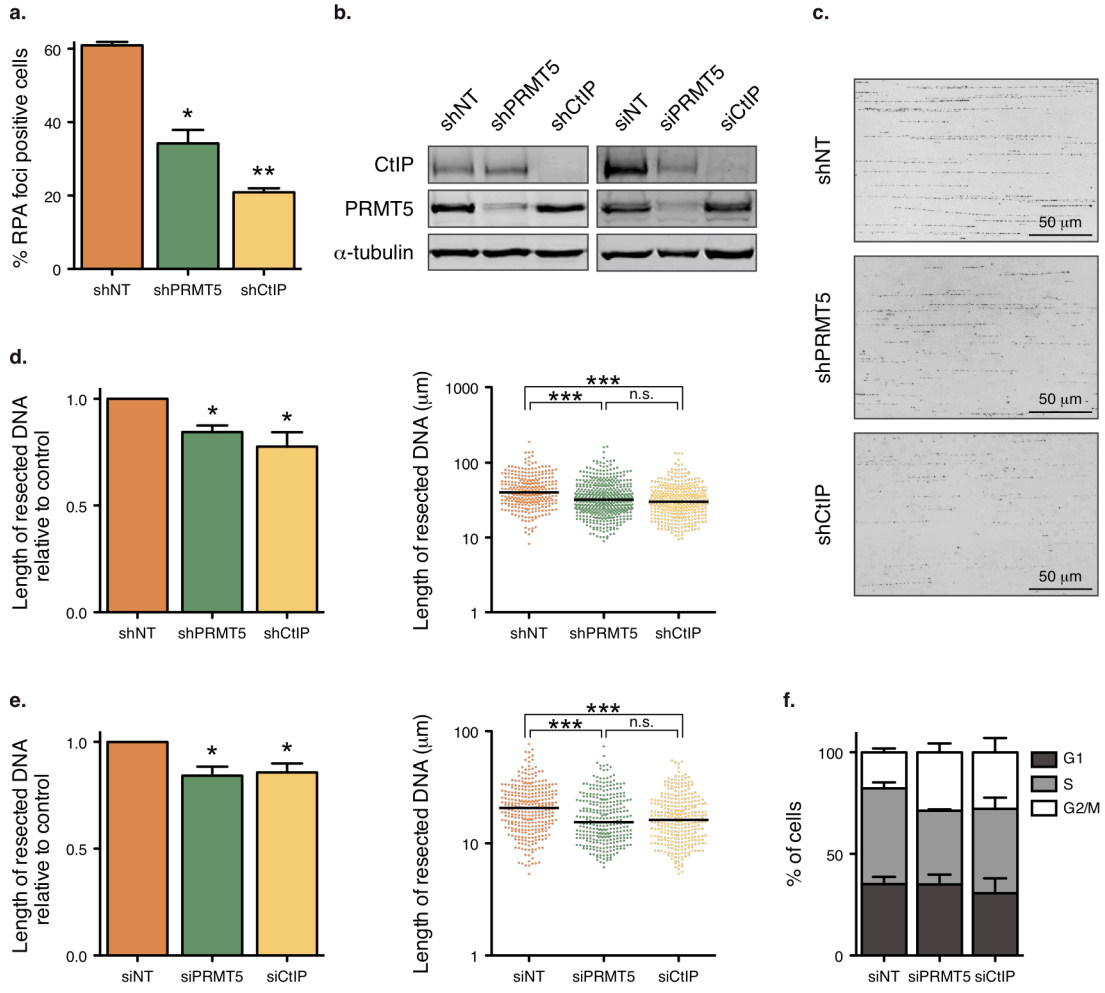

Figure R6. PRMT5 promotes initiation and extent of DNA end resection. a, Percentage of RPA foci positive cells detected by immunofluorescence in cells depleted of PRMT5 by shRNAs. A non-target shRNA (shNT) and an shRNA against CtIP were used as negative and positive controls, respectively. The graph represents the average and standard deviations of three independent experiments. For each replica, at least 200 cells were measured. A Student t-test was performed and one, two or three asterisk(s) denotes statistical significance at $p<0.05$, $p<0.01$ and $p<0.001$, respectively. **b,** Western blot displaying the expression levels of CtIP and

PRMT5 in cells transduced with lentiviruses harbouring the indicated shRNAs (left panel) or transfected with the indicated siRNAs (right panel). Antibody against α-tubulin was used as loading control. **c,** Representative images of the ssDNA fibers obtained upon SMART protocol in the different samples **d,** Length of resected DNA one hour after exposing cells infected with lentiviruses bearing the indicated shRNAs to 10 Gy of ionizing radiation, measured at individual DNA molecules using the SMART protocol. The plot on the left shows the average and standard deviation of the medians of at least three independent experiments, normalized to shNT. For each replica, at least 300 individual ssDNA fibers were measured. A Student t-test was performed to analyse statistical significance of the differences. The plot on the right displays the lengths of individual resected DNA fibers of a representative experiment, with the median indicated with a black line. A Mann-Whitney test was performed to analyse the difference in the dispersions. One, two or three asterisk(s) denotes statistical significance at $p<0.05$, $p<0.01$ and $p<0.001$, respectively. **e,** Same as (**d**), but using cells transfected with the indicated siRNAs. **f,**. Cell cycle distribution of cells upon transfection with the indicated siRNAs. The average and standard deviation of four independent experiments are plotted.

There are two non-exclusive ways to influence DNA end resection: either by affecting the number of cells that initiate resection at some breaks, or by modulating the length of DNA resected at each specific break. RPA foci formation is a good measurement of the former, but it is not sensitive enough to estimate the latter. To test whether PRMT5 also affects the length of resected DNA, we took advantage of a high-resolution technique to analyze DNA resection in single-molecules *in vivo* (Single-Molecule Analysis of Resection Tracks, SMART) (Cruz-García *et al*., 2014). See figure R6, panel c, for examples of DNA fibers obtained with this technique. Besides decreasing the number of cells that resect their DNA upon IR, depletion of PRMT5 also mildly limits the extent of DNA that is resected (figure R6, panel d). We used a non-target shRNA as negative control, and an shRNA against CtIP as positive control. In order to confirm that this effect was due to PRMT5 and was not caused by an off-target effect derived from the shRNA, we repeated the experiment but transfecting the U2OS with siRNA directed to a different part of PRMT5 transcript (figure R6, panel b, for depletion efficiency). Figure R6 (panel e) shows a decrease in the length of resected DNA similar to the previous experiment using shPRMT5. As mentioned, cell cycle is a major regulator

of DNA resection. Thus, we checked that this effect was not due to a change in the cell cycle distribution (figure R6, panel f). The results obtained lead us to assert that PRMT5, like CtIP, plays a role in DSB repair by promoting initiation and processivity of DNA end resection.

2.3. PRMT5 depletion by shRNA and siRNA affects CtIP transcription but not its stability

Careful observation of protein extracts by western blot of the different samples depleted of PRMT5 by either shRNAs or siRNAs (figure R6, panel b) lead us to a striking observation. Albeit downregulation of PRMT5 worked equally well with both approaches, CtIP expression was differently affected when PRMT5 was depleted with either shRNA or siRNA. On one hand, shRNA against PRMT5 seemed to slightly increase CtIP protein levels in the sample (figure R6, panel b, left). On the other hand, PRMT5 downregulation by siRNA consistently lead to a decrease in the amount of CtIP in the sample (figure R6, panel b, right). However, and despite the change in CtIP levels into the sample, both strategies used for PRMT5 depletion (shRNA or siRNA) promoted the same inhibitory effect in DNA end resection. Still, we wondered if PRMT5 could somehow affect CtIP stability. To do so, we treated the cells with cycloheximide (CHX), an inhibitor of protein biosynthesis that blocks translation elongation.

First, we downregulated PRMT5 by transducing cells with lentiviral particles bearing the indicated shRNA or by transfection with the indicated siRNA, using in both cases a non-target sequence (shNT and siNT) as control. Then, we added cycloheximide to the culture medium and harvested cells extracts at different times in order to assess CtIP degradation. We performed SDS-PAGE followed by western blot analysis (figure R7, panels a and b, right, for a representative western blot) and quantified the amount of CtIP in every sample, normalized with α-tubulin, used as loading control. According to the previously mentioned results, at the initial point we readily observed an increase in CtIP levels when using shPRMT5, while there was a CtIP reduction with siPRMT5 (figure R7, panels a and b, left graph). However, upon PRMT5 depletion CtIP stability was similar to the control sample in both cases. This was most obvious

when we normalized all data to the start time point to follow the degradation dynamic (figure R7, panels a and b, right graph). These outcomes lead us to suggest that PRMT5 depletion could only affect CtIP expression but not its stability. We hypothesize that this influence on CtIP expression should represent some off-target effect, as it was opposed using shRNA and siRNA as the downregulation method. However, the resection defect could be associated to an effect of PRMT5 as in both cases the results were consistent.

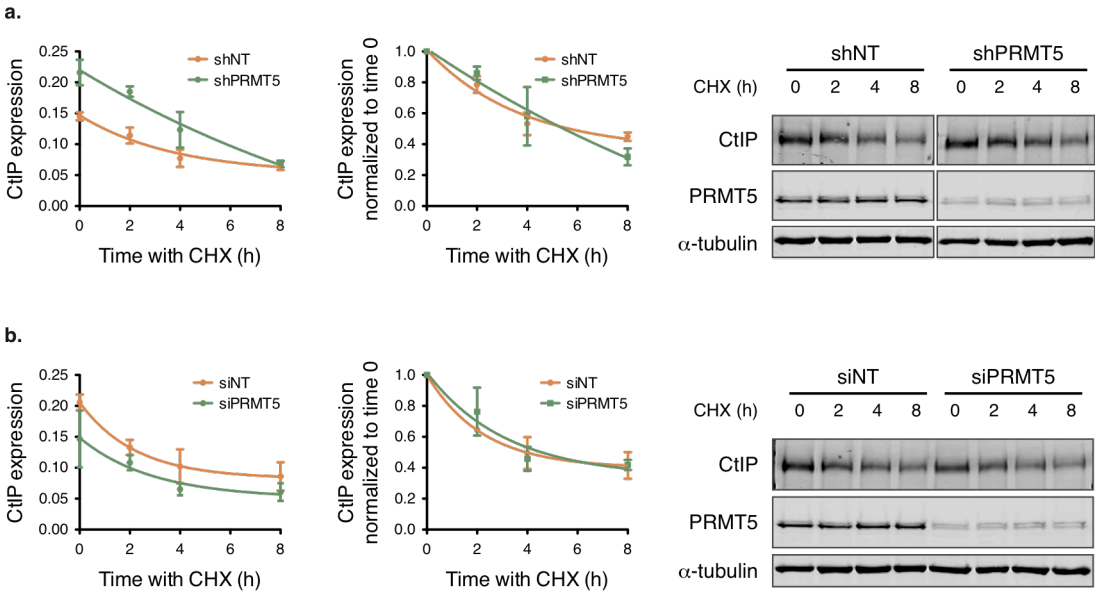

Figure R7. Downregulation of PRMT5 with shRNA and siRNA affects CtIP transcription but not its stability. a, U2OS cells depleted of PRMT5 using an shRNA and the control cells with shNT were treated with 150 μg/ml of cycloheximide (CHX) to determine CtIP stability. Protein samples were collected at the indicated time points after CHX addition. Point 0 corresponds to protein samples from cells before treatment. Protein extracts were resolved by SDS-PAGE and blotted using anti-CtIP, anti-PRMT5 and anti-α-tubulin antibodies. A representative western blot is shown on the right. The plot on the left displays CtIP expression of two independent experiments, calculated as the amount of CtIP divided by α-tubulin signal. The graph on the middle shows CtIP expression data but normalized to the start point in order to compare the degradation dynamic in both samples. Protein decay correlated from the time points using a nonlinear regression (one-phase decay equation) are plotted. **b,** Same as (**a**), but using cells transfected with the indicated siRNAs.

2.4. Downregulation of PRMT5 confers sensitivity to ionizing radiation and camptothecin, but does not influence the resistance to etoposide

It was previously described that CtIP depletion causes hypersensitivity to DNA double-strand break-inducing agents (Sartori *et al*., 2007). Thus, to test if the role of PRMT5 in DNA end resection could also have an effect in the response to DNA damage, we performed clonogenic assays and measured cell viability upon generation of DSBs by different agents. We used ionizing irradiation and etoposide, which break the DNA in all phases of the cell cycle, and camptothecin, which only causes DSBs in the S phase coupled to replication. CPT and VP16 are inhibitors of topoisomerases I and II, respectively, and stabilize the covalent binding of these enzymes to the cleaved DNA. This prevents DNA strands re-ligation and therefore promotes break formation.

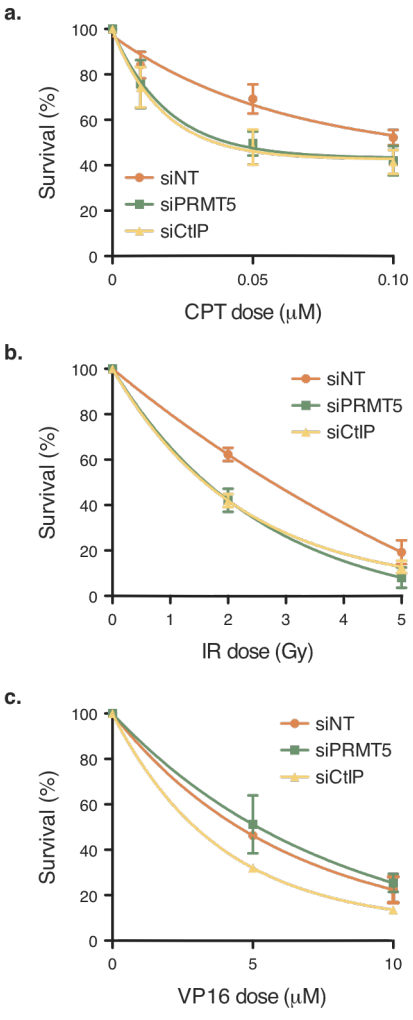

Figure R8. PRMT5 is required for survival to DSB-inducing agents. a, Cells transfected with the indicated siRNAs were exposed to different doses of campthotecin for 1 hour. Sensitivity of the cells to CPT was calculated based on surviving colonies after each treatment, normalizing to the control treated with DMSO (point 0). The mean and standard deviation of four independent experiments in triplicates are plotted. A nonlinear regression (one-phase decay equation) was used to fit the curve. **b,** Same as (**a**), but cells were subjected to different doses of ionizing radiation and undamaged cells were used as control. Other details as in (**a**). **c,** Same as (**a**), but treating the cells with different doses of etoposide, or DMSO as control. The mean and standard deviation of three independent experiments in triplicates are shown. Other details as in (**a**).

In order to study cell survival in absence of PRMT5, we transfected U2OS cells with siRNA against it, and also with siNT and siCtIP as negative and positive controls, respectively. On one hand, we treated U2OS depleted cells with different doses of IR and used non-irradiated cells as control. On the other hand, we employed acute (1 hour) treatment with different concentrations of topoisomerase inhibitors, including a control treatment with the vehicle dimethyl sulfoxide (DMSO). Cells were incubated several days until colonies acquired a suitable size to be counted upon staining with crystal violet. As seen in figure R8, PRMT5 is required, as CtIP, to promote CPT and IR resistance (panels a and b). However, in stark contrast with CtIP depletion, PRMT5 downregulation did not cause sensitivity to VP16 (panel c).

2.5. PRMT5 is implicated in the choice of DSB repair pathway

Our data implicated PRMT5 in homologous recombination by promoting initiation and extent of DNA end resection. Hence, it might regulate DSB repair pathway choice. To analyze this idea, we tested different DSB repair pathways upon PRMT5 downregulation. First, we generated U2OS cells stably expressing one single copy of the previously published SA-GFP reporter (Stark *et al*., 2004), which measures single-strand annealing by the formation of an active GFP gene upon I-SceI-induced DSB (see figure R9, panel a, left, for a schematic of the reporter). As expected, the absence of PRMT5 impaired DSB repair by this pathway (figure R9, panel a). SSA is a very specific type of HR that does not require strand invasion, but is heavily dependent on the extent of DNA end resection (Heyer *et al*., 2010). Thus, to test classical recombination, we used the DR-GFP reporter that render GFP positive cells of an I-SceI- induced DSB upon gene conversion (figure R9, panel b, left), but not if the break is repaired by SSA (Pierce *et al*., 1999). Indeed, we observed similar results with this reporter when PRMT5 was downregulated (figure R9, panel b). So, we concluded that the role of PRMT5 in homologous recombination is not specific for SSA, but is a general feature. These results were similar to those achieved by depleting CtIP.

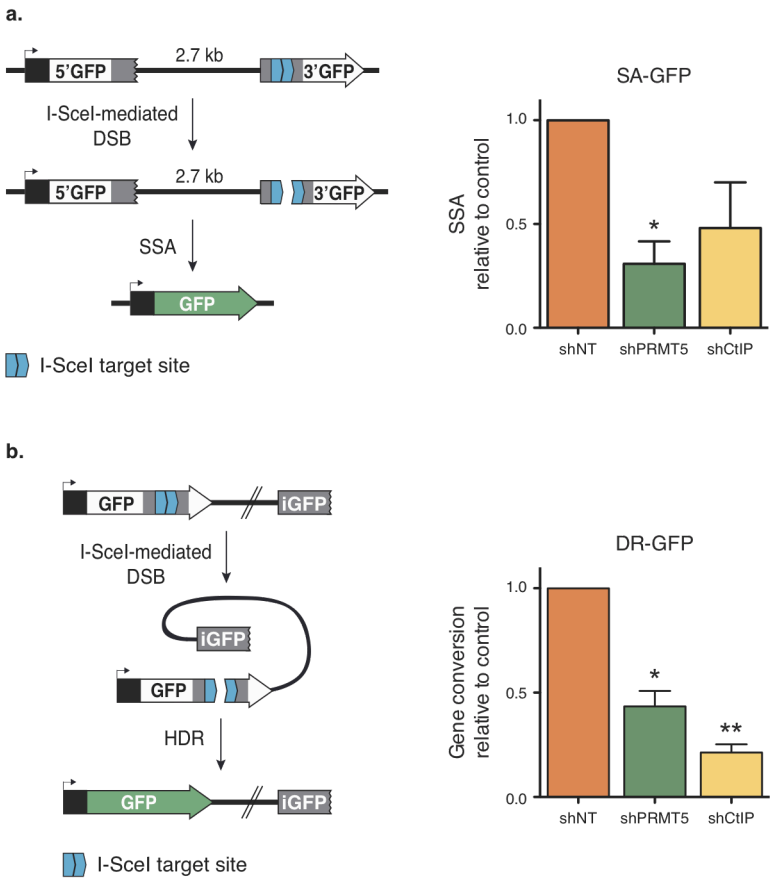

Figure R9. PRMT5 stimulates homologous recombination. a, Single Strand Annealing assay using cells bearing single-copy of the SA-GFP reporter and depleted for the indicated genes by shRNAs. A scheme of the reporter is shown on the left. The efficiency of SSA for repairing I-SceI-induced DSBs was calculated as the percentage of GFP positive cells. To facilitate the comparison between experiments, this percentage was normalized with control cells. The mean and standard deviation of three independent experiments are plotted on the right side. A Student t-test was performed and one or two asterisk(s) denotes statistical significance at $p<0.05$ and $p<0.01$, respectively. **b,** Same as (**a**) but using cells harbouring the DR-GFP reporter to measure short-tract gene conversion for repairing DSBs (scheme of the reporter shown on the left). Other details as in (**a**).

We also measured DSB repair by NHEJ using EJ5-GFP reporter (Bennardo *et al.*, 2008) that lead to GFP expression when an I-SceI-induced DSB is repair by classical NHEJ or alternative NHEJ (figure R10, left, for a schematic of the reporter). In stark contrast to CtIP downregulation, PRMT5 depletion did not promoted this repair pathway (figure R10).

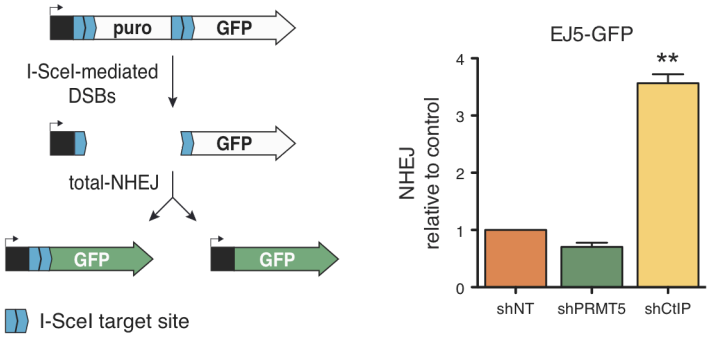

Figure R10. PRMT5 does not affect NHEJ. NHEJ assay using cells bearing single-copy of the EJ5-GFP reporter and depleted for the indicated genes by shRNAs. A scheme of the reporter is shown on the left. The efficiency of NHEJ for repairing I-SceI-induced DSBs was calculated as the percentage of GFP positive cells. To facilitate the comparison between experiments, this percentage was normalized with control cells. The mean and standard deviation of three independent experiments are plotted on the right side. Other details as figure R9, panel a.

Finally, we took advantage of the SeeSaw Reporter (SSR; Gomez-Cabello *et al.*, 2013). This system was designed in our lab with the aim to study the balance between repair pathways. When a DSB is produced by the expression of the meganuclease I-SceI, cells can repair it by NHEJ, leading to an active GFP gene, or by SSA, rendering an active RFP gene (figure R11, left, for a schematic of the reporter). Thus, the balance between NHEJ and SSA can be calculated as the ratio between green and red cells. Depletion of PRMT5 skewed the balance towards an increase in NHEJ (figure R11), which leads us to assert that the effect of PRMT5 in DNA end resection regulates DSB repair pathway choice, mainly by affecting HR.

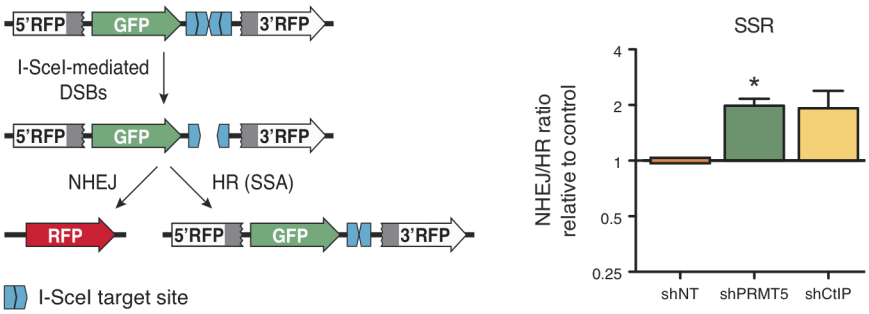

Figure R11. PRMT5 regulates DSB repair pathway choice. U2OS cells harbouring single-copy of the SeeSaw Reporter to measure the balance between NHEJ and HR were depleted of

the indicated genes. A scheme of the reporter is shown on the left side. In this case, the ratio between GFP (cells that have repaired by NHEJ) versus Red Fluorescent Protein (RFP; cells that have repaired by SSA) positive cells was calculated and normalized with the control. Those conditions that skew the balance towards an increase in NHEJ result in fold increase above 1. Otherwise, those conditions that reduced the ratio below 1 correspond to an enhancement in HR. For details, see Gómez-Cabello *et al.*, 2013. The mean and standard deviation of three independent experiments are plotted on the right side. Other details as in figure R9, panel a.

---

3. New role of CCAR2 as an antagonist of DNA end resection

3.1. CCAR2 interacts with CtIP in a damage-independent manner

As we did with PRMT5, we initially validated the physical interaction between CCAR2 and CtIP. We prepared protein extracts from U2OS stably expressing GFP-CtIP or GFP as negative control and performed immunoprecipitation using magnetic anti-GFP beads. Eluates obtained after boiling the resin with protein loading buffer were resolved by SDS-PAGE and blotted with the indicated antibodies. As shown in figure R12 (panel a), besides purifying and co-purifying the exogenous and the endogenous forms of CtIP (white and solid triangles, respectively), we were also able to co-immunoprecipitate CCAR2 in the same extracts (band marked with an arrow). Furthermore, the interaction was confirmed by the reciprocal experiment using protein extracts from U2OS overexpressing GFP-CCAR2 instead of GFP-CtIP construct (figure R12, panel b). In both assays, we used U2OS cells in undamaged conditions and 1 hour after 10 Gy of ionizing radiation. The presence of DSBs did not influence the interaction between CCAR2 and CtIP as no differences in the co-immunoprecipitate bands were observed. Moreover, only the non-phosphorilated form of CtIP (lower band), but not the damage-induced slower migrating form (top band in damaged conditions), was co-immunoprecipitated with GFP-CCAR2 after irradiation (figure R12, panel b), in agreement with a damage-independent interaction with the not activated form of the protein.

Complementary to this assay, we carried out Proximity Ligation Assays (PLA) to confirm interaction between CtIP and CCAR2 by immunofluorescence (figure R12, panel c). PLA is based on foci formation when antibodies against two proteins in close proximity are used, including those that are physically interacting (see figure R12, panel d, for an example of foci). These tests were performed in untreated cells or after exposing them to DNA damage conditions (10 Gy of IR) and proved that CtIP-CCAR2 are together and this proximity is not affected by the presence of DNA damage (figure R12, panel c). The specificity controls of the technique are shown in figure R12, panels c (CCAR2 depletion) and e (only one antibody). Both CCAR2 and CtIP have been shown to interact with BRCA1 (Hiraike *et al*., 2010; Yu & Chen, 2004). Thus, we wondered if the binding was direct or mediated by this factor. For that, U2OS cells depleted of BRCA1 were used and no significant differences were observed in the interaction between CCAR2 and CtIP (figure R12, panel c; panel f for a representative depletion).

Then, we detected *in vitro* interaction between the two proteins by using human whole cells extracts and purified, bacterial-expressed GST-CtIP as bait to pull-down GFP-CCAR2 (figure R12, panel g). We also mapped the region of CCAR2 where CtIP interacts with the pull-down assay by expressing three truncated versions of GFP-CCAR2. Carboxi-terminal part of CCAR2 was not able to interact with GST-CtIP, so we could constrain the interaction region to the first two thirds of the protein. Moreover, in a parallel approach in our laboratory, Dr. María Isabel Martínez Macías carried out an *in vitro* direct binding assay using full-length His_6-CCAR2 and a series of GST-CtIP fragments purified in all cases from bacteria and confirmed the direct interaction between both factors *in vitro* (López-Saavedra *et al*., 2016). In addition, she could map the region of CtIP where CCAR2 interacts to the carboxi-terminal region of CtIP (from amino acid 650 to the end of the protein), which covers the region that mediates the interaction between CtIP and the MRN complex (amino acids 790 to 897; Sartori *et al*., 2007).

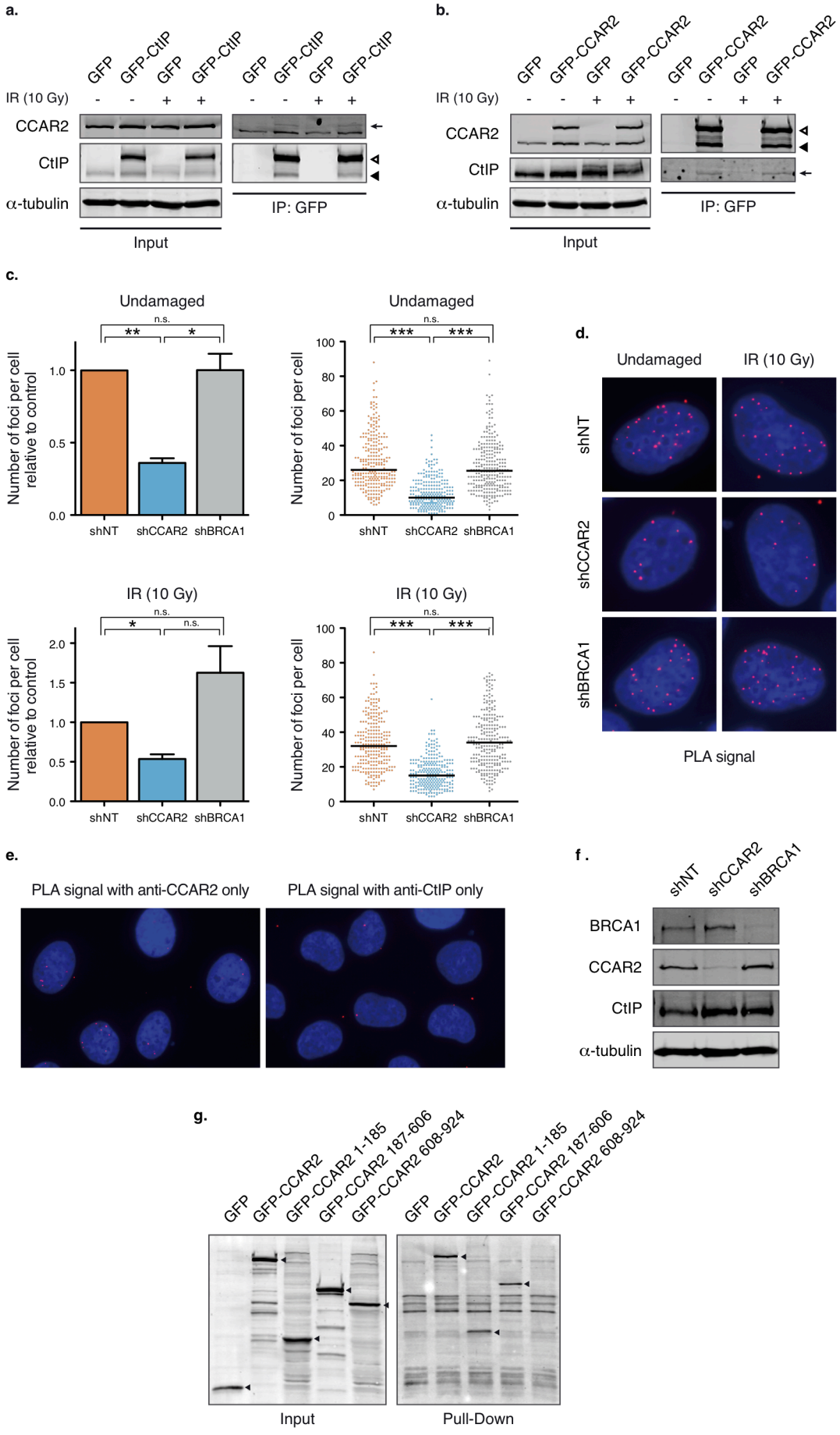
a.
GFP
GFP-CtIP
IR (10 Gy)
CCAR2
CtIP
α-tubulin
Input
IP: GFP
b.
GFP-CCAR2
c.
Undamaged
IR (10 Gy)
Number of foci per cell relative to control
Number of foci per cell
shNT
shCCAR2
shBRCA1
n.s.
d.
PLA signal
e.
PLA signal with anti-CCAR2 only
PLA signal with anti-CtIP only
f.
BRCA1
g.
GFP-CCAR2 1-185
GFP-CCAR2 187-606
GFP-CCAR2 608-924
Pull-Down

Figure R12. CCAR2 interacts with CtIP in a damage-independent manner. a, Protein samples from cells stably transfected with either GFP or GFP-CtIP in undamaged conditions or 1 hour after IR (10 Gy) were used for immunoprecipitation using anti-GFP resin. Proteins eluted were resolved by SDS-PAGE and immunoblotted for the indicated antibodies. The arrow points the band corresponding to CCAR2. White and solid triangles mark exogenous and endogenous CtIP, respectively. **b,** Same as (**a**) but with cells expressing GFP or GFP-CCAR2 constructs. In this case, the arrow marks CtIP band and the triangles endogenous and ectopic CCAR2. **c,** Cells depleted of the indicated genes by shRNAs were subjected to Proximity Ligation Assay using CtIP and CCAR2 antibodies. Top graphs were obtained with cells unchallenged with exogenous damage, while those at the bottom correspond to cells 1 hour after exposed to 10 Gy of IR. The average and standard deviations of the medians of three independent experiments are plotted on the left. For each replica, at least 200 cells were measured. A Student t-test was performed to compare the samples. Individual results of cells in a representative experiment are shown on the right. The median number of foci is marked with a dark line. A Mann-Whitney test was performed to analyse the difference in the dispersions. One, two or three asterisk(s) denotes statistical significance at $p<0.05$, $p<0.01$ and $p<0.001$, respectively. **d,** Representative images of each condition from PLA. Cell nuclei are shown in blue and red foci correspond to CtIP-CCAR2 interaction. **e,** PLA signal obtained when only one antibody is used. The foci observed represent background levels of the experiment. **f,** Representative western blot showing the expression levels of BRCA1, CtIP, CCAR2 and α-tubulin in cells transduced with lentiviruses harbouring the indicated shRNAs. **g,** GST-CtIP construct was used as bait for pull-down experiments from whole cells extracts of cells expressing GFP, GFP-CCAR2 full length or three deletion mutants of CCAR2, as indicated. Western blots with an anti-GFP antibody using inputs (left) and pull-downs (right) are shown. Black triangles label the position of GFP fusions.

3.2. CCAR2 inhibits DNA end resection through CtIP

Using the formation of RPA-coated ssDNA as readout, we confirmed that CCAR2 downregulation leaded to an enhancement of DNA end resection (figure R13, panel a) after challenging the cells with ionizing radiation. See figure R13 (panel b) for a representative example of CCAR2 and CtIP depletions. This result suggested CCAR2 might act as an inhibitor of DNA end resection. Considering that cell cycle is a major control point for DSB repair, we first discarded that the effect observed upon CCAR2 depletion was due to a change in the cell cycle profile (figure R13, panel c). As most S/G2 cells initiate resection, hence show RPA foci, it is hard to

observe an increase in the number of cells positive for RPA, limiting the sensitivity to detect increases in DNA end resection. Thus, it was already surprising that we could observe some increase in RPA foci positive cells upon CCAR2 downregulation. To have a better resolution in the increased resection resultant of CCAR2 depletion, we performed again SMART assays to check if CCAR2 also influence the length of resected DNA. Strikingly, not only the number of cells that resect their DNA was affected, but the reduction of CCAR2 levels also facilitates resection to continue deeper into the chromosomes (figure R13, panel d; panel e for an example of DNA fibers). Moreover, depletion of both CCAR2 and CtIP proteins (figure R13, panel b) lead to a decrease in the length of the DNA that is resected similar to the one observed upon CtIP downregulation (figure R13, panel d). This pointed out that the hyper-resection produced in the absence of CCAR2 is completely dependent on CtIP activity, genetically placing them in the same pathway.

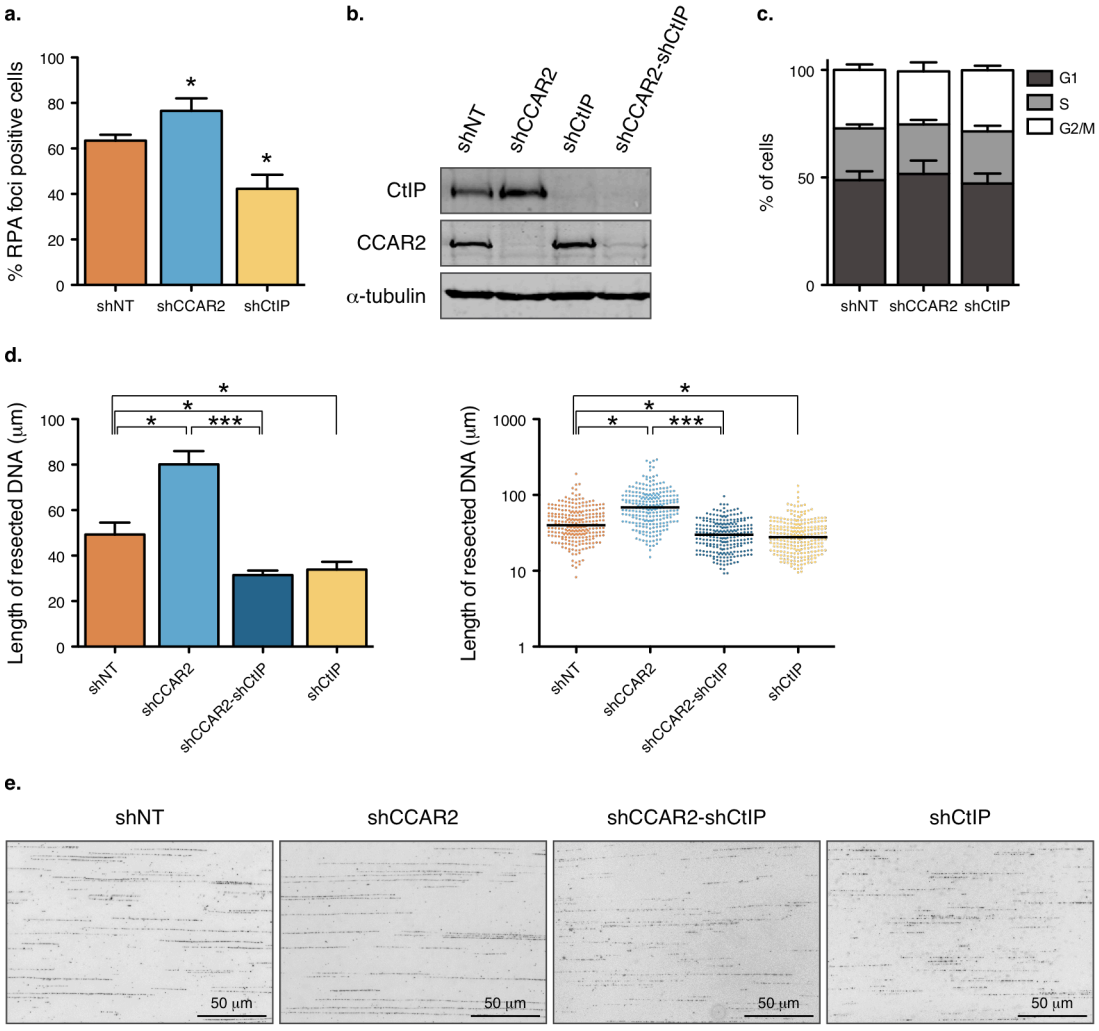

Figure R13. CCAR2 depletion increases CtIP-mediated DNA end resection. a, Percentage of RPA foci positive cells detected by immunofluorescence in cells depleted of CCAR2 by shRNAs. A non-target shRNA (shNT) and an shRNA against CtIP were used as negative and positive controls, respectively. The graph represents the average and standard deviations of three independent experiments. For each replica, at least 200 cells were measured. A Student t-test was performed and one, two or three asterisk(s) denotes statistical significance at $p<0.05$, $p<0.01$ and $p<0.001$, respectively. **b,** Representative depletion of CCAR2 and CtIP. Protein samples from cells depleted of the indicated proteins were resolved in SDS-PAGE and blotted with antibodies against CtIP, CCAR2 and α-tubulin as loading control. **c,** Cell cycle distribution upon infection with lentiviral particles harbouring the indicated shRNAs. The average and standard deviation of three independent experiments are plotted. **d,** Cells infected with lentiviruses bearing the indicated shRNAs were exposed to 10 Gy of ionizing radiation and collected 1 hour after damage. The length of resected DNA was measured using the SMART protocol at individual DNA molecules. The average and standard deviation of the medians of at least three independent experiments are shown in the plot on the left. For each replica, at least 300 individual ssDNA fibers were measured. A Student t-test was performed to analyse statistical significance of the differences. The plot on the right displays a representative experiment, with the median labelled with a black line. A Mann-Whitney test was performed to analyse the difference in the dispersions. One, two or three asterisk(s) denotes statistical significance at $p<0.05$, $p<0.01$ and $p<0.001$, respectively. **e**, Representative images of ssDNA fibers obtained upon SMART protocol in each condition.

3.3. CCAR2 does not affect CtIP interaction with MRE11A or BRCA1

It is established that CtIP physically and functionally interacts with the MRN complex, and both are required for efficient homologous recombination, in particular for the start of DNA processing during resection (Sartori *et al*., 2007). As mentioned before (see section 3.1.), Dr. María Isabel Martínez Macías mapped the interaction region where CCAR2 binds to CtIP to the carboxi-terminal domain of the protein, spreading over the region that mediates the interaction between CtIP and the MRN complex. Hence, we wondered if the inhibitory effect of CCAR2 in DNA end resection could be due to a competition for the binding site with this complex. For that, we performed immunoprecipitation using anti-MRE11A antibody and Dynabeads Protein A in U2OS cells transfected with siRNA against

CCAR2 or a control sequence. Our data suggested that there is no competition between CCAR2 and MRE11A in presence or absence of DNA damage (figure R14, panel a), despite the overlap of their interaction sites in CtIP structure.

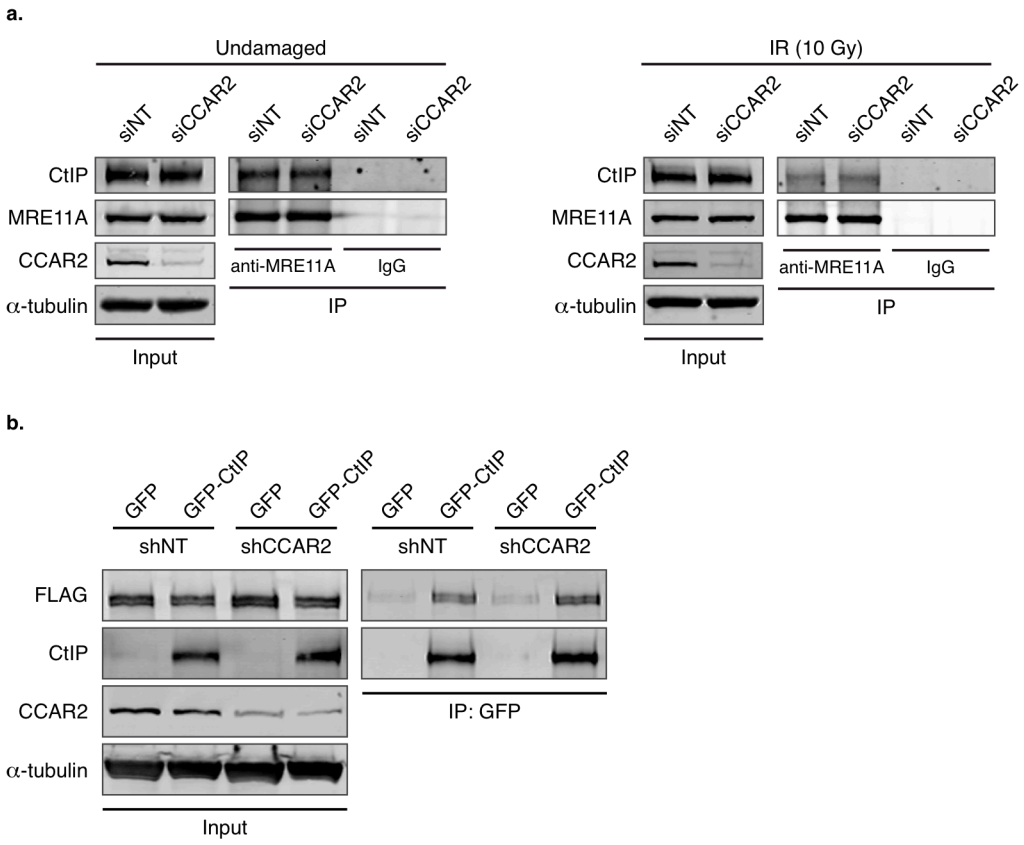

Figure R14. CCAR2 does not alter the interaction between CtIP and MRE11A or BRCA1. a, Protein samples from U2OS cells transfected with the indicated siRNAs and undamaged (left) or challenged with 10 Gy of IR (right) were subjected to immunoprecipitation using Dynabeads Protein A and anti-MRE11A antibody. IgG from rabbit serum was used as control of immunoprecipitation. Inputs and eluates samples were resolved by SDS-PAGE and blotted with antibodies that recognize the indicated proteins. **b,** HEK293 cells stably expressing GFP or GFP-CtIP were transduced with lentiviral particles harbouring shRNAs against CCAR2 or a non-target sequence. Then, cells were transfected with SFB-BRCA1 and HALO-BARD1 plasmids to overexpress BRCA1-BRD1 complex and endogenous CtIP was depleted using shRNAs. Protein extracts from these cells were immunoprecipitated using anti-GFP resin. Inputs and eluates samples were resolved by SDS-PAGE and blotted with antibodies that recognize the indicated proteins.

We previously observed by PLA that CtIP-CCAR2 interaction did not dependent on the presence of BRCA1. However, to elucidate how CCAR2 exerts its function in homologous recombination, we assessed whether CCAR2 could

influence the interaction between CtIP and BRCA1, a known regulator of resection processivity (Cruz-García *et al*., 2014). To do so, HEK293 cells stably expressing GFP-CtIP or GFP as control were infected with lentiviral particles harbouring shRNAs against CCAR2 or a non-target sequence. Then, cells were co-transfected with SFB-BRCA1 and HALO-BARD1 vectors to overexpress BRCA1-BARD1 complex. BARD1 is the major binding partner of BRCA1 and its expression is required for BRCA1 stability (Hashizume *et al*., 2001). Later, endogenous CtIP was downregulated by shRNA. Cells were harvested and we performed immunoprecipitation using protein extracts and anti-GFP magnetics beads. The results obtained after blotting with anti-FLAG antibody to observe co-immunoprecipitation of overexpressed BRCA1 suggested that CCAR2 does not impede DNA end resection by affecting CtIP-BRCA1 interaction (figure R14, panel b).

3.4. CCAR2 is a bona fide regulator of DSB repair pathway choice

As we did previously for PRMT5, we also performed DSB repair assays with different reporter systems to elucidate the influence of CCAR2 in the regulation of these repair pathways. First, we used cells harbouring a single copy of the SA-GFP reporter, which, as mentioned, measures SSA thus it readily reacts to DNA end resection proficiency but does not require strand invasion for repairing the breaks. As expected, and in agreement with previous RPA-foci and SMART results, we observed a hyper-activation of this repair pathway upon CCAR2 depletion (figure R15, panel a). In this experiment, proteins were downregulated by transfecting cells with siRNAs instead of using shRNAs. As we obtained an increase in DNA end resection in the absence of CCAR2 using both strategies, this confirmed that this phenotype was not caused by an off-target effect. Then, we wondered if the pro-recombination effect upon CCAR2 depletion was also observed specifically when DSBs are repaired by short tract gene conversion. Using DR-GFP reporter, we found that siRNA-mediated downregulation of CCAR2 rendered a significative increase in I-SceI-induced DSBs repaired by gene conversion, while depletion of the DNA resection protein CtIP impaired this repair pathway (figure R15, panel b).

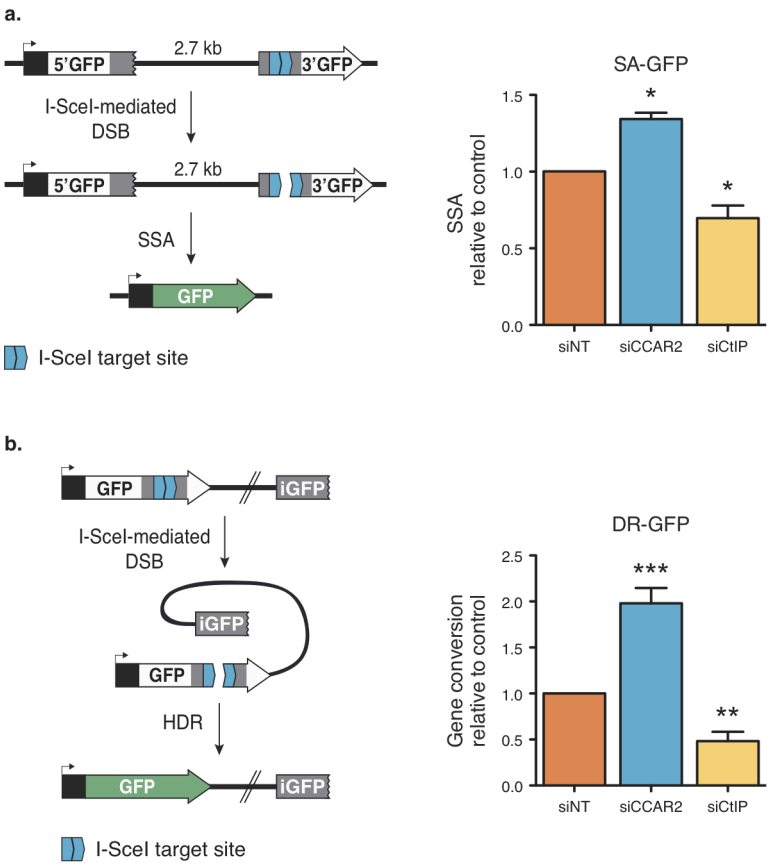

Figure R15. Downregulation of CCAR2 leads to hyper-recombination. a, U2OS cells harbouring single-copy of the SA-GFP reporter were used to measure Single Strand Annealing efficiency for repairing I-SceI-induced DSBs. Cells were depleted of CCAR2 by transfection with siRNAs. Non-target siRNA (siNT) and a siRNA against CtIP were used as negative and positive controls, respectively. The average and standard deviation of at least three independent experiments are shown. A Student t-test was performed and one, two or three asterisk(s) denotes statistical significance at $p<0.05$, $p<0.01$ and $p<0.001$, respectively. Other details as in figure R9, panel a. **b,** Same as (**a**) but with U2OS bearing the DR-GFP reporter for short-tract

Next, we took advantage of the EJ5-GFP reporter to assess the influence of CCAR2 in NHEJ. On this occasion, this repair pathway was not disturbed in cells transfected with siCCAR2 (figure R16). This mild effect in NHEJ compared with the strong phenotype observed for homologous recombination leads us to assert that the main contribution of CCAR2 in DSBs repair is to limit HR.

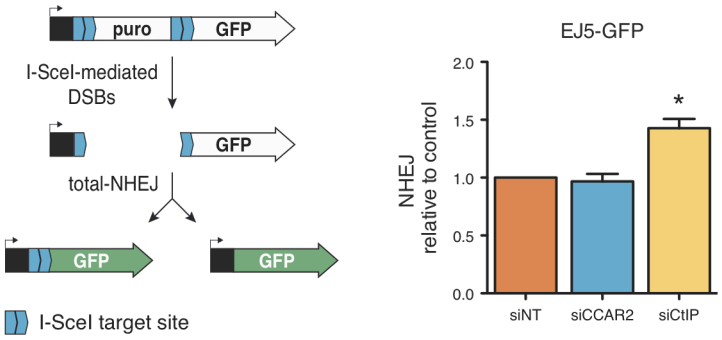

Figure R16. CCAR2 depletion does not affect NHEJ. NHEJ assay using cells bearing single-copy of the EJ5-GFP reporter to analyse NHEJ efficiency for repairing I-SceI-induced DSBs. Downregulation of the indicated genes was performed by siRNAs. The average and standard deviation of five independent experiments are shown. A Student t-test was performed and one, two or three asterisk(s) denotes statistical significance at $p<0.05$, $p<0.01$ and $p<0.001$, respectively. Other details as in figure R10.

Moreover, we wondered if this effect of CCAR2 in homologous recombination and NHEJ could be relevant in the choice between both DSBs repair pathways. Indeed, CCAR2 depletion by siRNA skewed the balance towards an increase in HR when using the SSR reporter (figure R17). With these results, we concluded that CCAR2 not only affects DNA end resection process, but as a consequence also alters the balance between DSBs repair pathways by inhibiting homologous recombination in human cells.

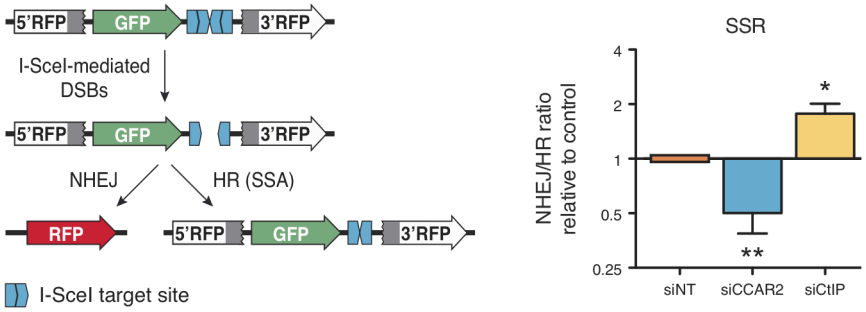

Figure R17. Downregulation of CCAR2 disturbs the balance between DSBs repair pathways. U2OS cells harbouring single-copy of the SSR reporter were used to measure the deviation from the balance between NHEJ and HR. The indicated proteins were depleted by transfection with siRNAs. The average and standard deviation of six independent experiments are shown. A Student t-test was performed and one, two or three asterisk(s) denotes statistical significance at $p<0.05$, $p<0.01$ and $p<0.001$, respectively. Other details as in figure R11.

CCAR2 has been shown to control the response to cellular stress by reducing SIRT1 activity and p53 acetylation (Kim *et al*., 2008; Zhao *et al*., 2008). Thus, one possible explanation of CCAR2 effect was that the upregulation of SIRT1 activity caused by CCAR2 depletion leaded to an increase in HR. In that scenario, decrease of SIRT1 should have the opposite effect, i.e. reduce HR. However, we were able to discard this hypothesis as SIRT1 depletion actually increased recombination when using DR-GFP reporter (figure R18, panel a). See figure R18, panel b and c, for an example of downregulation and cell cycle distribution, respectively. Hence, this result suggests that CCAR2 inhibits homologous recombination in a SIRT1-independent manner.

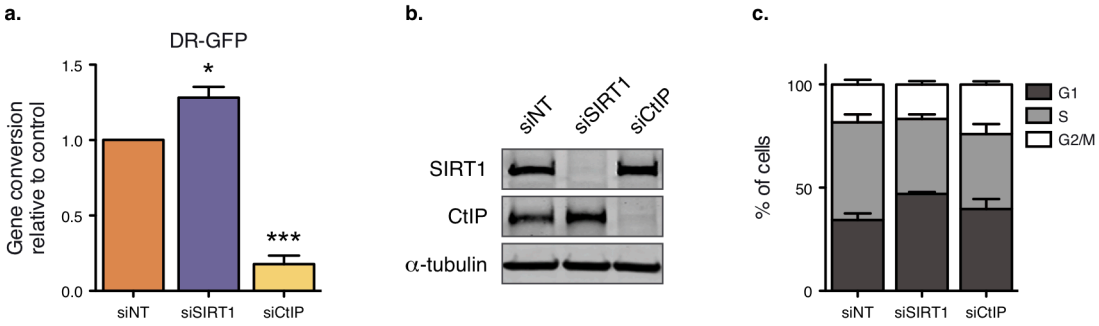

Figure R18. The recombination role of CCAR2 is SIRT1 independent. a, Effect of SIRT1 depletion in homologous recombination. U2OS cells harbouring the DR-GFP reporter were transfected with siRNA against SIRT1, and CtIP and a non-target sequence as positive and negative controls, respectively. The percentage of GFP-positive cells was normalized with control cells. The average and standard deviation of five independent repair experiments are shown. A Student t-test was performed and one, two or three asterisk(s) denotes statistical significance at $p<0.05$, $p<0.01$ and $p<0.001$, respectively. **b**, A representative western blot displaying the efficiency of SIRT1 and CtIP downregulation with siRNAs is shown. Antibody against α-tubulin was used as protein loading control. **c**, Cell cycle distribution of the cells used in the repair assay. The average and standard deviation of four independent experiments are plotted.

3.5. ATM controls CCAR2 role in DNA end resection and its recruitment to DSBs

Proteins involved in DSB repair commonly act locally at the vicinity of damaged DNA. Such local activity could be visualized through the accumulation of the protein to damaged chromatin. As we previously observed that CCAR2 regulates DSBs repair pathways (figures R15, R16 and R17), we performed immunofluorescence using CCAR2 antibody, and γH2AX antibody for labelling DSBs, to analyse its recruitment to the sites of the damage. We induced DNA damage by exposing U2OS cells at 10 Gy of ionizing radiation and then we fixed and stained them at different time points. As seen in figure R19, panel a, CCAR2 changed its localization pattern just 15 minutes after the cells were challenged with IR and accumulates at DSBs. Indeed, the presence of CCAR2 foci at the sites of damaged DNA steadily increased up to one hour after IR.

Recruitment of DNA repair proteins to the sites of DNA damage usually depends on the activation of the DNA damage response. To elucidate the factors involved in CCAR2 recruitment and retention at broken DNA, we treated the cells with inhibitors targeting the two major kinases that trigger the DDR, ATM and ATR, as well as the poly-(ADP-ribose) polymerase (PARP). ATM inhibition completely abolished CCAR2 foci formation upon exposure to ionizing radiation, whereas ATR inhibitor only partially reduced CCAR2 accumulation (figure R19, panel b). We want to point out that this effect was evident even for cells that retained some γH2AX foci despite the ATM inhibition. In contrast, cells treated with PARP inhibitor behaved as control cells treated with DMSO before damage (figure R19, panel b).

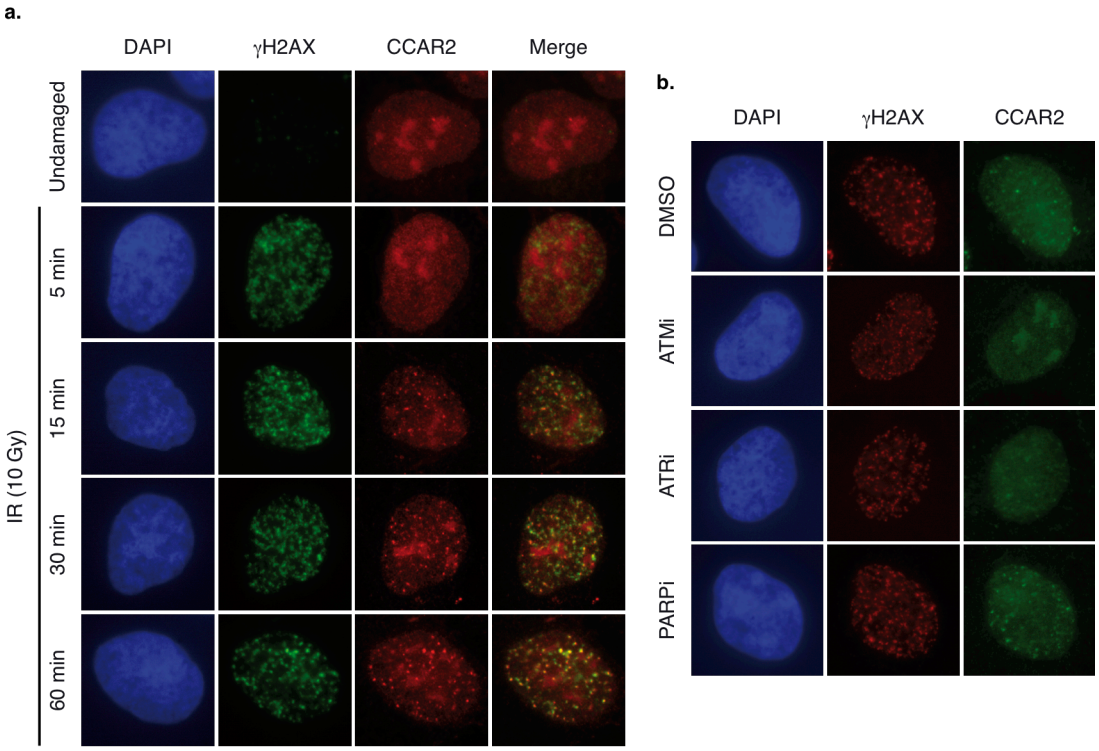

Figure R19. CCAR2 is recruited to sites of DNA damage in an ATM-dependent manner. a, CCAR2 (red) and the phosphorylated form of H2AX (γH2AX; green) were immunodetected in cells untreated or exposed to 10 Gy of IR. Immunofluorescence was performed at the indicated times after challenging the cells. Representative images are shown. **b,** Cells pretreated with inhibitors against ATM (ATMi; 10 μM), ATR (ATRi; 5 μM) or PARP (PARPi; 1 μM) and control cells pretreated with DMSO were irradiated (10 Gy). One hour after damage, these cells were subjected to immunofluorescence against CCAR2 (green) and γH2AX (red). Representative images are shown.

CCAR2 is a known ATM target (Zannini *et al*., 2012), thus it was possible that CCAR2 requires ATM activity to exert is antagonistic effect on DNA end resection and recombination. However, we could not test this idea by simply inhibiting ATM activity as this protein itself heavily affects DNA end resection by targeting other substrates, including CtIP itself. Hence, we used the mutant version of CCAR2 that could not be phosphorylated by ATM (T454A), to assess the influence of ATM in CCAR2-mediated resection inhibition. We performed SMART experiments with U2OS cells depleted of endogenous CCAR2 and complemented with either wild-type or the T454A mutant, using the non-target siRNA and cells expressing only the GFP protein as controls.

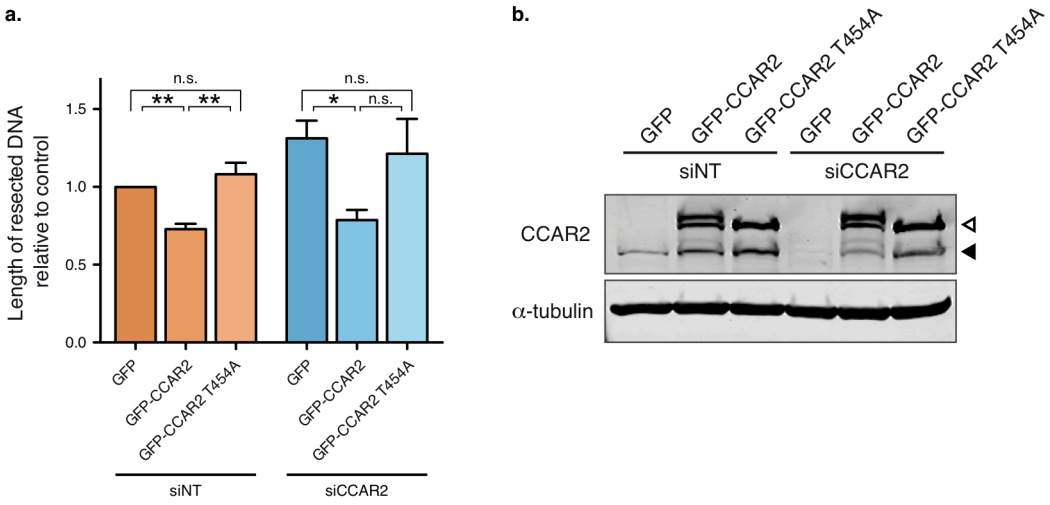

Figure R20. ATM-mediated phosphorylation of CCAR2 is essential for its role as a DNA end resection inhibitor. a, SMART assay with cells stably expressing GFP, GFP-CCAR2 or GFP-CCAR2 T454A constructs, and transfected with the indicated siRNAs. The plot represents the average and standard deviation of the normalized medians of resection length of at least three independent experiments. For each replica, at least 300 individual ssDNA fibers were measured. A Student t-test was performed and one, two or three asterisk(s) denotes statistical significance at $p<0.05$, $p<0.01$ and $p<0.001$, respectively. **b,** A representative western blot displaying CCAR2 expression in the cells used for the SMART assay. White and solid triangles indicate exogenous and endogenous CCAR2, respectively. Antibody against α-tubulin was used as protein loading control.

Unlike what happened with the depletion, overexpression of the wild-type version of CCAR2 markedly decreased the resection length of the DNA. Moreover, this construct complemented the effect of CCAR2 depletion as it completely supressed the hyper-resection phenotype observed (figure R20, panel a). Indeed, as exogenous CCAR2 expression lead to a slight overexpression of the protein (figure R20, panel b), the length of resected DNA in cells harbouring the wild-type gene was shorter than in control cells expressing GFP, reinforcing the idea that CCAR2 is antagonistic to DNA end resection (figure R20). However, this was not observed when the non-phosphorylatable version of the protein was introduced in the cells. Expression of the mutant T454A did not generate a defect in resection like the wild-type version in control cells and neither could rescue the effect of CCAR2 depletion (figure R20, panel a). Note that the lack of ATM phosphorylation

can be readily observed in the western blot by the absence of the slower migrating band (Figure R20, panel b). Thus, this result indicates that ATM-mediated phosphorylation of CCAR2 is truly required for the inhibitory role of CCAR2 on DNA end processing.

As seen for CCAR2, CtIP and the DNA end resection machinery are known to be also recruited to DSBs (Sartori *et al*., 2007). CCAR2 acts as inhibitor of CtIP and they both interact in a constitutive, damage-independent manner. Thus, we wondered if both proteins were recruited to the same set of DNA breaks or if, on the contrary, they were separated in order to be recruited to DSBs. To elucidate this point, we used PLA technique with CCAR2 and CtIP antibodies in cells expressing GFP-MDC1 construct, which is recruited and forms foci in the sites of the damage, independently if they are going to be repaired by either HR or NHEJ. As shown in figure R21, the CCAR2-CtIP PLA-signal almost never colocalized with DNA damage, suggesting that the interaction between both proteins rarely occurs on damaged chromatin, and that they are likely targeted to different subsets of DNA breaks to carry out their opposing roles in DNA repair. This was later confirmed by other members of the laboratory by using laser microirradiation (López-Saavedra *et al*., 2016; see the Discussion section for additional details).

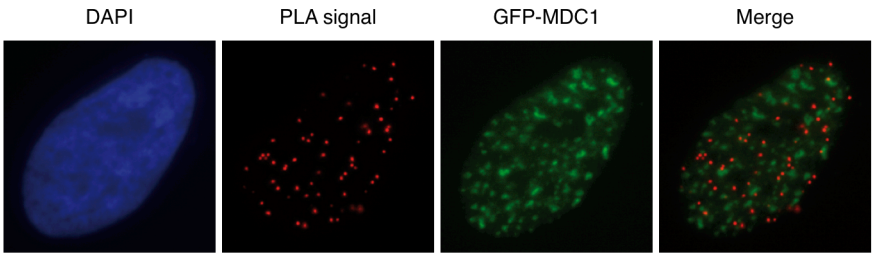

Figure R21. CtIP and CCAR2 do not interact on damaged DNA. PLA foci using anti-CtIP and anti-CCAR2 antibodies in cells expressing GFP-MDC1 that were collected 1 hour after 10 Gy of ionizing radiation.

DISCUSSION

1. Identification of new CtIP binding partners

In order to preserve genome stability, cells integrate complex and regulated processes that detect, signal and repair DNA damages (Jackson & Bartek, 2009). As mentioned, it is not only important to activate repair mechanisms, but to maintain an optimum balance between those that can act on a given DNA lesion (Huertas, 2010). DNA end resection is the major control point involved in the decision between DSBs repair pathways, as it commits cells to HR while, at the same time, impairs NHEJ (Huertas, 2010). CtIP is a key protein that acts in the initial step of this process, so its regulation is essential to ensure an accurate repair (Sartori *et al*., 2007). The role of CtIP in end resection, in addition to other aspects of the DNA metabolism, is controlled by post-translational modifications and protein-protein interactions (Makharashvili & Paull, 2015). Thus, in order to get new insights into the function of CtIP in response to DNA damage, we screened for novel CtIP interactors by a tandem affinity purification method using a GFP-6XFLAG tagged version of the protein. Besides the previously described interaction with members of the HNRNPU family (Polo *et al*., 2012), we isolated 10 new CtIP binding partners (table R1).

It is noteworthy that in the set of proteins we have found, 8 correspond to factors associated with RNA metabolism, including three subunits of the splicing-related SF3B complex. A likely explanation is that we purified CtIP-complexes more involved in CtIP function as a transcriptional regulator (Liu & Lee, 2006; Wu & Lee, 2006). However, several of these proteins have been already suggested to have a role in DNA repair and maintenance of genomic stability through their interaction with other repair factors. For instance, DHX9 associates with BRCA1, Ku80 and γH2AX (Anderson *et al*., 1998; Zhang *et al*., 2004; Mischo *et al*., 2005); SFPQ interacts with RAD51, RAD51 paralogues and the Ku70/Ku80 complex, and influences their activities in DSB repair (Bladen *et al*., 2005; Morozumi *et al*., 2009; Rajesh *et al*., 2011; Rajesh *et al*., 2009); and SF3B1 can form a complex with BRCA1 following DNA damage for stabilizing genes involved in the DDR (Savage *et al*., 2014). Thus, such a high incidence of RNA-related proteins interacting with a known DNA repair factor is not surprising. In fact, mRNA processing factors are commonly enriched in many genome-wide screenings aimed to find new proteins

involved in the DDR and the maintenance of genomic integrity, in which we can find subunits of the SF3B complex among others (López-Saavedra *et al*., 2016; Adamson *et al*., 2012; Hurov *et al*., 2010; Paulsen *et al*., 2009), and many RNA-related proteins have been detected as targets of DNA damage-induced post-translational modifications (Beli *et al*., 2012; Matsuoka *et al*., 2007; Smolka *et al*., 2007). Moreover, we favour the idea that our results are meaningful to understand DNA end resection and homologous recombination since depletion of the majority of the identified proteins hampers DNA end resection (figure R4). Indeed, in a parallel project carried out in our laboratory by Rosario Prados Carvajal that stems directly from this thesis, we have revealed that the SF3B complex participates in the control of DSB repair at differentlevels: first, by promoting DNA end resection through the regulation of the amount of CtIP; second, by controlling the splicing and mRNA abundance of many other factors such as EXO1, BRCA1 and ATR, which impact in DSB repair and cell survival to genotoxic treatments; and third, by regulating a DNA damage-induced change on splicing patterns of more than a thousands genes (Prados-Carvajal, López-Saavedra *et al*., second round of revision).

In spite of the emerging importance of RNA-related factors for the regulation of the cell response to DNA damages, in this thesis we focused on the study of PRMT5 and CCAR2 functions in DNA repair, both showing opposite roles in controlling DNA end resection (figure R4, R6 and R13).

2. PRMT5 interacts with CtIP and promotes DNA end resection

In addition to the aforementioned relevance of RNA-related factors in the regulation of DNA repair and the DDR, identification of post-translational modifiers and their targets, and understanding their functional significance remains a critical step to unravel how the cellular processes are coordinated in response to genotoxic stress. Phosphorylation is the best-characterized post-translational modification since it plays essential roles in DDR and DNA repair (Maréchal & Zou, 2013). However, other post-translational modifications, such as

ubiquitylation, sumoylation, neddylation, acetylation and methylation, are becoming increasingly important for regulation of these processes (Polo & Jackson, 2011; Brown & Jackson, 2015) (several examples of post-translational modifications are shown in figure I2 and figure I6). Indeed, P53, a key protein involved in DDR, has been shown to be phosphorylated, ubiquitylated, sumoylated, acetylated and methylated with the aim of regulating its function (Dai & Gu, 2010). Among these modifications, protein arginine methylation has been implicated in the regulation of many cellular processes, including more recently DNA repair (Hu *et al*., 2016). Strikingly, as a result of the TAP purification, we isolated PRMT5 as a novel CtIP interactor. PRMT5 is a member of the *N*-arginine methyltransferases family, which catalyzes the addition of one or two methyl groups to arginine residues (Gary & Clarke, 1998). Transfer of one methyl group results in monomethylarginines, while incorporation of two methyl groups can be performed symmetrically or asymmetrically, leading to symmetric dimethylarginines or asymmetric dimethylarginines, respectively (Bedford & Richard, 2005). Currently, nine members of this family have been identified and they are classified into three types according to its methylation features (Hu *et al*., 2016). PRMT5 is the predominant type II enzyme, which produces monomethylarginines and symmetric dimethylarginines (Branscombe *et al*., 2001).

From our data, it is clear that PRMT5 promotes homologous recombination, DNA end resection and is important for survival upon exposure to DNA damaging agents (figures R6, R8-R11). A surprising result was that PRMT5 is required for survival to CPT and IR, while its depletion does not generate sensitivity to VP16 (figure R8). These DSB-inducing agents differ in the modifications they generate at the ends. CPT stabilizes the complex between DNA and topoisomerase I at 3' ends, whereas VP16 does the same but with DNA and topoisomerase II at 5' ends. IR results in complex modifications in both DNA ends. Thus, our results suggest that PRMT5 is more required for processing of ends with 3' alterations. Despite this stronger requirement for 3'-modified ends, it is also clear that the role of PRMT5 is more general, as PRMT5 is also essential for repairing simple DSBs generated by I-SceI (figure R9 and R11). In agreement with our data, PRMT7, a methyltranferase

closely related with PRMT5, is also especially important for survival to treatments with CPT (Verbiest *et al*., 2008).

Although the molecular role of PRMT5 in resection remains elusive, we can speculate based on the known roles of this factor and related proteins in other cellular events. Arginine methylation can regulate multiple cellular processes including RNA processing, transcriptional regulation, signal transduction and DNA repair (Bedford & Richard, 2005). A key function of arginine methyltransferases is the methylation of histone tails, which participates in the regulation of many of these biological pathways (Di Lorenzo & Bedford, 2011). Indeed, histones H2A, H3 and H4 have been described as targets of PRMT5 (Pollack *et al*., 1999). Recognition of methylated arginines in histone proteins can recruit or block the binding of effector proteins and it is shown that these modifications influence transcription processes, acting as coactivators or repressors depending on the modification site and status (Di Lorenzo & Bedford, 2011; Musselman *et al*., 2012). Type I arginine methyltransferases are described as transcriptional coactivators, while the others, including PRMT5, participates in transcriptional repression through modification of histones located in specific promoters. Indeed, PRMT5-mediated symmetrical dimethylation of histones H3 (residue arginine-8) and H4 (residue arginine-3) found in promoter regions of the Retinoblastoma family have been shown to repress transcription of these tumour suppressor genes (Wang *et al*., 2008). In addition, PRMT7 also negatively regulates expression of its target DNA repair genes through methylation of histones H2A and H4 present in their promoters (Karkhanis *et al*., 2012). Thus, an obvious hypothesis is that PRMT5 might control resection through its effect on histone methylation, either by altering expression of resection factors or by mediating its recruitment to damaged DNA. We have not been able to see large decreases in protein levels of any resection factor so far, with the exception of the mentioned difference between shRNA- and siRNA-mediated depletion of PRMT5 in CtIP levels (figure R7). However, we could not completely discard that such indirect effect is partially responsible of the observed phenotypes. This can even be related with CtIP interaction, as CtIP is a well-established transcription regulator of, among others, its own promoter or cell cycle relevant genes such as cyclin D1 (Liu & Lee, 2006). In a similar way, PRMT5 is responsible for arginine methylation of P53 after DNA damage and this

modification is required for P53 expression and cell cycle progression (Jansson *et al*., 2008; Scoumanne *et al*., 2009). On the other hand, and in a more direct effect, examples of histone methylation requirements for the recruitment of DDR factors are well documented. The classical example is 53BP1, which accumulates at DSB sites by interacting with histone H4 dimethylated on lysine-20 through its Tudor domain, as well as recognizing other nucleosome modifications such as H2A ubiquitylation (Botuyan *et al*., 2006; Fradet-Turcotte *et al*., 2013; Wilson *et al*., 2016). Tudor domains are also able to recognize and bind symmetrical dimethylated arginines (Côté & Richard, 2005), suggesting that arginine methylation could play a role in controlling localization of proteins. So, it is possible that PRMT5-mediated histone modifications affect the recruitment or retention of key repair factors.

Despite the possibility that PRMT5 might affect resection by histone methylation, we favour a more central role as a core component of the resection machinery through the methylation of non-histone proteins. Besides the interaction with CtIP, immunoprecipitation experiments carried out by Dr. Cristina Cepeda García in our laboratory reveal that PRMT5 also associates with other DNA repair proteins, such as BRCA1, MRE11A, RAD50 and even CCAR2 (Cepeda García and Huertas, unpublished results), all closely related proteins that interact with each other's. Proteomic analysis revealed that several DNA repair proteins are targets for arginine-methylation (Boisvert *et al*., 2003). For instance, PRMT1-mediated methylation of glycine and arginine-rich (GAR) motifs of MRE11A and 53BP1 allows their localization to sites of DNA damage (Boisvert, Hendzel *et al*., 2005; Boisvert, Rhie *et al*., 2005; Déry *et al*., 2008). Moreover, this methylation also regulates exonuclease activity of MRE11A (Boisvert, Déry *et al*., 2005; Déry *et al*., 2008). This modification might affect several distinct functions of those proteins and not only their repair roles. In that regard, PRMT1 also methylates BRCA1 and controls its bind at specific promoters, hence affecting its role in modulating gene transcription (Guendel *et al*., 2010). Although PRMT1 and PRMT5 are fundamentally different enzymes with an opposite dimethylation activity (asymmetric and symmetric, respectively), they have been connected before through sharing some substrates. In that case, they usually display opposing biological consequences depending on the methylation pattern. For instance,

PRMT1-mediated asymmetric methylation of arginine-3 of histone H4 is associated with active transcription, whereas its symmetric methylation performed by PRMT5 is a mark for gene silencing (Bedford & Richard, 2005). MRE11A was a likely target for this kind of regulation since it was described as a substrate for PRMT1 methylation (Boisvert, Déry *et al*., 2005) and interacts with PRMT5 (Cepeda-García and Huertas, unpublished results). However, in this case, PRMT1 and PRMT5 do not seem to play opposite roles owing to both enzymes exhibit an effect in promoting DNA end resection (figure R6; Boisvert, Déry *et al*., 2005). Moreover, western blots using antibodies that recognize symmetric dimethylation on immunoprecipitated samples performed in our laboratory by Dr. Cristina Cepeda García discarded that either CtIP or MRE11A are targets for PRMT5-mediated methylation. Despite that, she could observe symmetric methylation in response to DNA damage of specific proteins that were co-immunoprecipitated with CtIP (Cepeda-García and Huertas, unpublished results). This indicates that PRMT5 may function in DNA end resection through methylation of other substrates rather than CtIP or MRE11A, but likely forming a complex with them. Our working model is that CtIP may function in regulating PRMT5 activity on yet unknown repair/resection factors. This is supported by evidences of non-target proteins that interact with arginine methyltransferases and activate or inhibit their catalytic activity (Lin *et al*., 1996; Singh *et al*., 2004). In this regard, it was shown that association of PRMT5 with chromatin remodelers BRG and BRM enhances its mediated methylation of histones H3 and H4 (Pal *et al*., 2004). Interestingly, interaction of PRMT5 and CtIP seems to be constitutive (figure R3) and damage-independent (figure R5, panel a), suggesting that CtIP may regulate PRMT5 methyltransferase activity by facilitating the encounter with its substrate proteins, likely through promoting PRMT5 recruitment to DSBs after DNA damage. This spatial control that influences proximity between substrates and PRMT5 was also described for certain SUMO E3-ligases, which require localization to DSBs for sumoylation of their targets (Galanty *et al*., 2009). Moreover, it has already been described a PRMT5-MEP50 complex required for substrate recognition and efficient histone methylation (Burgos *et al*., 2015). MEP50 may function in binding histones H2A and H4 and orienting and presenting histone tail substrates to the

catalytic domain of PRMT5, thus promoting its methyltransferase activity (Ho *et al*., 2013; Burgos *et al*., 2015).

Along these lines, recent studies reveal a role of PRMT5 in promoting homologous recombination through methylation of specific substrates. For example, PRMT5 methylates RUVBL1, a cofactor of the TIP60 complex (Clarke *et al*., 2017). This methylation is required for the acetyltransferase activity of TIP60, allowing acetylation of lysine-16 of histone H4 that facilitates the displacement of 53BP1 from sites of DNA damage (Clarke *et al*., 2017). Since 53BP1 is a known inhibitor of DNA end resection, these data agree with our results showing PRMT5 as activator of DNA end resection. In addition, Cintia Checa Rodríguez in our laboratory is studying how depletion of KLF4 impairs DNA end resection (Checa-Rodríguez and Huertas, unpublished results). KLF4 was described as target of PRMT5-mediated methylation, which inhibits its ubiquitylation and thus stabilizes its protein levels (Hu *et al*., 2015). Strikingly, whereas ectopic expression of wild-type KLF4 is able to supress the defect in DNA end resection mediated by endogenous KLF4 downregulation, a mutant of KLF4 that abrogates its PRMT5-dependent methylation fails, even when expressed at higher levels than the endogenous protein. This reveals an additional layer of regulation of resection by PRMT5 through KLF4.

Hence, we think that a key question for future studies is what are the actual substrate(s) of PRMT5 involved in resection and what brings this methylation to them. A tantalizing idea is that such post-translational modification might affect other relevant modifications of such factors and/or influence several protein-protein interactions. In this regard, FEN1, a flap endonuclease that can form a complex with PCNA, is a target of PRMT5. PRMT5-mediated methylation of FEN1 abolish its phosphorylation, facilitating its association with PCNA and enhancing DNA replication and repair (Guo *et al*., 2010).

Despite the lack of a complete molecular mechanism, we suggest that PRMT5 plays a central role in controlling DNA end resection and homologous recombination, most likely by acting at many different levels. Future studies that are currently on going in our laboratory will shed some light on how this function is exerted and regulated.

3. CCAR2 antagonizes CtIP and inhibits DNA end resection and homologous recombination

Cell Cycle and Apoptosis Regulator 2 (CCAR2), formerly known as Deleted in Breast Cancer 1 (DBC1), was the only isolated protein from the TAP purification that revealed an inhibitory effect on DNA end resection. CCAR2 is a well-known tumour suppressor that has been widely studied by its role in promoting P53-mediated apoptosis through negative regulation of SIRT1 activity. CCAR2 interacts with SIRT1 and inhibits its P53-deacetylase function, leading to P53 upregulation that drives cells to apoptosis (Kim *et al*., 2008; Zhao *et al*., 2008). ATM- or ATR-mediated phosphorylation of CCAR2 on threonine-454 after DNA lesions controls its association with SIRT1, and hence its influence on cell proliferation (Zannini *et al*., 2012). Our results show that SIRT1 is not involved in the function of CCAR2 in HR (figure R18), which agrees with the already described idea that CCAR2 contributes to DNA repair independently of SIRT1 (Kim & Kim, 2013; Magni *et al*., 2015). However, phosphorylation of threonine-454 of CCAR2 by ATM/ATR is also required for its role in homologous recombination (figure R20). Besides the aforementioned function in regulation of apoptosis, cell survival and DNA repair, CCAR2 is also involved in other biological processes such as RNA metabolism as part of the DBIRD complex (Close *et al*., 2012) and transcription regulation through association with BRCA1 (Hiraike *et al*., 2010).

In this thesis we got new insights into the role of CCAR2 in DNA repair by showing a direct physical and functionally antagonistic relationship with CtIP (figures R12 and R13). CCAR2 acts as a bona fide inhibitor of DNA end resection that not only regulates which cells resect their DNA (detected by RPA foci formation), but also limits the length of the produced resected DNA (measured by SMART assays). This leads us to hypothesize that CCAR2 might constrain the spreading of CtIP along the DNA, thereby spatially confining end resection. Interestingly, a proteomic screening revealed CCAR2 as interactor of the three subunits of the RPA complex (Maréchal *et al*., 2014), hence suggesting that such an interaction might be required for this role in limiting resection. CCAR2 depletion affects all HR subpathways (figure R15), whereas it seems not influence repair by

NHEJ (figure R16), which is consistent with the fact that it does not affect the recruitment of NHEJ proteins such as 53BP1 (Magni *et al*., 2015). Thus, we conclude that the major role of CCAR2 in DSB repair is to limit resection spreading. In recent years, it has been proposed that resection has to be constrained to ensure an accurate repair and the maintenance of genomic stability (Roberts *et al*., 2012; Jimeno *et al*., 2015; Chen *et al*., 2015; Kijas *et al*., 2015; Tkáč *et al*., 2016; Zong *et al*., 2016). In addition, such a role in HR could contribute to CCAR2 sensitivity to DSB-inducing agents (Kim *et al*., 2014; Tanikawa *et al*., 2013). Our data are in apparent contrast to a previously published report that proposes CCAR2 to be an enhancer of HR, using a recombination reporter in SW480sn3 cells (Tanikawa *et al*., 2013). However, this might reflect differences in the reporters used and, more specifically, the length of gene conversion tracts required to render positive colonies. This hypothesis is supported by the fact that CCAR2 not only affects the number of DSBs to be resected but also mainly controls the length of DNA that will be resected, hence modulating gene conversion tracts and crossovers (Prado & Aguilera, 2003).

Although CCAR2 interacts constitutively with CtIP and in a damage-independent manner (figure R3 and R12), a probable explanation for the role of CCAR2 antagonizing CtIP-mediated resection is that it might influence CtIP interaction with other factors such as MRE11A or BRCA1, required for its function in DNA end resection. The physical relationship between CtIP, CCAR2 and BRCA1 suggested the possibility that each of them may affect the interaction between the others. In this regard, it was evidenced that CCAR2 depletion does not influence the relationship between CtIP and BRCA1 (figure R14). In addition, we show by PLA assay that BRCA1 does not bridge the interaction of CtIP with CCAR2 as it was maintained or even increased in the absence of BRCA1 (figure R12). Also, we demonstrate that there is no competition between CCAR2 and MRN despite the proximity of their interaction sites in CtIP (figure R14). It should be noted that carboxi-terminal region of CtIP has much relevance to its role in DNA end resection since it is responsible for the binding of CCAR2 and the MRN complex (Sartori *et al*., 2007), as well as is subjected to several post-translational modifications, such as phosphorylations and sumoylation, which are described as essentials for promoting DNA end resection (Huertas & Jackson, 2009a; Peterson *et al*., 2013 ;

Soria-Bretones and Huertas, personal communication; see figure I6). Thus, a likely scenario is that, although CCAR2 does not hamper CtIP complexes formation, the physical presence of CCAR2 negatively affects one or several of those post-translational modifications and impairs the activity of those complexes.

We have demonstrated that CCAR2 localizes to DNA damage sites and forms foci like other repair proteins (figure R19). In addition, several experiments were performed in collaboration with Jiri Bartek to monitor the recruitment of CCAR2 and CtIP to the breaks using a laser microirradiation. CCAR2 accumulates at DSBs in 7% of cells, while is excluded from damaged DNA in 37% of the cells, suggesting that CCAR2 is recruited to DNA damage sites in a subset of breaks but is actively removed from them in another subset (López-Saavedra *et al*., 2016). Strikingly, the majority of the cells that showed CCAR2 recruitment did not accumulate CtIP, as well as more than 50% of cells that accumulate CtIP displayed clear CCAR2 exclusion from damaged chromatin. Colocalization of both proteins was observed in less than 20% of the cells (López-Saavedra *et al*., 2016). The influence of cell cycle position on CCAR2 retention at or exclusion from DSBs sites has also been studied. CCAR2 accumulation appeared throughout the cell cycle, mainly in G1 and G2 phases, whereas exclusion was more present in S phase, and also in G2 phase with a slower kinetic, suggesting that CCAR2 removal from damaged sites was mainly restricted to replicating cells (López-Saavedra *et al*., 2016). Moreover, cells showing accumulation of both CtIP and CCAR2 revealed that these proteins tended not to colocalize (López-Saavedra *et al*., 2016). An interesting hypothesis is that cells that use NHEJ for repair recruit CCAR2 to inhibit HR, while cells that use HR for repair exclude CCAR2 from damaged chromatin to allow recombination to take place.

Mechanistically, we proposed that the relationship between CtIP and CCAR2 acts accordingly to the following model. CtIP and CCAR2 interact constitutively and in a DNA damage-independent manner in the nucleoplasm (figure D1, i). Since CCAR2 does not compete with MRN for its binding to CtIP even though they share interaction regions (figure R14), it is likely that the physical presence of CCAR2 negatively regulates the activity of the CtIP-MRN complex. When DSB occurs, the recruitment of CtIP and CCAR2 to the site of DNA damage depends on the cell cycle phase. Thus, in G1 cells only CCAR2 is recruited, as resection will be inactive

(Huertas, 2010; Ferretti *et al*., 2013). Otherwise, CtIP and CCAR2 are probably recruited together to chromatin in G2 and, perhaps, S phase, accounting for the cells that show accumulation of both proteins after laser microirradiation (figure D1, ii). The fact that CCAR2 limits CtIP-dependent resection spreading along the DNA (figure R13) and CtIP presence at sites of DNA damage promotes CCAR2 exclusion, reinforces the idea that inhibition of CtIP by CCAR2 depends on the physical interaction between the two. While the bulk of CtIP and CCAR2 in the nucleoplasm retain their interaction upon DNA damage, the CtIP-CCAR2 complex appears to be disrupted locally on damaged chromatin (figure D1, iii and iv). In this scenario, either one factor or the other rapidly takes command of the situation to allow DSB repair by the appropriate mechanism. Which one dominates depends on several factors, such as cell cycle distribution or chromatin status. Indeed, CCAR2 affects the repair kinetics of breaks that occur in heterochromatin but not in euchromatin (Magni *et al*., 2015). Strikingly, CCAR2 has no effect on breaks that are always repaired by NHEJ (figure R16), but is critical for DSB repair pathway choice for breaks that could be repaired by NHEJ or HR (figure R17). When a break will be repaired by NHEJ (figure D1, iii), CtIP exits the damaged chromatin but CCAR2 stays on, constraining DNA end resection and allowing NHEJ to ensue. This occurs in breaks that arise in G1 and many of those that arise in G2. Retention of CCAR2 at sites of damage and its role as an antagonist of resection requires ATM activity and ATM-mediated phosphorylation of threonine-454 of CCAR2 (figures R19 and R20). The function of CCAR2 limiting resection parallels the 53BP1-RIF1 and 53BP1-PTIP anti-resection pathways, which are also triggered by ATM-mediated phosphorylation of 53BP1 (Chapman *et al*., 2013; Escribano-Díaz *et al*., 2013; Callen *et al*., 2013). Alternatively, DSBs that will be resected maintain CtIP on damaged chromatin and do not accumulate (G2 phase) or even actively exclude (S phase) CCAR2 from these sites of damage (figure D1, iv and v), probably thereby allowing the catalytic activity of the MRN complex. Such behaviour of CCAR2 is CtIP-dependent and allows CtIP and DNA end resection to be activated. Indeed, it is noteworthy that CCAR2 only interacts with the non-phosphorylated form of CtIP (figure R12). An interesting hypothesis is that resection will spread along the chromatin region devoid of CCAR2 and will stop as soon as it enters a region in which CCAR2 is still present (figure D1, v). This might explain the increased length

of resected DNA tracts upon CCAR2 depletion (figure R13). The model predicts that the extent of resection in human cells is higher in the S phase than in the G2 phase, a phenomenon that has been observed in budding yeast (Zierhut & Diffley, 2008). Moreover, this will also suggest that HR is probably different between S and G2 phases as the length of resection will affect the balance between different recombination subpathways, controlling the size of gene conversion tracts and interfering with crossover formations (Prado & Aguilera, 2003).

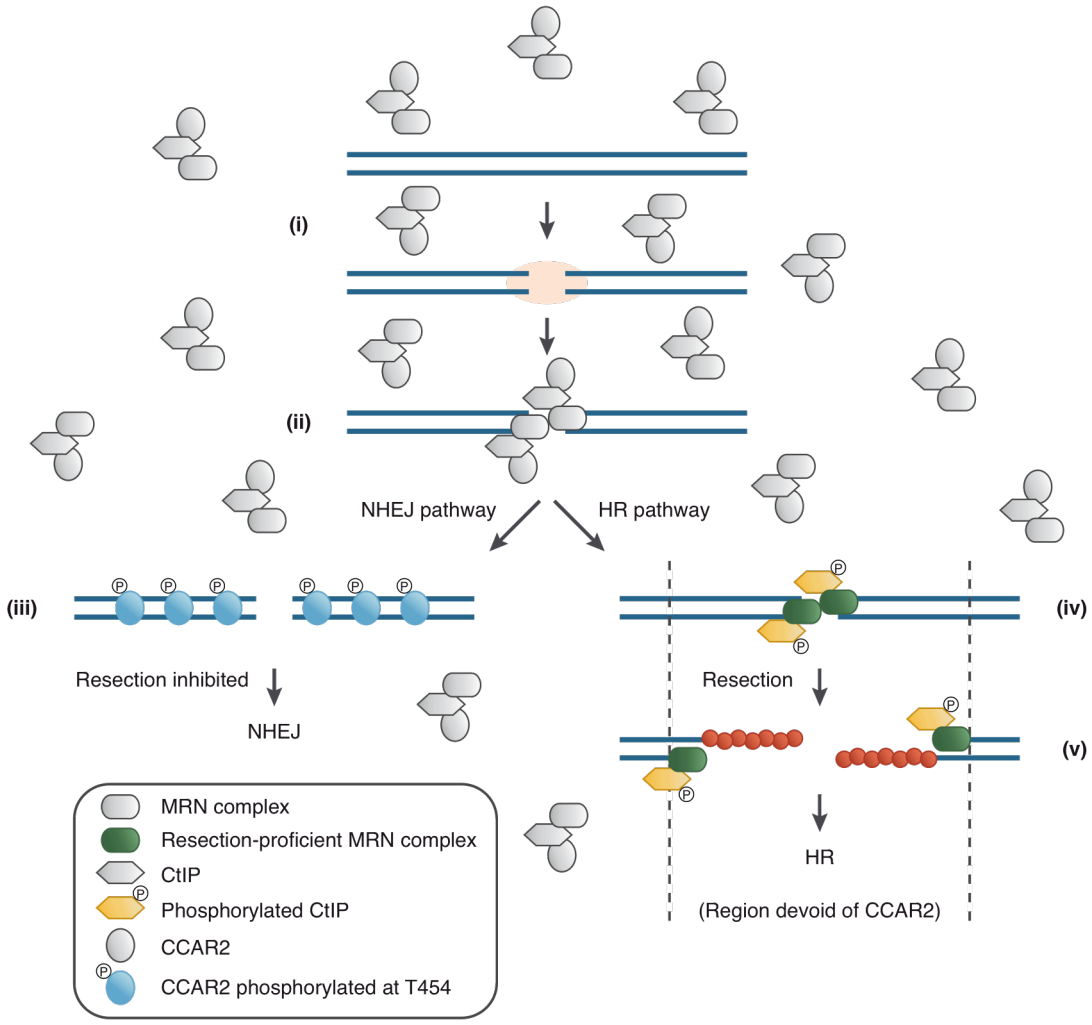

Figure D1. Scheme representing the role of CCAR2 in DNA end resection. CtIP and CCAR2 interact constitutively in a damage-independent manner (**i**). Upon the appearance of a DSB, they are both recruited to the site of damage (**ii**), but rapidly the complex is dissociated and only one of them remains at the breaks (**iii** and **iv**). DSBs repaired by NHEJ maintain CCAR2 in an ATM-dependent manner, facilitating repair through preventing DNA end resection (**iii**). In contrast, DSBs that require DNA end resection retain only CtIP at the break and exclude CCAR2 from this region in a CtIP and/or DNA end resection manner (**iv**). This allows resection to progress until it covers the region devoid of CCAR2 (**v**).

In summary, we propose a role for CCAR2 acting as a DNA end resection inhibitor that would limit its spreading along chromatin in order to generate confined tracts of ssDNA that are suitable for homology search by the RAD51 filament, leading to productive and error-free HR. This mechanism for regulation of the extent of DNA end resection would minimize the chance of hyper-resection, generally associated with genomic instability (Roberts *et al*., 2012; Jimeno *et al*., 2015; Chen *et al*., 2015; Kijas *et al*., 2015; Tkáč *et al*., 2016; Zong *et al*., 2016). Our data imply that during normal DNA repair, CtIP-CCAR2 complexes have to be locally disrupted. Albeit it is still unclear which is/are the factor(s) responsible for this dissociation, our findings suggest that cell cycle and post-translational modifications have been shown to play a role in regulating their activities.

4. CtIP, PRMT5 and CCAR2. Implication in genomic instability, genetic disorders and cancer

In this thesis, we have revealed novel and opposite roles for PRMT5 and CCAR2 in DNA end resection through their interaction with CtIP. These functions result in activation or inhibition of homologous recombination, respectively. Despite the contrary influence of CtIP and PRMT5 in resection process compared with CCAR2, depletion of each of these three factors leads to disturbance of the balance between NHEJ and HR for the repair of DSB (figures R11 and R17). This unbalance might have consequences for cells since improperly repaired breaks generate an increase in genomic instability and, in humans, it would drive towards the appearance of diseases as cancer and premature aging (Aguilera & Gómez-González, 2008; Jackson & Bartek, 2009). Their roles in DNA repair, as well as their implication in a wide range of other cellular processes, reveal that PRMT5 and CCAR2 could function either in promoting tumorigenesis or as tumour suppressors (Qin *et al*., 2015; Tanikawa *et al*., 2013; Kim & Kim, 2013; Scoumanne *et al*., 2009; Wang *et al*., 2008; Stopa *et al*., 2015). Thus, further studies to get new insights in their influence in DNA repair might contribute to better understand the relationship between these factors and cancer appearance, as wells as their use as indicators of tumour prognosis and targets for anti-cancer therapies.

CONCLUSIONS

1. We have identified 10 proteins as new constitutive interactors of CtIP using a Tandem Affinity Purification assay with a double-tagged (GFP and FLAG) construct. Most of them are related with CtIP resection role as their depletion either promotes (CCAR2) or impairs (PRMT5, SF3B3, DHX15, DHX9 and KIF11) DNA end processing.

2. PRMT5 association with CtIP is DNA damage-independent and requires CtIP phosphorylation at serine-327.

3. PRMT5 stimulates initiation and processivity of DNA end resection, hence promoting homologous recombination and keeping the balance between HR and NHEJ.

4. Depletion of PRMT5 confers sensitivity to DSB-inducing agents, such as ionizing radiation and camptothecin, but not etoposide.

5. CCAR2-CtIP interaction is damage-independent and occurs mainly outside of damaged chromatin. Such interaction does not require the carboxi-terminal part of CCAR2.

6. CCAR2 acts as an inhibitor of CtIP-mediated DNA end resection that limits resection initiation as well as the length of resected DNA. As a consequence, CCAR2 regulates the balance between HR and NHEJ by controlling recombination.

7. CCAR2 localizes at DSBs in an ATM-dependent manner. ATM-mediated phosphorylation of threonine-454 of CCAR2 is required for its function limiting end resection.

MATERIALS AND METHODS

1. Cell culture procedures

1.1. Growth media and conditions

Cells were cultured in high-glucose Dulbecco's Modified Eagle Medium (DMEM, D6546, Sigma), supplemented with 10% fetal bovine serum (F7524, Sigma), 2 mM L-glutamine (25030024, Gibco), 100 U/ml penicillin and 100 μg/ml streptomycin (15140122, Gibco) at 37ºC in 5% CO_2. Cell lines used in this thesis were U2OS (human osteosarcoma), HEK293 and HEK293T (human embryonic kidney) or cells lines derived from them stably harbouring the indicated constructs (Table M1) obtained by plasmid transfection or by infection with lentiviral particles. These cell lines were cultured in the same conditions and were selected by adding 0.5 mg/ml G418 (A1720, Sigma) or 1 μg/ml puromycin (P8833, Sigma) to the culture medium, according to the selection marker of the plasmid inserted.

Table M1. Human cell lines used in this study.

Cell name	Description	Selection	Source/Reference
U2OS	Human osteosarcoma	No	ATCC HTB-96
HEK293	Human embryonic kidney	No	ATCC CRL-1573
HEK293T	Human embryonic kidney	No	ATCC CRL-11268
U2OS GFP-6XFLAG-CtIP	U2OS cell line stably expressing GFP-6XFLAG-CtIP construct	G418	This study

Cell name	Description	Selection	Source/Reference
U2OS GFP	U2OS cell line stably expressing GFP	G418	Generated in Steve Jackson's lab by Dr. Pablo Huertas (Huertas & Jackson, 2009)
U2OS GFP-CtIP	U2OS cell line stably expressing GFP-CtIP construct	G418	This study
U2OS GFP-CtIP S327D	U2OS cell line stably expressing GFP-CtIP S327D construct	G418	Generated in Steve Jackson's lab by Dr. Pablo Huertas
U2OS GFP-CtIP S327A	U2OS cell line stably expressing GFP-CtIP S327A construct	G418	Generated in Steve Jackson's lab by Dr. Pablo Huertas
U2OS GFP-CCAR2	U2OS cell line stably expressing GFP-CCAR2 construct	G418	This study
U2OS GFP-CCAR2 T454A	U2OS cell line stably expressing mutant GFP-CCAR2 T454A construct	G418	This study
U2OS GFP-MDC1	U2OS cell line stably expressing GFP-MDC1 construct	G418	Kind gift from Dr. Steve Jackson
U2OS DR-GFP	U2OS cell line with DR-GFP reporter integrated	Puromycin	Kind gift from Dr. Maria Jasin (Pierce *at al.*, 1999)

Cell name	Description	Selection	Source/Reference
U2OS SA-GFP	U2OS cell line with SA-GFP reporter integrated	Puromycin	Generated in our lab from hprtSAGFP plasmid (Addgene, 41594)
U2OS EJ5-GFP	U2OS cell line with EJ5-GFP reporter integrated	Puromycin	Generated in our lab from pimEJ5GFP plasmid (Addgene, 44026)
U2OS SSR	U2OS cell line with SSR reporter integrated	G418	Generated in our lab by Dr. Daniel Gómez Cabello (Gómez-Cabello *et al*., 2013)
293 GFP	293 cell line stably expressing GFP	G418	This study
293 GFP-CtIP	293 cell line stably expressing GFP-CtIP construct	G418	This study

Cells were grown in different types of plates depending on the experiment. Trypsin-EDTA solution (T4049, Sigma) was used to detach the cells when required. For seeding, the number of cells was quantified with an automatic cell counter (Z2™ Coulter Counter®, Beckman Coulter).

For long-term preservation of the cells, they were harvested and pelleted by centrifugation at 500 g for 5 minutes. Cells were resuspended in freezing solution (10% DMSO in fetal bovine serum), aliquoted in tubes and deposited in freezing containers (C1562, Sigma) that allowed an optimal freezing of the cells with a gradual temperature decrease of 1ºC/minute. Containers were stored at -80ºC at least 24 hours and then vials were transferred to liquid nitrogen tanks for long-term preservation.

1.2. Double thymidine synchronization of U2OS

In order to analyse CtIP complexes over the cell cycle, TAP assay was performed with protein extracts from cells in each phase of the cell cycle. Cells were synchronized using high concentration of thymidine to interrupt the deoxynucleotide metabolism pathway, thereby halting DNA replication. As treatment with thymidine arrests cells throughout S phase, a double thymidine protocol was used to ensure blocking of the cells at the end of G1, before starting S phase.

Cells were seeded at 20% of confluence in different plates and the following day medium with 3 mM thymidine (T9250, Sigma) was added and incubated for 18 hours. Then, thymidine was removed by washing three times with phosphate buffered saline (PBS) and cells were released from block by adding fresh medium supplemented with 24 μM deoxycytidine (D0776, Sigma). Cells should be out S phase after 12 hours, so medium with 3 mM thymidine was added again at that point and then cells were incubated for another 24 hours. After that time, cells were mostly arrested at the G1/S border. A sample for G1 cells was harvested at that point for protein extraction. The rest of the cells were released by washing three times with PBS and adding fresh medium with 24 μM deoxycytidine. New samples were collected three and eight hours later (cells in S and G2 phases, respectively) for protein extraction.

1.3. Transfection

1.3.1. siRNAs

One of the strategies used for specific protein downregulation was gene silencing mediated by siRNAs using the transfection reagent Lipofectamine® RNAiMAX (13778, Invitrogen). The list of siRNAs used in this thesis is shown in table M2.

Table M2. siRNAs used in this study.

Target gene	Description	Source/Reference
Non-target	ON-TARGETplus Non-targeting Pool	Dharmacon (D-001810-10-20)
CtIP	GCUAAAACAGGAACGAAUC	Sigma
PRMT5	CCGCUAUUGCACCUUGGAA	Sigma
CCAR2	ON-TARGETplus human CCAR2	Dharmacon (J-010427-08)
SIRT1	ON-TARGETplus SMARTpool human SIRT1	Dharmacon (L-003540-00)

siRNA transfection was performed in different plate formats, accordingly to the requirements of each specific experiment. For 60-mm plates, 300.000 cells were seeded the day before transfection. Then, the media was removed and 3 ml of fresh DMEM supplemented with L-glutamine but without antibiotics was added. Nine μl siRNA (10 μM) were diluted in 150 μl Opti-MEM® (11058-021, Gibco) and, on a separate tube, 9 μl lipofectamine RNAiMAX reagent were diluted in 150 μl Opti-MEM. Next, 150 μl from each tube were mixed gently and incubated for 5 minutes at room temperature to allow siRNA-lipofectamine complex formation. Transfection solution was added dropwise while carefully rocking the plate. Plates were incubated at 37ºC for 6 hours before replacing the media with 5 ml of fresh complete DMEM to minimise cell death. All volumes were reduced or increased by a factor of two in case of 6-well or 100-mm plates, respectively.

1.3.2. Plasmid DNA

Plasmids used in this thesis are described in table M3.

Table M3. Plasmids used in this study.

Plasmid	Description	Resistance	Source/Reference
pEGFP-C1	Vector used for EGFP expression	Kanamycin/ G418	Clontech (6084-1)
pGFP-CtIP	pEGFP-C1 vector containing *CtIP* gene fused to *EGFP*	Kanamycin/ G418	Kind gift from Dr. Steve Jackson (Sartori *et al.*, 2007)
pGFP-6XFLAG-CtIP	pEGFP-C1 vector containing 6XFLAG and *CtIP* gene fused to *EGFP*	Kanamycin/ G418	Generated in Steve Jackson's lab by Dr. Pablo Huertas
pGFP-CCAR2	pEGFP-C1 vector containing *CCAR2* gene fused to *EGFP*	Kanamycin/ G418	This study
pGFP-CCAR2 T454A	pEGFP-C1 vector containing mutant T454A *CCAR2* gene fused to *EGFP*	Kanamycin/ G418	This study
pGFP-CCAR2 1-185	pEGFP-C1 vector containing a CCAR2 fragment from aminoacid 1 to 185 fused to *EGFP*	Kanamycin/ G418	Generated in our lab by Dr. Mª Jesús Fernández Ávila
pGFP-CCAR2 187-606	pEGFP-C1 vector containing a CCAR2 fragment from aminoacid 187 to 606 fused to *EGFP*	Kanamycin/ G418	Generated in our lab by Dr. Mª Jesús Fernández Ávila

Plasmid	Description	Resistance	Source/Reference
pGFP-CCAR2 608-924	pEGFP-C1 vector containing a CCAR2 fragment from aminoacid 608 to 924 fused to *EGFP*	Kanamycin/ G418	Generated in our lab by Dr. Mª Jesús Fernández Ávila
SFB-BRCA1	Vector used to overexpress BRCA1 fused to SFB tag (streptavidine-binding peptide, FLAG epitope and S-protein)	Kanamycin	Kind gift from Dr. Ko Sato
HALO-BARD1	Vector used to overexpress BARD1 fused to HALO tag	Ampicillin	Kind gift from Dr. Ko Sato
hprtSAGFP	Vector harbouring the SA-GFP reporter for SSA analysis (see section 1.8.)	Ampicillin/ Puromycin	Addgene (41594) (Stark *et al.*, 2004)
pimEJ5GFP	Vector bearing the EJ5-GFP reporter for total NHEJ measurement (see section 1.8.)	Ampicillin/ Puromycin	Addgene (44026) (Bennardo *et al.*, 2008)
SSR 2.0	Vector harbouring the SeeSaw Reporter to analyse the balance between NHEJ and HR (see section 1.8.)	Kanamycin/ G418	Generated in our lab by Dr. Daniel Gómez Cabello (Gómez-Cabello *et al.*, 2013)
pBFP-ISceI	Vector containing the I-SceI and *BFP* genes for simultaneous induction of the endonuclease and labelling of the transfected cells	Ampicillin	Addgene (31484) (Certo *et al.*, 2011)

Plasmid	Description	Resistance	Source/Reference
p8.91	Vector used for expression of lentiviral capside proteins	Ampicillin/ Puromycin	Kind gift from Dr. Felipe Cortés Ledesma
pVSVG	Vector used for expression of lentiviral envelope proteins	Ampicillin/ Puromycin	Kind gift from Dr. Felipe Cortés Ledesma
pLKO.1-shNT	Vector used for expression of shRNA against a non-target sequence	Ampicillin/ Puromycin	Sigma (SHC016V)
pLKO.1-shCtIP	Vector used for expression of shRNA against CtIP	Ampicillin/ Puromycin	Sigma (NM_002894.1-3008s1c1)
pLKO.1-shPRMT5	Vector used for expression of shRNA against PRMT5	Ampicillin/ Puromycin	Sigma (NM_006109.2-1577s1c1)
pLKO.1-shCCAR2	Vector used for expression of shRNA against CCAR2	Ampicillin/ Puromycin	Sigma (NM_021174.4-1443s1c1)
pLKO.1-shDHX9	Vector used for expression of shRNA against DHX9	Ampicillin/ Puromycin	Sigma (NM_001357.x-515s1c1)
pLKO.1-shDHX15	Vector used for expression of shRNA against DHX15	Ampicillin/ Puromycin	Sigma (NM_001358.x-2632s1c1)
pLKO.1-shRBM10	Vector used for expression of shRNA against RBM10	Ampicillin/ Puromycin	Sigma (NM_005676.3-491s21c1)
pLKO.1-shSF3B3	Vector used for expression of shRNA against SF3B3	Ampicillin/ Puromycin	Sigma (NM_012426.x-3898s1c1)
pLKO.1-shSFPQ	Vector used for expression of shRNA against SFPQ	Ampicillin/ Puromycin	Sigma (NM_005066.x-1855s1c1)
pLKO.1-shKIF11	Vector used for expression of shRNA against KIF11	Ampicillin/ Puromycin	Sigma (NM_004523.2-3927s1c1)

Different strategies were used to introduce plasmid DNA into the cells.

1.3.2.1. FuGENE transfection

FuGENE® HD Transfection Reagent (E2311, Promega) was used in order to transfect expression vectors. Again, different types of plates were used for transfection depending on the requirements of each specific experiment, scaling the volumes following manufacturer's instructions. For 100-mm plates, between 500.000 and 10^6 cells were seeded the day before transfection. Then, 7.2 μg of plasmid DNA were diluted in Opti-MEM to a final volume of 336 μl. Afterwards, 21 μl of FuGENE HD Transfection Reagent were added and gently mixed. Solution was incubated 10-15 minutes at room temperature and finally was added dropwise while carefully rocking the plate.

1.3.2.2. Calcium phosphate transfection

Calcium phosphate transfection protocol was used to introduce the plasmids required for lentivirus production in HEK293T cells. For 100-mm plates, $3.5x10^6$ cells were seeded the previous day and the media was changed at least 30 minutes before transfection. A mixture with the three plasmid required was prepared with a 3:2:1 ratio, i.e. 15 μg of the vector containing DNA of interest, 10 μg of the vector with virus capsid genes (p8.91) and 5 μg of the vector with virus envelope genes (pVSVG). Then, 64 μl of calcium chloride was added and volume was topped up to 500 μl with mili-Q water. Furthermore, 500 μl of 2x HEPES buffered saline (HBS; 51558, Sigma) were added to a fresh 15 ml tube. Solution with DNA and calcium chloride was added dropwise to the tube while bubbling air through HBS using a glass Pasteur pipette. The blend was incubated 30 minutes at room temperature. Transfection mixture was finally added dropwise to the cells while carefully rocking the plate. The protocol was carried out in a P2 biological safety room or plates were moved there just after transfection. The following day, the media was removed and exchanged with fresh completed DMEM after a wash with PBS. Some experiments required the use of larger or smaller plates, so volumes used were scaled accordingly in those cases.

1.4. Lentiviral production and transduction

The other strategy used for protein downregulation was infection with lentiviral particles harbouring shRNAs vectors targeted against the protein of interest. Moreover, lentiviral transduction was also used to introduce pBFP-ISceI vector to express the restriction enzyme I-SceI and the blue fluorescent protein (BFP) in cells harbouring a repair reporter system. HEK293T cells were used for lentivirus production for its high transfectability. Cells were seeded and the vector of interest was co-transfected with p8.91 and pVSVG plasmids for lentivirus capsid and envelope formation, using calcium phosphate transfection protocol as described previously in paragraph 1.3.2.2.

Two different procedures were followed for lentivirus collection and transduction, depending on the plasmid that harboured, and both were carried out in a P2 biological safety room.

On the one hand, lentiviruses produced for pBFP-ISceI plasmid expression were harvested 48 hours after changing the media upon transfection (see section 1.3.2.2.). Culture medium of each plate was collected with 10 ml syringes and was filtered using 0.45 μm polyvinylidene difluoride (PVDF) filters (SLHV035RS, Millex®-HV, Millipore) to remove cellular debris. For larger production of viruses, medium from plates of the same lentivirus were pooled together. Then, lentiviruses were pelleted by centrifugation for 1 hour and 30 minutes at 22.000 rpm at 4ºC. Supernatant was removed and viruses were resuspended in 500 μl DMEM for each 100-mm plate pooled. Finally, samples were aliquoted and stored at -80ºC until use. Before infection, viral production was titrated by BFP expression using flow cytometer (see paragraph 1.7.2.). For transduction, lentiviral particles were diluted in DMEM supplemented with 4 μg/ml hexadimethrine bromide (H9268, Sigma) with a multiplicity of infection (MOI) of 10, i.e. 10 times more than the number of particles needed for 100% cell infection, and this solution was added to the plates. Cells were washed the next day with new media to remove viral residues and hexadimethrine bromide.

On the other hand, lentiviruses harbouring shRNAs vectors to deplete specific proteins were harvested in two steps without centrifugation. The day after changing the media upon transfection, culture medium was collected and filtered

as previously described, and 8 μg/ml hexadimethrine bromide was added. Aliquots were made as required and stored at -80ºC. Fresh medium was added to the plates and the following day it was harvested and stored in the same way. Cells were seeded the day before, and medium with lentiviruses was thawed and added to the plates for transduction. These viruses could not be titrated by fluorescence, so lentiviruses produced in one 100-mm plate were used to infect two 100-mm plates, after combining both harvests. The media was replaced 8 hours later to remove viral residues and hexadimethrine bromide.

1.5. Single clone stable cell line generation

The following procedure was performed to generate a stable cell line clonally pure after transfection. Cells were transfected to integrate a specific DNA construct using FuGENE HD transfection reagent as described in paragraph 1.3.2.1. The day after, cells were diluted 1:50, 1:100 and 1:200 and seeded in 150-mm plates to isolate colonies grown from single cells. When clones had grown and formed isolated colonies of a suitable size, they were picked up with the aid of an automatic pipette under an inverted optical microscope. To do so, first cells have to be partially detached from the bottom of the plates. Instead of trypsin, the chelating agent ethylenediaminetetraacetic acid (EDTA) was used to weaken cell adhesion to the plate without completely detaching cells. Culture medium was removed and 10 ml of 5mM EDTA diluted in PBS were added to the plate. Each colony was identified under the microscope, picked up by aspirating 150 μl of solution while scrapping the surface to detach the cells and was seeded in a well of 24-well plate containing 500 μl DMEM. The media was replaced 24 hours later and fresh DMEM containing G418 or puromycin according to the plasmid selection marker was added. Between 24 and 48 clones were picked up and were grown separately before freezing them. Finally, different clones were analysed to check DNA insertion.

1.6. Clonogenic cell survival assays

Clonogenic assays with different DSB-inducing agents were performed to study cell survival after damage essentially as published (Puck and Marcus, 1956). Double-strand breaks were produced by ionizing radiation (see section 1.9.) or by treatment with topoisomerase inhibitors camptothecin (C9911, Sigma) and etoposide (E1383, Sigma). First, cells were seeded in 6-well plates at two different concentrations in triplicates. For IR, 250 and 500 cells were seeded and for CPT and VP16 treatments, 500 and 1.000 cells were seeded per well. The following day, DNA was damage by different procedures. On the one hand, cells were irradiated with doses of 0, 2 or 5 Gy. On the other hand, acute treatments (1 hour) with different concentrations of topoisomerase inhibitors were used, using DMSO as control. Concentrations used for such treatments were 0.01 μM, 0.05 μM and 0.1 μM of camptothecin and 5 μM and 10 μM of etoposide. Cells were incubated with drugs or DMSO for 1 hour and then were washed twice with PBS and fresh medium was added to each well.

Cells were incubated at 37ºC for 7-12 days to allow colonies formation. Afterwards, cells were stained and visualized using crystal violet. For that, culture medium was removed, cells washed with PBS and treated with a solution of 0.5 % crystal violet (1.15940.0025, Merck) and 20% ethanol (1.00983.1000, Merck). Once the colonies were stained, this solution was removed and plates were washed with water and let them dry. The number of colonies per well was scored.

1.7. Flow cytometry

1.7.1. Cell cycle analysis

To analyse cell cycle, cells were harvested by trypsinization and spinned down at 500 g for 5 minutes. Then, they were washed with PBS and resuspended in 200 μl ice-cold PBS. Cells were fixed by adding 5 ml of cold 70% ethanol dropwise while vortexing at low speed and they were incubated at 4ºC for at least 2 hours. Cells were centrifuged at 500 g for 5 minutes, washed with PBS and treated with 250 μg/ml RNAse A (R6148, Sigma) and 10 μg/ml propidium iodide (81845, Fluka)

diluted in PBS for 30 minutes at 37ºC, keeping the samples in the dark. Finally, cell cycle was analysed using BD FACSCalibur Flow Cytometer (342975, BD Biosciences) and CellQuest Pro software.

1.7.2. Titration of lentiviral production

As mentioned before (section 1.4.), production of lentiviruses harbouring pBFP-ISceI plasmid was titrated by measuring BFP expression using a flow cytometer. To do so, 25.000 cells per well were seeded in 12-well plates. The following day, culture medium was removed and 300 μl fresh DMEM supplemented with 8 μg/ml hexadimethrine bromide were added. Then, one aliquot of viruses was thawed and diluted 1/10 in DMEM, and 0, 5, 10 or 20 μl of this solution were added to each well for infection. After 6 hours of incubation at 37ºC in a P2 biological safety room, the volume was completed with 700 μl fresh DMEM. Next day, cells were washed with DMEM and incubated another 24 hours upon addition of fresh medium. Finally, cells were harvested by trypsinization and pelleted by centrifugation at 800 g for 5 minutes in FACs tubes. Samples were washed with PBS and resuspended in 150 μl PBS, keeping them at 4ºC and in the dark until they were further analysed. BFP expression in each cell was then measured by cytometry using BD FACSAria™ (BD Biosciences) and FACSDiva v5.0.3 software. The highest dilution factor that still resulted in 25-50% of the cells positive for BFP signal was used to calculate viral titer.

1.7.3. Fluorescent proteins analysis by flow cytometry

DNA double-strand breaks repair systems restore expression of a fluorescent protein when a specific pathway repairs the damage (see paragraph 1.8.1.). Cells bearing a single copy integration of the reporters SA-GFP, DR-GFP, EJ5-GFP or SSR were downregulated for the indicated genes and infected with lentiviruses harbouring pBFP-ISceI plasmid to generate the break. Cells were then harvested with trypsin, spinned down at 800 g for 5 minutes and washed with PBS. To prevent losing fluorescence, cells were fixed with 4% paraformaldehyde for 20 minutes at 4ºC in the dark, and later rinsed and resuspended in 150 μl of fresh

PBS. Samples were kept on ice in the dark until they were analysed by flow cytometry using BD FACSAria™ and FACSDiva v5.0.3 software. The percentage of green cells, and red cells in the case of SSR system, was calculated from a total of 10.000 events that were BFP positive, i.e. harbouring the I-SceI nuclease.

1.8. DSBs repair assays *in vivo*

To study the influence of PRMT5 and CCAR2 in DSB repair pathways, we took advantage of different repair systems, which we described below. In all of them, the DSB is generated by the rare-cutting endonuclease I-SceI, whose 18-pb recognition sequence has been integrated in the sequence. The repair of the damage results in the expression of a fluorescent protein (GFP, or also RFP in SSR) that could be quantified by flow citometry.

1.8.1. Description of repair systems used

To test DSB repair by homologous recombination, SA-GFP and DR-GFP reporters (figure M1, panels a and b) were used since each one measures a different HR pathway. SA-GFP (Stark *et al*., 2004) consists of two *GFP* gene fragments (5'GFP and 3'GFP) that share 266 bp of homology (marked in grey) and are separated by 2.7 kb. I-SceI site is present in the downstream *GFP* fragment inside the region of homology. Repair of the I-SceI-induced DSB by single-strand annealing gives rise to a functional *GFP* gene after annealing of complementary strands of both *GFP* fragments in an intramolecular event, followed by appropriate DNA-processing steps that produce a 2.7 kb deletion in the chromosome. This reporter could also be repaired by other homology-directed repair (HDR), but without restoration of a functional *GFP* gene.

DR-GFP (Pierce *et al*., 1999) system, which is not sensitive to study SSA, was used to measure HDR efficiency, specifically short tract gene conversion. This reporter is composed of a full-length *GFP* gene mutated at a BcgI restriction site to contain the recognition site for the I-SceI endonuclease. This mutation consists of a substitution of 11 bp of the wild-type GFP sequence that supplies two in-frame stop-codons, which terminate translation and inactivate the protein. Downstream

of this gene and oriented as direct repeat, is integrated an 812-bp internal *GFP* fragment (iGFP). Homologous sequences in the two mutated *GFP* genes (marked in grey) are separated along 3.7 kb by the puromycin N-acetyltransferase gene. When I-SceI-induced DSB is produced, iGFP sequence could act as a donor of wild-type sequence information to the broken gene for repairing by noncrossover gene conversion within the limited amount of homology. Then, a short tract gene conversion product is generated with restoration of an intact *GFP* gene. There are other possible homologous recombination outcomes, including crossover recombination, long tract gene conversion or SSA pathway. These events retain only the 5' fragment of the *GFP* gene that would encode a carboxy-terminal truncation, so there will be no accumulation of fluorescence in the cells.

Otherwise, NHEJ was measured by EJ5-GFP (Bennardo *et al*., 2008; figure M1, panel c). This reporter contains a promoter that is separated from a GFP coding cassette by the puromycin (puro) gene flanked by two I-SceI sites in the same orientation. Once the two DSBs are produced after I-SceI expression, they are repaired by NHEJ. Then, puromycin gene is excised and the promoter is joined to the rest of the expression cassette, leading to restoration of *GFP* gene. The repair of the breaks results in reconstitution of the I-SceI site as the two I-SceI-induced DSBs have complementary 3' overhangs. Alternatively, NHEJ could fail to restore the I-SceI site, generating an I-SceI resistant site that shows evidence of microhomology, suggesting that this repair product is one measure of alternative-NHEJ. Hence, EJ5-GFP reporter could detect different end-joining events, each giving rise to green cells, considering it as an assay to study total-NHEJ.

Finally, SSR system (Gómez-Cabello *et al*., 2013; figure M1, panel d) was used to analyse the influence in the repair pathway choice by measuring the balance between NHEJ and HR. This reporter consists of the *GFP* gene flanked by a 5'- and a 3'-end truncated fractions of the *RFP* gene that share 302 bp of homology with each other (marked in grey). Two I-SceI restriction sites were inserted downstream of the *GFP* gene, close to each other in an inverted orientation. Since the I-SceI target site is not palindromic, the repair of the inverted I-SceI-mediated breaks by NHEJ destroys the target sequence. Once DSBs are induced by the expression of the I-SceI meganuclease, cells could repair the damage through a classical NHEJ-type of repair, leading to *GFP* gene restoration and hence

fluorescence in green. Alternatively, these breaks could be resected, thereby inhibiting classical NHEJ, and the homologous regions of the RFP fragments are then exposed and used to repair the damage by SSA. This type of homologous recombination excises the *GFP* gene and creates a functional *RFP* gene, giving rise to cells that fluoresce in red.

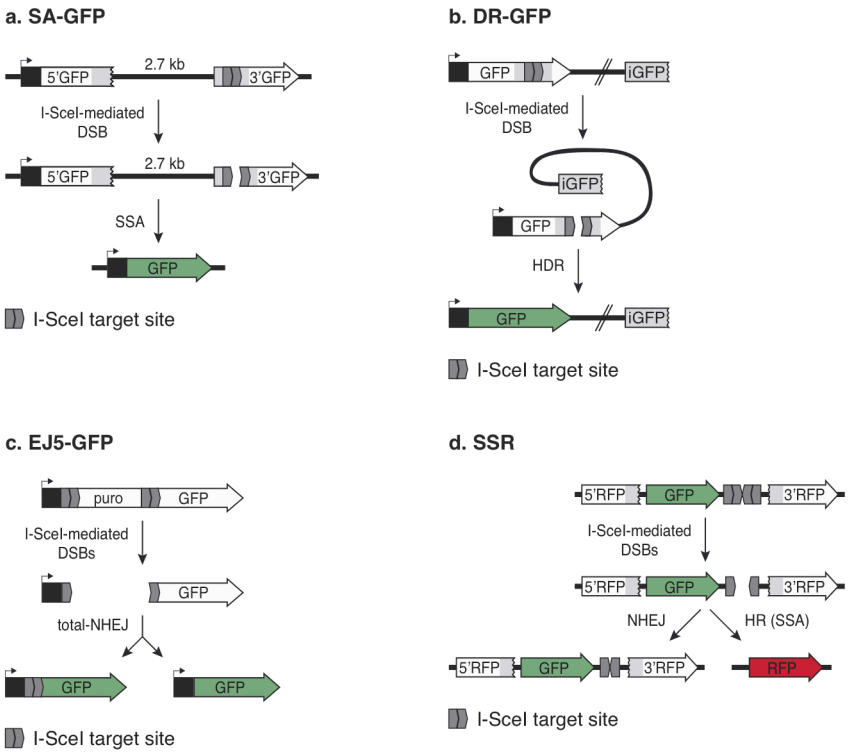

Figure M1. Schematic representation of the DSBs repair systems used. a, SA-GFP reporter that measures SSA. **b**, DR-GFP reporter that measures gene conversion. **c**, EJ5-GFP reporter that measures total-NHEJ. **d**, SSR system that measures the balance between NHEJ and HR. Homology regions in the different reporters are marked in grey.

1.8.2. DSBs repair assays *in vivo*

Cells bearing a single copy integration of SA-GFP, DR-GFP, EJ5-GFP or SSR systems were used to analyse the role of PRMT5 and CCAR2 in the different DSB repair pathways. To carry out the repair assays, 50.000 cells/well were plated in 6-well plates. One day after seeding, the indicated proteins were downregulated by using different siRNAs or shRNAs against them, including CtIP and a non-target sequence as positive and negative controls. The medium was changed after 6-8 hours. The

following day, cells were infected with lentivirus harbouring I-SceI and BFP with a MOI of 10. DMEM containing lentiviral particles was supplemented with 4 μg/ml hexadimethrine bromide to enhance transduction, as indicated in section 1.4. DMEM including hexadimethrine bromide but without lentivirus was added to another set of depleted cells as control of basal fluorescence. After 24 hours, cells were washed with fresh medium and maintained in culture during an additional day. Cells were then harvested and fixed with 4% paraformaldehyde followed by the analysis by flow citometry of the blue, green and, in the case of SSR, red fluorescence, as described in paragraph 1.7.3.

The repair frequency for SA-GFP, DR-GFP and EJ5-GFP reporters was calculated as the percentage of green cells from 10.000 events positive for blue fluorescence, considering the background of green fluorescence obtained in the samples without infection with lentivirus harbouring pBFP-ISceI plasmid as previously described (Stark *et al.*, 2004; Pierce *et al.*, 1999; Bennardo *et al.*, 2008). Otherwise, the balance between NHEJ and HR with the SSR was calculated by dividing the number of cells expressing GFP by the number of cells expressing RFP from the total 10.000 blue-positive events analysed, again normalizing with the basal fluorescence observed in the samples without I-SceI infection (Gómez-Cabello *et al.*, 2013). To facilitate the comparison between experiments, the percentage or the ratio calculated were normalized with the control siNT or shNT in each case.

1.9. DSB induction by ionizing radiation

An irradiator device that emits gamma rays (BIOBEAM GM 8000, Gamma-Service Medical GmbH) was used to induce double-strand breaks in the cells. The damage was generated by exposure of the samples to an encapsulated radioactive source (Cs-137). Cells were irradiated in plates containing culture medium, using a dose of 10 Gy, or 2 and 5 Gy in the case of clonogenic assays. The irradiator is adjusted to the dose rate on the cover surface does not exceed 3 μSv/h.

2. Molecular Biology procedures

2.1. DNA manipulations

2.1.1. Plasmid DNA amplification

Plasmid DNA was amplified using competent cells of the DH5α strain of *Escherichia coli*. To do so, bacteria were transformed using heat shock protocol and DNA was later purified. Briefly, 100 μl competent bacteria were mixed with plasmid DNA and incubated for 30 minutes on ice. Then, cells were placed at 42ºC for 85 seconds and returned into ice for a heat shock. After 3-5 minutes, 1 ml LB (LB-Broth Lennox, Formedium™) media was added and the transformed cells were incubated at 37ºC for 30 minutes. Cells were harvested by centrifugation at 6000 rpm for 2 minutes and plated in LB supplemented with 100 μg/ml ampicillin (A9518, Sigma) or 25 μg/ml kanamycin (K4000, Sigma), according to the selection marker of the plasmid. DNA was purified from one single bacterial colony using PureYield™ Plasmid Maxiprep System (A2393, Promega) following the manufacturer's instructions. DNA concentration in the sample was quantified by measuring the absorbance at 260 nm using a spectrophotometer ND-1000 (NanoDrop®).

2.1.2. DNA digestion with restriction enzymes

For DNA cloning and plasmids checking, restriction endonucleases from Takara or New England Biolabs were used according to the manufacter's instructions.

2.1.3. Site-directed mutagenesis

Changes in DNA sequence of some plasmids were performed using a QuickChange Lightning Site-Directed Mutagenesis kit (210518, Agilent Technologies) according to the manufacter's instructions. Briefly, mutated plasmid was generated after thermal cycling with designed mutagenic primers (Table M4) containing the

desired mutation(s). Then, methylated and hemimethylated DNA, corresponding with the non-mutated template, was digested using DpnI endonuclease. Finally, mutation-containing synthesized DNA was transformed into competent bacteria and amplified.

Table M4. DNA primers used in this study.

Primer	Sequence 5'-3'	Use
Mut.siDBC1 Fw	GTGACCCCGCTTATAGCAGCAAGGTACTGCTGCTCTCTTCC	Mutagenesis in *CCAR2* sequence to avoid siRNA-mediated depletion
Mut.siDBC1 Rv	GCAGCAGTACCTTGCTGCTATAAGCGGGGTCACTGTCTGC	
Mut2.DBC1 Fw	GCAGCTCCCCCAGCCCAGGAGGCACAAGGGG	Mutagenesis in *CCAR2* sequence to obtain T454A mutant
Mut2.DBC1 Rv	GTGCCTCCTGGGCTGGGGGAGCTGCCTCTGC	
EGFP*-C	CACGAACTCCAGCAGGACCATG	PCR amplification of a *GFP* fragment to obtain a DNA probe used in Southern blot
EGFP*-N	CTGGTCGAGCTGGACGGCGACG	

2.1.4. DNA electrophoresis in agarose gels

DNA electrophoresis was performed on gels containing a variable percentage of agarose (8014, pronadisa), depending on the size of the bands to differentiate, and RedSafe™ (21141, Intron Biotechnology) for nucleic acid staining, both diluted in TAE 1X buffer (40 mM Tris pH 7.6, 20 mM acetic acid and 1 mM EDTA). Loading

Buffer (Takara) was added to the DNA samples (1X concentrated) prior to loading in the gel and 1 kb DNA ladder (GTPBM0002, gTPbio) was used to identify the approximate size of the bands. Stained DNA was visualized using an ultraviolet transilluminator (Bio-Rad) and the Quantity One software.

2.1.5. Southern blot analysis of human cells

U2OS cells stably expressing SA-GFP or EJ5-GFP systems were generated in our lab and they were later analysed by Southern blot to select a clone of each cell line that harboured single-copy integration of the reporters (Figure M2).

First, to extract genomic DNA, cells were harvested, resuspended in 300 μl of lysis buffer (50 mM Tris-HCl pH7.5, 100 mM NaCl, 5 mM EDTA and 0.5% sodium dodecyl sulphate (SDS)) containing 20 μg/ml proteinase K (P2308, Sigma) and incubated 2 hours at 55ºC with shaking. To facilitate DNA precipitation, 1.2 M NaCl was added and shaken before centrifuged at 13000 rpm for 5 minutes at 4ºC. DNA was precipitated overnight at -80ºC with 1 volume of isopropanol (131090.1211, AppliChem), and centrifuged at 13000 g for 15 minutes. The DNA pellet was washed with ice-cold 70% ethanol and resuspended in 50 μl mili-Q water. Then, 50 μg of genomic DNA were digested for 4 hours with BamHI (at 30ºC) or EcoRV (at 37ºC) endonucleases (Takara), which generate a single cut in hprtSAGFP or pimEJ5GFP plasmids, respectively. Simultaneously, 50 ng of plasmidic DNA were also digested as control. Samples were resolved on 0.8% agarose gel at 50 V overnight. Gel was treated 30 minutes with denaturing solution (1.5 M NaCl and 0.5 M NaOH) to denature double-stranded DNA, followed by a wash with distilled water and two washes of 15 minutes each with neutralizing solution (0.5 M Tris-HCl pH 7.5 and 1.5 M NaCl). DNA was then transferred to a Hybond-N+ membrane (RPN303N, Amersham) by capillarity blotting overnight and crosslinked at 700J/cm^2 in an UV Stratalinker® 2400 (Stratagene).

Southern blot analyses were performed according to standard procedures with ^{32}P-radiolabelled probes. The DNA probe consisted of a GFP fragment obtained by Polymerase Chain Reaction (PCR) amplification from pEGFP-C1 plasmid using primers indicated in table M4. The purified DNA product was denatured by incubation at 90ºC for 5 minutes and was quickly chilled on ice for 5

minutes. Afterwards, the probe was labelled with 500 μg/ml N6 random primers, 0.25 mM of each dATP, dGTP and dTTP, 0.025 mM dCTP, 1 mCi/ml [^{32}P]dCTP and 5U Klenow polymerase (2140A, Takara) during 2 hours at 37ºC. Labelled probe was purified using G50 columns.

The membrane was hybridized with the GFP-labelled fragment in hybridization buffer (0.25 M Na_2HPO_4, 0.2% H_3PO_4, 7% SDS and 1 mM EDTA) overnight at 65ºC, washed three times at 50ºC with washing buffer (0.1X SSC 20X (150 mM NaCl and 15 mM Na-Citrate), 1 mM EDTA and 1% SDS) and radioactive signals were acquired using PhosphorImager Fujifilm FLA-5100. Clones bearing a single-copy integration of the reporters were used for further DSBs repair assays (Figure M2).

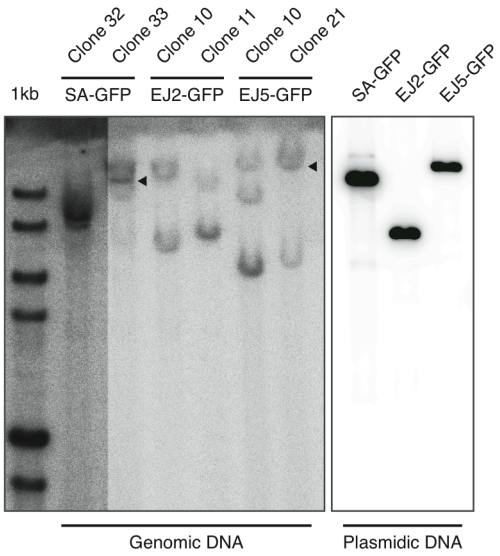

Figure M2. Analysis of the repair systems integrated in different clones. Southern blot analysis of different U2OS clones transfected with SA-GFP, EJ2-GFP or EJ5-GFP reporters. Clones used in DSBs repair assays, which harboured a single-copy DNA insertion, are marked with a black triangle. 1Kb means 1Kb DNA ladder from gTPbio.

2.2. Protein analysis

2.2.1. Protein extraction under denaturing conditions

For protein extraction, Laemmli 2X buffer (125 mM Tris-HCl pH 6.8, 4% SDS and 20% glycerol (49770, Sigma)) was added directly on the plates, previously washed with PBS, and adherent cells were scraped off the dish using a plastic cell scraper

(83.1830, Sarstedt). The cell suspension was then transferred into a microcentrifuge tube. Alternatively, cells were harvested with trypsin, rinsed with PBS and resuspended in Laemmli 2X buffer. Chromatin was sheared by passing the solution through a syringe with a 0.5x16 mm needle (BD Plastipak) at least 10 times. Cellular debris was removed by spinning down the samples at 13000 rpm for 5 min. Supernatant was collected and quantified (see paragraph 2.2.3.).

2.2.2. Protein extraction under native conditions

For immunoprecipitation and pull-down assays, protein extracts were prepared under native conditions to keep protein interactions. Thus, protease (11873580001, Roche) and phosphatase inhibitors cocktails (P0044, Sigma) had to be added into the lysis buffer. Cells growing in 150-mm plates were placed on ice, rinsed with cold PBS and scraped off the dish after adding cold lysis buffer. Lysis buffer used for maintaining native conditions had no SDS and a low detergent concentration, but its composition varied according to the requirements of each experiment (see paragraphs 2.2.7. and 2.2.8.). Cell suspension was passed through a syringe with a 0.5x16 mm needle (BD Plastipak) at least 10 times and was centrifuged at 13000 rpm for 5 min at 4ºC to remove cellular debris. Supernatant was collected and quantified (see section 2.2.3.).

2.2.3. Protein quantification

Two different quantification procedures were used depending on the samples. For protein extracts obtained under native conditions, concentration of proteins was measured using Bradford assay. This method is based on the formation of a complex between the dye (brilliant blue G) and proteins in solution, which shift the absorbance of the dye in proportion to the protein present. Bovine serum albumin (BSA) dilutions were used in order to create a standard curve used to determine the concentration of the unknown protein. Samples containing 0, 1, 2, 5, 10 and 20 μg/ml BSA (A4503, Sigma) diluted in mili-Q water up to a final volume of 100 μl were prepared, and 900 μl Bradford reagent (B6916, Sigma) was added. Next, our samples were prepared in mili-Q water up to a final volume of 100 μl with a

dilution factor that gave a concentration in the range of BSA dilutions, and 900 μl Bradford reagent was added. Optical density was measured at a wavelength of 595 nm using a spectrophotometer DU® 800 (Beckman Coulter). BSA concentration was plotted on the X-axis and its absorbance on the Y-axis to create the standard curve. Then, the equation that represents the graph was determined by linear regression and used to calculate protein concentration in our samples based on their absorbance.

Nevertheless, SDS used in Laemmli buffer for protein extraction under denaturing conditions interferes with the Bradford assay, generating erroneous results. Thus, an approximate value of protein concentration in these samples was obtained by measuring the absorbance at 280 nm using a spectrophotometer ND-1000 (NanoDrop®).

2.2.4. Sodium dodecyl sulphate polyacrylamide gel electrophoresis (SDS-PAGE)

Proteins were separated by size in 29:1 acrylamide:bis-acrylamide gels with concentrations appropriate to the molecular weight of the proteins to analyse. SDS-PAGE was performed according to previously described method (Laemmli, 1970). Samples were prepared with 50-100 μg protein extracts and protein loading buffer 4X (250 mM Tris-HCl pH 6.8, 8% SDS, 40 % glycerol, 20% β-mercaptoethanol (M6250, Sigma) and bromophenol blue) to a final concentration of 1X, and were boiled at 100ºC for 5 minutes. Prestained protein ladder (GTPBM003, gTPbio) was also loaded in the gel. Electrophoresis was performed in a Mini-PROTEAN® Tetra Cell (Bio-Rad) with Running Buffer (25 mM Tris-HCl pH 8.3, 194 mM glycine and 0.1% SDS) at 100-150 V.

However, samples obtained after Tandem Affinity Purification were resolved using a gradient gel with an acrylamide:bis-acrylamide (29:1) percentage from 6% to 15%, prepared with a gradient mixer (Z340413, Sigma). In this case, electrophoresis was performed in a Tall Standard Dual Cooled Vertical Unit (SE660, Hoefer) at 200 V until dye front moved through the stacking gel and then at 70 V overnight.

2.2.5. Immunoblotting (western blot analysis)

For western blot, proteins were wet-transferred using Mini Trans-Blot® system (Bio-Rad) for 1.5-2 hours at 400 mA in Transfer Buffer (25 mM Tris-HCl pH 8.3, 190 mM glycine, 20% methanol and with or without 0.1% SDS). Two different procedures were used for immunoblotting. ECL detection protocol was used during the set up of TAP, but the rest of the western blot analyses were performed according to Odyssey protocol.

2.2.5.1. ECL detection

Proteins were transferred to nitrocellulose membranes (Hybond ECL RPN203D, Amersham), which were stained with Ponceau S (0.1% w/v Ponceau S (78376, Sigma) in 5% acetic acid (45726, Sigma)) to check protein loading and transference. Transfer buffer used did not contain any detergent. Then, membranes were blocked with 5% powder milk or BSA (depending on the antibodies used) diluted in a solution of TBS with 0.05% Tween-20 (TBS-T) for at least 1 hour at room temperature with shaking. Primary antibodies (Table M5) diluted in TBS-T were incubated for at least 2 hours at room temperature or overnight at 4ºC with shaking. After three washes with TBS-T of 5 minutes each, membranes were incubated with the corresponding secondary antibodies conjugated with the horseradish peroxidase (Table M6) for 1 hour at room temperature and washed again three times for 15 minutes. Finally, peroxidase substrate for enhanced chemiluminescence (ECL; K-12045-D20, Advansta) was used for signal detection with a Kodak X-OMAT 2000 Processor in a developing room.

2.2.5.2. Odyssey scanning

A PVDF membrane with low fluorescence background (IPFL00010, Immobilon-FL, Millipore) was used. This membrane was first activated in methanol for 1 minute, washed in water and equilibrated in transfer buffer (containing 0,1% SDS) before the transference. Commercial Odyssey Blocking Buffer (927-40000, LI-COR

Biosciences) was used for blocking the membrane for at least 1 hour at room temperature. Primary antibodies (Table M5) were diluted in blocking buffer containing 0.1% Tween-20 and were incubated for at least 2 hours at room temperature or overnight at 4ºC with shaking. Then, three washes of 5 minutes were performed with 0.1% Tween-20 in TBS, followed by 1 hour incubation with the corresponding IRDye secondary antibodies (Table M6) diluted in blocking buffer containing 0.1% Tween-20. Finally, membranes were washed again three times for 10 minutes, rinsed in TBS and immediately scanned or left to dry. Image acquisition was performed in an Odyssey CLx Imaging System (LI-COR Biosciences) at two infrared wavelengths (700 and 800 nm) and using Image Studio v.2.1 software.

Table M5. Primary antibodies used in this study. WB, western blotting. IF, immunofluorescence. SMART, Single Molecule Analysis of Resection Tracks. IP, immunoprecipitation. PLA, Proximity Ligation Assay

Target protein	Source	Supplier/Reference	Application	Dilution
CtIP	Mouse	R. Baer (14.1)	WB, PLA	1:500, 1:200
FLAG	Mouse	Sigma (F3165)	WB	1:1000
GFP	Rabbit	Santa Cruz (sc-8334)	WB	1:1000
α-tubulin	Mouse	Sigma (T9026)	WB	1:50000
PRMT5	Rabbit	Abcam (ab31751)	WB	1:1000
CCAR2	Rabbit	Bethyl Laboratories (A300-433A-1)	WB, IF	1:1500, 1:150
CCAR2	Rabbit	Bethyl Laboratories (IHC-00135)	PLA	1:200
SF3B3	Goat	Abcam (ab3608)	WB	1:2000
SFPQ	Rabbit	Abcam (ab38148)	WB	1:1000

Target protein	Source	Supplier/Reference	Application	Dilution
DHX9	Rabbit	Bethyl Laboratories (A300-855A-1)	WB	1:1500
DHX15	Rabbit	Bethyl Laboratories (A300-118A-1)	WB	1:500
KIF11	Mouse	Novus Biologicals (NB100-78467)	WB	1:1000
RBM10	Rabbit	Bethyl Laboratories (A301-006A)	WB	1:5000
RPA32	Mouse	Abcam (ab2175)	IF	1:500
γ-H2AX	Rabbit	Cell Signaling (2577L)	IF	1:500
γ-H2AX	Mouse	Millipore (05-636)	IF	1:1000
BRCA1	Mouse	Santa Cruz (sc-6954)	WB	1:1000
SIRT1	Rabbit	Novus Biologicals (NB110-57573)	WB	1:1000
MRE11A	Rabbit	Novus Biologicals (NB100-142)	WB, IP	1:5000, 5 μl
IgG from rabbit serum	Rabbit	Sigma (I8140)	IP	5 μg
BrdU	Mouse	Amersham (RPN202)	SMART	1:1000

Table M6. Secondary antibodies used in this study. WB, western blotting. IF, immunofluorescence. SMART, Single Molecule Analysis of Resection Tracks.

Antibody	Supplier/Reference	Application	Dilution
Anti-mouse IgG, HRP-linked whole antibody	GE Healthcare (NA931V)	WB	1:10000

Antibody	Supplier/Reference	Application	Dilution
Anti-rabbit IgG, HRP-linked whole antibody	GE Healthcare (NA934V)	WB	1:10000
IRDye 680RD goat anti-mouse IgG (H+L)	LI-COR (926-68070)	WB	1:5000-1:25000
IRDye 800CW goat anti-rabbit IgG (H+L)	LI-COR (926-32211)	WB	1:5000-1:25000
IRDye 800CW donkey anti-goat IgG (H+L)	LI-COR (926-32214)	WB	1:5000-1:25000
Alexa Fluor 594 goat anti-mouse IgG (H+L)	Invitrogen (A11032)	IF, SMART	1:1000
Alexa Fluor 488 goat anti-rabbit IgG (H+L)	Invitrogen (A11034)	IF	1:1000
Alexa Fluor 568 goat anti-mouse IgG (H+L)	Invitrogen (A11031)	IF	1:1000
Alexa Fluor 647 goat anti-rabbit IgG (H+L)	Invitrogen (A21245)	IF	1:1000

2.2.6. Silver staining

Silver staining was performed to detect proteins after electrophoresis. Besides its sensitivity, this protocol was mainly used because is also compatible with downstream processing such as mass spectrometry. To get better staining, 1 mm thick gels were prepared because silver solution could not completely penetrate the ones 1,5 mm thick.

After SDS-PAGE, gel was fixed in a solution of 50% methanol, 12% acetic acid and 0.5 ml/l 37% formaldehyde (33220, Sigma) for at least 2 hours up to overnight. Then, gel was rinsed in 50 % ethanol for at least 30 minutes and sensitized by soaking for exactly 1 minute in 0.2 g/l sodium thiosulfate (217263, Sigma) with gentle shaking. Gel was washed three times in distilled water for 20

seconds each and impregnated in another container with a solution of 2 g/l silver nitrate (1015120025, Merck) and 0.75 ml/l formaldehyde for 1 hour. Gel was washed twice in distilled water for 30 seconds each time and moved to another container to develop with a solution of 60 g/l sodium carbonate (71358, Sigma), 4 mg/l sodium thiosulfate and 0.5 ml/l formaldehyde with gentle shaking. Bands appeared after one or several minutes and reaction was stopped just before correct exposure was reached by soaking the gel in 1% acetic acid. Finally, gel was rinsed and kept in water until cutting the bands or drying and imaging it.

2.2.7. Protein immunoprecipitation

2.2.7.1. Tandem Affinity Purification

The final protocol set up for Tandem Affinity Purification assay was performed with protein extracts from U2OS GFP-6XFLAG-CtIP and U2OS as control, and also from the clone synchronized in different phases of the cell cycle. These protein extracts were prepared under native conditions to keep protein complexes (see paragraph 2.2.2.) with lysis buffer (50 mM Tris-HCl pH 7.5, 100 mM NaCl, 1 mM EDTA, 0.2% Triton X-100, 1X protease inhibitors and 1X phosphatase inhibitor cocktail 3), and 6 mg were used for purification.

In the first step of immunoprecipitation, 300 μl of anti-FLAG resin (ANTI-FLAG® M2 Affinity Gel, A2220, Sigma) for each sample were pre-equilibrated by washing three times with lysis buffer, and next were incubated with protein extracts overnight at 4ºC with gentle rocking. Proteins that did not bind to the beads were removed by washing the samples three times 15 minutes with lysis buffer. Afterwards, three rounds of incubation with 300 μg/ml 3XFLAG peptide diluted in lysis buffer for 1 hour at room temperature were performed to elute CtIP complexes.

After elution with 3XFLAG peptide, a second step of immunoprecipitation was performed using anti-GFP resin (GFP-Trap®_M, Chromotek). Eluates obtained from the three rounds of elution were mixed and incubated overnight at 4ºC with gentle rocking with 50 μl of pre-equilibrated beads. Then, samples were washed three times for 15 minutes with lysis buffer, transferring the resin to a new tube

after each wash to eliminate proteins bound to the tube. Finally, precipitated proteins were eluted by boiling the samples for 5 minutes in protein loading buffer. Next, the samples were resolved by SDS-PAGE and silver stained.

2.2.7.2. Immunoprecipitation using magnetic GFP beads

Cells overexpressing GFP or GFP-tagged proteins were seeded and treated accordingly to the requirements of the experiment. Protein extracts were prepared under native conditions (see paragraph 2.2.2.) using lysis buffer (50 mM Tris-HCl pH 7.5, 50 mM NaCl, 1 mM EDTA, 0.2% Triton X-100, 1X protease inhibitors and 1X phosphatase inhibitor cocktail 3). Protein extracts (1 mg) were mixed with 20 μl of pre-equilibrated magnetic anti-GFP resin and incubated overnight at 4ºC with gentle rocking. Beads were then washed three times with lysis buffer and elution was carried out by boiling the samples for 5 minutes in lysis buffer with 1X protein loading buffer. Finally, precipitated proteins were resolved by SDS-PAGE and analysed by western blotting.

2.2.7.3. Immunoprecipitation using protein A resin

Dynabeads® Protein A (10001D, Novex, Life Technologies) and anti-Mre11 antibody were used for Mre11 immunoprecipitation. U2OS cells were seeded in 150-mm plates and the following day were transfected with siNT and siCCAR2 for downregulation. To avoid reaching confluence, cells were divided into two plates and 48 hours after transfection were harvested. In those experiments performed under damage conditions, cells were irradiated (10 Gy) and incubated for 1 hour at 37ºC before harvested. Proteins extracts were prepared under native conditions (see paragraph 2.2.2.) using lysis buffer (50 mM Tris-HCl pH 7.5, 50 mM NaCl, 1 mM EDTA, 0.2% Triton X-100, 1X protease inhibitors and 1X phosphatase inhibitor cocktail 3). Before incubation with protein extracts, 70 μl Dynabeads Protein A for each sample were pre-equilibrated by washing the resin three times for 5 minutes at 4ºC with lysis buffer without protease and phosphatase inhibitors, and a fourth wash with lysis buffer containing the mentioned inhibitors. Then, 1 mg protein extract was pre-cleared to reduce non-specific binding by incubation with 20 μl

pre-equilibrated beads for 1 hour at 4ºC with gentle rocking. After pre-clearing, extracts were recovered and incubated with 5 μl anti-Mre11 antibody, or 5 μg Rabbit IgG as negative control, for 30 minutes at 4ºC. The remaining pre-equilibrated beads (50 μl for each sample) were added to the mixture of proteins and antibody and were incubated overnight at 4ºC with gentle rocking. The day after, beads were washed three times with lysis buffer for 5 minutes at 4ºC and, finally, samples were boiled for 5 minutes in 40 μl lysis buffer with 1X protein loading buffer to elute proteins complexes bound to the resin. Precipitated proteins were then resolved by SDS-PAGE and analysed by immunoblotting.

2.2.8. Pull-down assay from whole cell extracts

Protein extracts from cells transfected with the different versions of GFP-CCAR2 and the control GFP plasmid were prepared in lysis buffer (20 mM Tris-HCl pH7.5, 50 mM NaCl, 1 mM EDTA, 0.5 % Triton X-100, 1X protease inhibitors and 1X phosphatase inhibitor cocktail 3). The amount of expression of GFP and each CCAR2 fragment in the samples was calculated by western blotting. Similar amounts of GFP, GFP-CCAR2 and each CCAR2 truncated version were used for pull down assays. After adding β-mercaptoethanol to the samples to a final concentration of 10 mM, cell extracts were pre-cleared by incubating with 50 μl of pre-equilibrated glutathione sepharose 4B resin (17-0756-01, GE Healthcare) for 1 hour at 4ºC with gentle rocking.

Eighty pmol of bacterial-purified GST-CtIP (a gift from Dr. María Isabel Martínez Macías) were resuspended in a final volume of 500 μl with PBS, mixed with 100 μl of pre-equilibrated glutathione sepharose 4B resin and incubated for 1 hour at 4ºC. The resin was washed twice with binding buffer (lysis buffer with 10 mM β-mercaptoethanol but without protease and phosphatase inhibitors) and then incubated with the pre-cleared cell extracts for 2 hours at 4ºC with gentle rocking. Beads were washed twice with wash buffer (binding buffer with 3 mM L-glutathione reduced (G4251, Sigma)) and proteins were eluted by boiling the slurry for 5 minutes in wash buffer with 1X protein loading buffer. Precipitated proteins were resolved by SDS-PAGE (with a 10% acrylamide:bis-acrylamide gel),

transferred to PVDF membranes and analysed by western blot using anti-GFP antibody.

2.2.9. Cycloheximide chase assay

In order to analyse the effect of PRMT5 in CtIP stability, cells were exposed to cycloheximide, an inhibitor of protein biosynthesis that prevents translational elongation. U2OS cells were depleted of PRMT5 by shRNAs or siRNAs, and a non-target sequence was used as control (shNT and siNT). Then, cells were treated with fresh medium containing 150 μg/ml cycloheximide (C7698, Sigma) 48 hours post infection or transfection. Cells were collected 2, 4 and 8 hours after the cycloheximide addition and protein samples were prepared as described in section 2.2.1. Protein extracts from cells before the treatment were used as control of the initial amount of proteins. Finally, samples were resolved by SDS-PAGE, analysed by immunoblotting and protein quantification was made using Image Studio v.2.1 software. CtIP expression was calculated as the amount of CtIP divided by α-tubulin signal.

3. Microscopy procedures

3.1. RPA/γH2AX foci immunofluorescence

U2OS cells were infected with lentivirus harbouring the indicated shRNA or a control sequence. After 48 hours, cells growing on coverslips were irradiated (10 Gy) or mock treated, incubated 1 hour to allow foci formation, washed once with ice-cold PBS and collected. Coverslips were treated for 5 minutes on ice with pre-extraction buffer (25 mM Tris-HCl pH 7.5, 50 mM NaCl, 1 mM EDTA, 3 mM MgCl2, 300 mM sucrose and 0.2% Triton X-100) to remove the nucleoplasmic and cytoplasmic proteins, leaving behind the chromatin-bound and matrix-associated proteins. Cells were then washed once with cold PBS, fixed with 4% paraformaldehyde (w/v) in PBS for 15 minutes on ice, washed three times with PBS and blocked for at least 1 hour with blocking solution (5% FBS diluted in PBS).

Afterwards, cells were incubated for at least 2 hours at room temperature or overnight at 4ºC with the adequate primary antibodies (Table M5) diluted in blocking solution. Coverslips were washed three times with cold PBS, incubated with secondary antibodies (Table M6) for 1 hour at room temperature in the dark, washed again with PBS, dried and mounted with Vectashield Antifade mounting medium (H-1200, Vector Laboratories) containing 4',6-diamidino-2-phenylindole (DAPI). At least 200 cells per sample per experiment were analysed using Leica Fluorescence microscope.

3.2. CCAR2 foci immunofluorescence

U2OS cells were irradiated (10 Gy) or mock treated and incubated 5, 15, 30 and 60 minutes at 37ºC for foci formation before being collected. In the experiments performed with the inhibitors, the medium was exchanged with fresh DMEM containing 10 μM ATMi, 5 μM ATRi, 1 μM PARPi or DMSO as vehicle, 30 minutes before irradiation, followed by incubation for 1 hour after the damage. Cells were washed once with cold PBS, fixed with 4% paraformaldehyde (w/v) in PBS for 15 minutes on ice, washed twice with PBS and permeabilized for 10 minutes on ice with 0.2% Triton X-100 diluted in PBS. Coverslips were washed twice PBS and blocked for at least 1 hour with 5% FBS diluted in PBS. Incubation with primary and secondary antibodies, coverslips mounting and analysis were carried out as for RPA/γH2AX foci immunofluorescence (paragraph 3.1.), using the appropriate antibodies (Tables M5 and M6).

3.3. Proximity ligation assay

Proximity ligation assay was performed using the Duolink PLA kit (Olink Bioscience) according to the manufacturer's protocol. This technique allows visualization and quantification of protein interactions in cells samples prepared for microscopy. For that, two primary antibodies raised in different species were used to detect the target proteins, and then secondary antibodies conjugated with oligonucleotides (PLA probes) were added to the reaction. If they are in close proximity, ligation solution containing ligase and two oligonucleotides hybridized

the two PLA probes generating a closed circle that acted as a template for rolling-circle amplification. Finally, fluorescently labelled oligonucleotides hybridized with the amplification product generating the signal, visualized as an individual fluorescent spot.

U2OS cells were infected with lentivirus harbouring shRNA against the indicated gene or a control sequence. After selection with 1 μg/ml puromycin during 3 days, cells growing on coverslips were treated with ionizing radiation (10 Gy) or mock treated, incubated for 1 hour, and then collected. Coverslips were washed with cold PBS, fixed on ice with methanol for 10 minutes followed by acetone for 30 seconds, washed three times with cold PBS and blocked with blocking solution from the Duolink PLA kit for 30 minutes at 37ºC in a wet chamber. Samples were incubated with primary antibodies against CCAR2 and CtIP (Table M5) overnight at 4ºC, followed by incubation with MINUS and PLUS secondary PLA probes (anti-mouse MINUS and anti-rabbit PLUS) for 1 hour at 37ºC in a humidity chamber. Detection was carried out with the Duolink Detection kit Red (Olink Biosciences). Separate incubations with only one or the other primary antibody was carried out as control of the background signal. At least 200 cells were analysed using a Leica Fluorescence microscope and foci were counted automatically using the command *Granularity* of MetaMorph software.

3.4. Single-molecule analysis of resection tracks

SMART assay was performed as previously described (Cruz-García *et al*., 2014). The different cell lines transfected with the indicated shRNAs, siRNAs or plasmids were grown in the presence of 10 μg/ml bromodeoxyuridine (BrdU; B5002, Sigma) for 20-24 hours. Cultures were then irradiated (10 Gy), incubated for 1 hour at 37ºC and harvested using accutase (00-4555-56, eBioscience) instead of trypsin to gently detach the cells. Then, cells were resuspended in PBS and embedded in 1% low melting agarose (161-3111, Bio-Rad) diluted in PBS and poured in a casting mold to create agarose plugs. For DNA extraction, plugs were incubated in a solution of TE-50 (10 mM Tris-HCl pH 8 and 50 mM EDTA) with 1% sarkosyl (L5125, Sigma) and 0.2-0.4 mg/ml proteinase K at 50ºC overnight and 6 hours more with a new preparation of the same buffer. Plugs were washed four

times with TE-50 for 10 minutes with gentle shaking, stained with YOYO-1 (Y3601, Molecular Probes) for 30 minutes in the dark to check DNA fibers integrity and were washed again four times with TE (10 mM Tris-HCl pH 8 and 1 mM EDTA) for 5 minutes. Afterwards, each plug was melted in 2.5 ml of 50 mM 2-(N-morpholino)ethanesulfonic acid (MES) pH 5.7 by incubating 30-40 minutes at 66ºC. Then, solution was cooled down to 42ºC before adding 3U of β-Agarase I (M0392L, New England Biolabs) diluted in 100 μl MES. Samples were incubated overnight at 42ºC. To stretch the DNA fibers, silanized coverslips (COV-001, Genomic Vision) were dipped into the DNA solution for 15 minutes and pulled out at a constant speed (300 μm/sec). Coverslips were baked for at least 2 hours at 65ºC for DNA crosslinking.

For immunodetection, coverslips were fixed to slides and first dipped into blocking solution (1% BSA diluted in PBS with 0.1% Triton X-100 (PBS-T)) for 15 minutes. Then, DNA fibers were incubated directly without denaturation with an anti-BrdU mouse monoclonal antibody (Table M5) for 45 minutes. Slides were washed five times with PBS-T for 2 minutes each and then incubated with the secondary antibody (Table M6) for 30 minutes in the dark. Finally, coverslips were washed again with PBS-T, dried, mounted with 20 μl ProLong® Gold Antifade Reagent (P36930, Molecular Probes) and stored at -20ºC.

DNA fibers were observed with a Nikon Eclipse NI-E microscope and a Plan Fluor 40x/0.75 OFN25 Ph2 DLL objective. The images were recorded and processed with NIS ELEMENTS Nikon software. For each experiment, at least 200 DNA fibers were analysed, and their length was measured with Adobe Photoshop CS4 Extended version 11.0 (Adobe Systems Incorporated).

4. Statistical analysis

Unless otherwise specified, statistical significance was determined with a paired t-Student test using the PRISM software (Graphpad Software Inc.). Statistically significant differences were labelled with one, two or three asterisks if $P < 0.05$, $P < 0.01$ or $P < 0.001$, respectively. A nonparametric Mann-Whitney test was used to establish statistically significant differences between populations such as those of foci analysed by PLA or the length of resected DNA ends detected by SMART.

REFERENCES

Adamson, B., Smogorzewska, A., Sigoillot, F.D., King, R.W. & Elledge, S.J., 2012. A genome-wide homologous recombination screen identifies the RNA-binding protein RBMX as a component of the DNA-damage response. Nature Cell Biology, 14(3), pp.318–328.

Aguilera, A. & Gómez-González, B., 2008. Genome instability: a mechanistic view of its causes and consequences. Nature Reviews Genetics, 9(3), pp.204–217.

Anand, R., Ranjha, L., Cannavo, E. & Cejka, P., 2016. Phosphorylated CtIP Functions as a Co-factor of the MRE11-RAD50-NBS1 Endonuclease in DNA End Resection. Molecular Cell.

Anderson, S.F., Schlegel, B.P., Nakajima, T., Wolpin, E.S. & Parvin, J.D., 1998. BRCA1 protein is linked to the RNA polymerase II holoenzyme complex via RNA helicase A. Nature genetics, 19(3), pp.254–6.

Andres, S.N. et al., 2012. A human XRCC4-XLF complex bridges DNA. Nucleic acids research, 40(4), pp.1868–78.

Arcas, A., Fernández-Capetillo, O., Cases, I. & Rojas, A.M., 2014. Emergence and evolutionary analysis of the human DDR network: implications in comparative genomics and downstream analyses. Molecular biology and evolution, 31(4), pp.940–61.

Bartek, J. & Lukas, J., 2003. Chk1 and Chk2 kinases in checkpoint control and cancer. Cancer Cell, 3(5), pp.421–429.

Bartek, J. & Lukas, J., 2007. DNA damage checkpoints: from initiation to recovery or adaptation. Current Opinion in Cell Biology, 19(2), pp.238–245.

Bedford, M.T. & Richard, S., 2005. Arginine methylation an emerging regulator of protein function. Molecular cell, 18(3), pp.263–72.

Beli, P. et al., 2012. Proteomic Investigations Reveal a Role for RNA Processing Factor THRAP3 in the DNA Damage Response. Molecular Cell, 46(2), pp.212–225.

Bennardo, N., Cheng, A., Huang, N. & Stark, J.M., 2008. Alternative-NHEJ is a mechanistically distinct pathway of mammalian chromosome break repair. PLoS Genetics, 4(6).

Bertocci, B., De Smet, A., Weill, J.-C. & Reynaud, C.-A., 2006. Nonoverlapping Functions of DNA Polymerases Mu, Lambda, and Terminal Deoxynucleotidyltransferase during Immunoglobulin V(D)J Recombination In Vivo. Immunity, 25(1), pp.31–41.

Bhatti, S. et al., 2011. ATM protein kinase: the linchpin of cellular defenses to stress.

Cellular and Molecular Life Sciences, 68(18), pp.2977–3006.

Bilbao, C. et al., 2010. Double strand break repair components are frequent targets of microsatellite instability in endometrial cancer. European Journal of Cancer, 46(15), pp.2821–2827.

Bladen, C.L., Udayakumar, D., Takeda, Y. & Dynan, W.S., 2005. Identification of the polypyrimidine tract binding protein-associated splicing factor.p54(nrb) complex as a candidate DNA double-strand break rejoining factor. The Journal of biological chemistry, 280(7), pp.5205–10.

Boersma, V. et al., 2015. MAD2L2 controls DNA repair at telomeres and DNA breaks by inhibiting 5' end resection. Nature, 521(7553), pp.537–40.

Boisvert, F.-M., Côté, J., Boulanger, M.-C. & Richard, S., 2003. A proteomic analysis of arginine-methylated protein complexes. Molecular & cellular proteomics : MCP, 2(12), pp.1319–30.

Boisvert, F.-M., Déry, U., Masson, J.-Y. & Richard, S., 2005. Arginine methylation of MRE11 by PRMT1 is required for DNA damage checkpoint control. Genes & development, 19(6), pp.671–6.

Boisvert, F.-M., Hendzel, M.J., Masson, J.-Y. & Richard, S., 2005. Methylation of MRE11 Regulates its Nuclear Compartmentalization. Cell Cycle, 4(7), pp.981–989.

Boisvert, F.-M., Rhie, A., Richard, S. & Doherty, A.J., 2005. The GAR Motif of 53BP1 is Arginine Methylated by PRMT1 and is Necessary for 53BP1 DNA Binding Activity. Cell Cycle, 4(12), pp.1834–1841.

De Bont, R. & van Larebeke, N., 2004. Endogenous DNA damage in humans: a review of quantitative data. Mutagenesis, 19(3), pp.169–185.

Botuyan, M.V. et al., 2006. Structural Basis for the Methylation State-Specific Recognition of Histone H4-K20 by 53BP1 and Crb2 in DNA Repair. Cell, 127(7), pp.1361–1373.

Boucas, J. et al., 2012. Posttranscriptional regulation of gene expression-adding another layer of complexity to the DNA damage response. Frontiers in genetics, 3, p.159.

Bouwman, P. et al., 2010. 53BP1 loss rescues BRCA1 deficiency and is associated with triple-negative and BRCA-mutated breast cancers. Nature structural & molecular biology, 17(6), pp.688–95.

Branscombe, T.L. et al., 2001. PRMT5 (Janus kinase-binding protein 1) catalyzes the formation of symmetric dimethylarginine residues in proteins. The Journal of

biological chemistry, 276(35), pp.32971–6.

Broderick, R. et al., 2016. EXD2 promotes homologous recombination by facilitating DNA end resection. Nature Cell Biology, (January).

Brown, J.S. & Jackson, S.P., 2015. Ubiquitylation, neddylation and the DNA damage response. Open biology, 5(4), p.150018.

Buisson, R. et al., 2010. Cooperation of breast cancer proteins PALB2 and piccolo BRCA2 in stimulating homologous recombination. Nature structural & molecular biology, 17(10), pp.1247–54.

Bunting, S.F. et al., 2010. 53BP1 Inhibits Homologous Recombination in Brca1-Deficient Cells by Blocking Resection of DNA Breaks. Cell, 141(2), pp.243–254.

Burgos, E.S. et al., 2015. Histone H2A and H4 N-terminal tails are positioned by the MEP50 WD repeat protein for efficient methylation by the PRMT5 arginine methyltransferase. The Journal of biological chemistry, 290(15), pp.9674–89.

Burkhart, D.L. & Sage, J., 2008. Cellular mechanisms of tumour suppression by the retinoblastoma gene. Nature Reviews Cancer, 8(9), pp.671–682.

Byun, T.S., Pacek, M., Yee, M., Walter, J.C. & Cimprich, K.A., 2005. Functional uncoupling of MCM helicase and DNA polymerase activities activates the ATR-dependent checkpoint. Genes & development, 19(9), pp.1040–52.

Cadet, J. et al., 1997. Effects of UV and visible radiation on DNA-final base damage. Biological chemistry, 378(11), pp.1275–86.

Callen, E. et al., 2013. 53BP1 mediates productive and mutagenic DNA repair through distinct phosphoprotein interactions. Cell, 153(6), pp.1266–80.

Certo, M.T. et al., 2011. Tracking genome engineering outcome at individual DNA breakpoints. Nature methods, 8(8), pp.671–6.

Chapman, J.R. et al., 2013. RIF1 is essential for 53BP1-dependent nonhomologous end joining and suppression of DNA double-strand break resection. Molecular cell, 49(5), pp.858–71.

Chapman, J.R., Sossick, A.J., Boulton, S.J. & Jackson, S.P., 2012. BRCA1-associated exclusion of 53BP1 from DNA damage sites underlies temporal control of DNA repair. Journal of cell science, 125(Pt 15), pp.3529–34.

Chen, L., Gilkes, D.M., Pan, Y., Lane, W.S. & Chen, J., 2005. ATM and Chk2-dependent phosphorylation of MDMX contribute to p53 activation after DNA damage. The EMBO journal, 24(19), pp.3411–22.

Chen, P.-L. et al., 2005. Inactivation of CtIP leads to early embryonic lethality mediated by G1 restraint and to tumorigenesis by haploid insufficiency. Molecular and cellular biology, 25(9), pp.3535–42.

Chen, X. et al., 2015. 14-3-3 proteins restrain the Exo1 nuclease to prevent overresection. The Journal of biological chemistry, 290(19), pp.12300–12.

Chen, X., Paudyal, S.C., Chin, R.-I. & You, Z., 2013. PCNA promotes processive DNA end resection by Exo1. Nucleic Acids Research, 41(20), pp.9325–9338.

Choi, J.-H., Lindsey-Boltz, L.A. & Sancar, A., 2009. Cooperative activation of the ATR checkpoint kinase by TopBP1 and damaged DNA. Nucleic acids research, 37(5), pp.1501–9.

Ciccia, A. & Elledge, S.J., 2010. The DNA Damage Response: Making It Safe to Play with Knives. Molecular Cell, 40(2), pp.179–204.

Clarke, T.L. et al., 2017. PRMT5-Dependent Methylation of the TIP60 Coactivator RUVBL1 Is a Key Regulator of Homologous Recombination. Molecular Cell, 65(5), p.900–916.e7.

Close, P. et al., 2012. DBIRD complex integrates alternative mRNA splicing with RNA polymerase II transcript elongation. Nature, 484(7394), pp.386–389.

Côté, J. & Richard, S., 2005. Tudor domains bind symmetrical dimethylated arginines. The Journal of biological chemistry, 280(31), pp.28476–83.

Cruz-García, A., López-Saavedra, A. & Huertas, P., 2014. BRCA1 accelerates CtIP-mediated DNA-end resection. Cell reports, 9(2), pp.451–9.

Dai, C. & Gu, W., 2010. p53 post-translational modification: deregulated in tumorigenesis. Trends in molecular medicine, 16(11), pp.528–36.

Daley, J.M., Gaines, W.A., Kwon, Y. & Sung, P., 2014. Regulation of DNA pairing in homologous recombination. Cold Spring Harbor perspectives in biology, 6(11), p.a017954.

Daley, J.M., Kwon, Y., Niu, H. & Sung, P., 2013. Investigations of homologous recombination pathways and their regulation. The Yale journal of biology and medicine, 86(4), pp.453–61.

Davies, O.R. et al., 2015. CtIP tetramer assembly is required for DNA-end resection and repair. Nat Struct Mol Biol, 22(2), pp.150–157.

Davis, A.J. & Chen, D.J., 2013. DNA double strand break repair via non-homologous end-joining. Translational cancer research, 2(3), pp.130–143.

Déry, U. et al., 2008. A glycine-arginine domain in control of the human MRE11 DNA repair protein. Molecular and cellular biology, 28(9), pp.3058–69.

Downs, J.A. & Jackson, S.P., 2004. A means to a DNA end: the many roles of Ku. Nature Reviews Molecular Cell Biology, 5(5), pp.367–378.

Dubin, M.J. et al., 2004. Dimerization of CtIP, a BRCA1- and CtBP-interacting protein, is mediated by an N-terminal coiled-coil motif. The Journal of biological chemistry, 279(26), pp.26932–8.

Escribano-Díaz, C. et al., 2013. A Cell Cycle-Dependent Regulatory Circuit Composed of 53BP1-RIF1 and BRCA1-CtIP Controls DNA Repair Pathway Choice. Molecular Cell, 49(5), pp.872–883.

Falck, J., Coates, J. & Jackson, S.P., 2005. Conserved modes of recruitment of ATM, ATR and DNA-PKcs to sites of DNA damage. Nature, 434(7033), pp.605–611.

Ferretti, L.P. et al., 2016. Cullin3-KLHL15 ubiquitin ligase mediates CtIP protein turnover to fine-tune DNA-end resection. Nature communications, 7, p.12628.

Ferretti, L.P., Lafranchi, L. & Sartori, A.A., 2013. Controlling DNA-end resection: a new task for CDKs. Frontiers in genetics, 4, p.99.

Finkel, T. & Holbrook, N.J., 2000. Oxidants, oxidative stress and the biology of ageing. Nature, 408(6809), pp.239–247.

Fortune, J.M. & Osheroff, N., 2000. Topoisomerase II as a target for anticancer drugs: When enzymes stop being nice. Progress in Nucleic Acid Research and Molecular Biology, 64, pp.221–253.

Fradet-Turcotte, A. et al., 2013. 53BP1 is a reader of the DNA-damage-induced H2A Lys 15 ubiquitin mark. Nature, 499(7456), pp.50–54.

Frit, P., Barboule, N., Yuan, Y., Gomez, D. & Calsou, P., 2014. Alternative end-joining pathway(s): Bricolage at DNA breaks. DNA Repair, 17, pp.81–97.

Fusco, C., Reymond, A. & Zervos, A.S., 1998. Molecular Cloning and Characterization of a Novel Retinoblastoma-Binding Protein. Genomics, 51(3), pp.351–358.

Galanty, Y. et al., 2009. Mammalian SUMO E3-ligases PIAS1 and PIAS4 promote responses to DNA double-strand breaks. Nature, 462(7275), pp.935–9.

Gary, J.D. & Clarke, S., 1998. RNA and protein interactions modulated by protein arginine methylation. Progress in nucleic acid research and molecular biology, 61, pp.65–131.

Gaymes, T.J. et al., 2013. Microsatellite instability induced mutations in DNA repair

genes CtIP and MRE11 confer hypersensitivity to poly (ADP-ribose) polymerase inhibitors in myeloid malignancies. Haematologica, 98(9), pp.1397–406.

Genois, M.-M. et al., 2014. DNA repair pathways in trypanosomatids: from DNA repair to drug resistance. Microbiology and molecular biology reviews : MMBR, 78(1), pp.40–73.

Gómez-Cabello, D., Jimeno, S., Fernández-Ávila, M.J. & Huertas, P., 2013. New tools to study DNA double-strand break repair pathway choice. M. Lichten, ed. PloS one, 8(10), p.e77206.

Greene, E.C., 2016. DNA Sequence Alignment during Homologous Recombination. The Journal of biological chemistry, 291(22), pp.11572–80.

Gu, B. & Chen, P.-L., 2009. Expression of PCNA-binding domain of CtIP, a motif required for CtIP localization at DNA replication foci, causes DNA damage and activation of DNA damage checkpoint. Cell Cycle, 8(9), pp.1409–1420.

Gu, J., Lu, H., Tsai, A.G., Schwarz, K. & Lieber, M.R., 2007. Single-stranded DNA ligation and XLF-stimulated incompatible DNA end ligation by the XRCC4-DNA ligase IV complex: influence of terminal DNA sequence. Nucleic acids research, 35(17), pp.5755–62.

Guendel, I. et al., 2010. Methylation of the tumor suppressor protein, BRCA1, influences its transcriptional cofactor function. PloS one, 5(6), p.e11379.

Guo, Z. et al., 2010. Methylation of FEN1 suppresses nearby phosphorylation and facilitates PCNA binding. Nature chemical biology, 6(10), pp.766–73.

Hammel, M. et al., 2010. Ku and DNA-dependent protein kinase dynamic conformations and assembly regulate DNA binding and the initial non-homologous end joining complex. The Journal of biological chemistry, 285(2), pp.1414–23.

Harbour, J.W., Luo, R.X., Santi, A.D., Postigo, A.A. & Dean, D.C., 1999. Cdk Phosphorylation Triggers Sequential Intramolecular Interactions that Progressively Block Rb Functions as Cells Move through G1. Cell, 98(6), pp.859–869.

Harper, J.W. & Elledge, S.J., 2007. The DNA Damage Response: Ten Years After. Molecular Cell, 28(5), pp.739–745.

Hartlerode, A., Odate, S., Shim, I., Brown, J. & Scully, R., 2011. Cell Cycle-Dependent Induction of Homologous Recombination by a Tightly Regulated I-SceI Fusion Protein W. El-Deiry, ed. PLoS ONE, 6(3), p.e16501.

Hartlerode, A.J. & Scully, R., 2009. Mechanisms of double-strand break repair in somatic mammalian cells. The Biochemical journal, 423(2), pp.157–68.

Hashizume, R. et al., 2001. The RING heterodimer BRCA1-BARD1 is a ubiquitin ligase inactivated by a breast cancer-derived mutation. The Journal of biological chemistry, 276(18), pp.14537–40.

Heyer, W.-D., Ehmsen, K.T. & Liu, J., 2010. Regulation of homologous recombination in eukaryotes. Annual review of genetics, 44, pp.113–39.

Hiraike, H. et al., 2010. Identification of DBC1 as a transcriptional repressor for BRCA1. British journal of cancer, 102(6), pp.1061–7.

Ho, M.-C. et al., 2013. Structure of the Arginine Methyltransferase PRMT5-MEP50 Reveals a Mechanism for Substrate Specificity S. Cotterill, ed. PLoS ONE, 8(2), p.e57008.

Hoeijmakers, J.H.J., 2009. DNA Damage, Aging, and Cancer. New England Journal of Medicine, 361(15), pp.1475–1485.

Hoeijmakers, J.H.J., 2001. Genome maintenance mechanisms for preventing cancer. Nature, 411(6835), pp.366–374.

Hsiang, Y.H., Hertzberg, R., Hecht, S. & Liu, L.F., 1985. Camptothecin induces protein-linked DNA breaks via mammalian DNA topoisomerase I. The Journal of biological chemistry, 260(27), pp.14873–8.

Hu, D. et al., 2015. Interplay between arginine methylation and ubiquitylation regulates KLF4-mediated genome stability and carcinogenesis. Nature Communications, 6, p.8419.

Hu, H., Qian, K., Ho, M.-C. & Zheng, Y.G., 2016. Small Molecule Inhibitors of Protein Arginine Methyltransferases. Expert Opinion on Investigational Drugs, 25(3), pp.335–358.

Huen, M.S. & Chen, J., 2008. The DNA damage response pathways: at the crossroad of protein modifications. Cell Research, 18(1), pp.8–16.

Huertas, P., 2010. DNA resection in eukaryotes: deciding how to fix the break. Nature structural & molecular biology, 17(1), pp.11–6.

Huertas, P., Cortés-Ledesma, F., Sartori, A.A., Aguilera, A. & Jackson, S.P., 2008. CDK targets Sae2 to control DNA-end resection and homologous recombination. Nature, 455(7213), pp.689–92.

Huertas, P. & Jackson, S.P., 2009. Human CtIP mediates cell cycle control of DNA end

resection and double strand break repair. The Journal of biological chemistry, 284(14), pp.9558–65.

Hung, P.J. et al., 2017. Deficiency of XLF and PAXX prevents DNA double-strand break repair by non-homologous end joining in lymphocytes. Cell Cycle, 16(3), pp.286–295.

Hurov, K.E., Cotta-Ramusino, C. & Elledge, S.J., 2010. A genetic screen identifies the Triple T complex required for DNA damage signaling and ATM and ATR stability. Genes & development, 24(17), pp.1939–50.

Isono, M. et al., 2017. BRCA1 Directs the Repair Pathway to Homologous Recombination by Promoting 53BP1 Dephosphorylation. Cell Reports, 18(2), pp.520–532.

Ivanov, E.L., Sugawara, N., Fishman-Lobell, J. & Haber, J.E., 1996. Genetic requirements for the single-strand annealing pathway of double-strand break repair in Saccharomyces cerevisiae. Genetics, 142(3), pp.693–704.

Jackson, S.P. & Bartek, J., 2009. The DNA-damage response in human biology and disease. Nature, 461(7267), pp.1071–1078.

de Jager, M. et al., 2001. Human Rad50/Mre11 Is a Flexible Complex that Can Tether DNA Ends. Molecular Cell, 8(5), pp.1129–1135.

Jansson, M. et al., 2008. Arginine methylation regulates the p53 response. Nature Cell Biology, 10(12), pp.1431–1439.

Jasin, M. & Rothstein, R., 2013. Repair of strand breaks by homologous recombination. Cold Spring Harbor perspectives in biology, 5(11), p.a012740.

Jensen, R.B., Carreira, A. & Kowalczykowski, S.C., 2010. Purified human BRCA2 stimulates RAD51-mediated recombination. Nature, 467(7316), pp.678–83.

Jiang, W. et al., 2015. Differential phosphorylation of DNA-PKcs regulates the interplay between end-processing and end-ligation during nonhomologous end-joining. Molecular cell, 58(1), pp.172–85.

Jimeno, S. et al., 2015. Neddylation inhibits CtIP-mediated resection and regulates DNA double strand break repair pathway choice. Nucleic acids research, 43(2), pp.987–99.

Kaidi, A., Weinert, B.T., Choudhary, C. & Jackson, S.P., 2010. Human SIRT6 promotes DNA end resection through CtIP deacetylation. Science (New York, N.Y.), 329(5997), pp.1348–53.

Karkhanis, V. et al., 2012. Protein arginine methyltransferase 7 regulates cellular

response to DNA damage by methylating promoter histones H2A and H4 of the polymerase δ catalytic subunit gene, POLD1. The Journal of biological chemistry, 287(35), pp.29801–14.

Khanna, K.K. & Jackson, S.P., 2001. DNA double-strand breaks: signaling, repair and the cancer connection. Nature Genetics, 27(3), pp.247–254.

Kijas, A.W. et al., 2015. ATM-dependent phosphorylation of MRE11 controls extent of resection during homology directed repair by signalling through Exonuclease 1. Nucleic Acids Research, 43(17), pp.8352–8367.

Kim, J.-E., Chen, J. & Lou, Z., 2008. DBC1 is a negative regulator of SIRT1. Nature, 451(7178), pp.583–6.

Kim, J.-H. et al., 2006. Isolation of human Dna2 endonuclease and characterization of its enzymatic properties. Nucleic acids research, 34(6), pp.1854–64.

Kim, W., Jeong, J.-W. & Kim, J.-E., 2014. CCAR2 deficiency augments genotoxic stress-induced apoptosis in the presence of melatonin in non-small cell lung cancer cells. Tumor Biology, 35(11), pp.10919–10929.

Kim, W. & Kim, J.-E., 2013. Deleted in breast cancer 1 (DBC1) deficiency results in apoptosis of breast cancer cells through impaired responses to UV-induced DNA damage. Cancer Letters, 333(2), pp.180–186.

Kinner, A., Wu, W., Staudt, C. & Iliakis, G., 2008. Gamma-H2AX in recognition and signaling of DNA double-strand breaks in the context of chromatin. Nucleic acids research, 36(17), pp.5678–94.

Koipally, J. & Georgopoulos, K., 2002. Ikaros-CtIP interactions do not require C-terminal binding protein and participate in a deacetylase-independent mode of repression. The Journal of biological chemistry, 277(26), pp.23143–9.

Krejci, L. et al., 2002. Interaction with Rad51 is indispensable for recombination mediator function of Rad52. The Journal of biological chemistry, 277(42), pp.40132–41.

Krejci, L., Altmannova, V., Spirek, M. & Zhao, X., 2012. Homologous recombination and its regulation. Nucleic acids research, 40(13), pp.5795–818.

Krogh, B.O. & Symington, L.S., 2004. Recombination Proteins in Yeast. Annual Review of Genetics, 38(1), pp.233–271.

Kumagai, A., Lee, J., Yoo, H.Y. & Dunphy, W.G., 2006. TopBP1 Activates the ATR-ATRIP Complex. Cell, 124(5), pp.943–955.

Kunkel, T.A. & Bebenek, K., 2000. DNA Replication Fidelity. Annual Review of Biochemistry, 69(1), pp.497–529.

Kusumoto-Matsuo, R. et al., 2014. Serines 440 and 467 in the Werner syndrome protein are phosphorylated by DNA-PK and affects its dynamics in response to DNA double strand breaks. Aging, 6(1), pp.70–81.

Lafranchi, L. et al., 2014. APC/C(Cdh1) controls CtIP stability during the cell cycle and in response to DNA damage. The EMBO journal, 33(23), pp.2860–79.

Lee, J.-H., Goodarzi, A.A., Jeggo, P.A. & Paull, T.T., 2010. 53BP1 promotes ATM activity through direct interactions with the MRN complex. The EMBO journal, 29(3), pp.574–85.

Li, S. et al., 1999. Binding of CtIP to the BRCT repeats of BRCA1 involved in the transcription regulation of p21 is disrupted upon DNA damage. The Journal of biological chemistry, 274(16), pp.11334–8.

Li, S. et al., 2000. Functional link of BRCA1 and ataxia telangiectasia gene product in DNA damage response. Nature, 406(6792), pp.210–5.

Lieber, M.R., 2010. The mechanism of double-strand DNA break repair by the nonhomologous DNA end-joining pathway. Annual review of biochemistry, 79, pp.181–211.

Lieber, M.R., 2008. The Mechanism of Human Nonhomologous DNA End Joining. Journal of Biological Chemistry, 283(1), pp.1–5.

Lin, W.J., Gary, J.D., Yang, M.C., Clarke, S. & Herschman, H.R., 1996. The mammalian immediate-early TIS21 protein and the leukemia-associated BTG1 protein interact with a protein-arginine N-methyltransferase. The Journal of biological chemistry, 271(25), pp.15034–44.

Lindahl, T., 1993. Instability and decay of the primary structure of DNA. Nature, 362(6422), pp.709–715.

Liu, F. & Lee, W.-H., 2006. CtIP activates its own and cyclin D1 promoters via the E2F/RB pathway during G1/S progression. Molecular and cellular biology, 26(8), pp.3124–34.

Liu, X., Shao, Z., Jiang, W., Lee, B.J. & Zha, S., 2017. PAXX promotes KU accumulation at DNA breaks and is essential for end-joining in XLF-deficient mice. Nature communications, 8, p.13816.

Llorente, B., Smith, C.E. & Symington, L.S., 2008. Break-induced replication: What is it

and what is it for? Cell Cycle, 7(7), pp.859–864.

López-Saavedra, A. et al., 2016. A genome-wide screening uncovers the role of CCAR2 as an antagonist of DNA end resection. Nature communications, 7, p.12364.

Di Lorenzo, A. & Bedford, M.T., 2011. Histone arginine methylation. FEBS letters, 585(13), pp.2024–31.

Lou, Z. et al., 2006. MDC1 Maintains Genomic Stability by Participating in the Amplification of ATM-Dependent DNA Damage Signals. Molecular Cell, 21(2), pp.187–200.

Lydeard, J.R. et al., 2010. Break-induced replication requires all essential DNA replication factors except those specific for pre-RC assembly. Genes & development, 24(11), pp.1133–44.

Ma, Y., Schwarz, K. & Lieber, M.R., 2005. The Artemis:DNA-PKcs endonuclease cleaves DNA loops, flaps, and gaps,

Magni, M. et al., 2015. CCAR2/DBC1 is required for Chk2-dependent KAP1 phosphorylation and repair of DNA damage. Oncotarget, 6(19), pp.17817–17831.

Makharashvili, N. et al., 2014. Catalytic and Noncatalytic Roles of the CtIP Endonuclease in Double-Strand Break End Resection,

Makharashvili, N. & Paull, T.T., 2015. CtIP: A DNA damage response protein at the intersection of DNA metabolism. DNA Repair, 32, pp.75–81.

Maréchal, A. et al., 2014. PRP19 transforms into a sensor of RPA-ssDNA after DNA damage and drives ATR activation via a ubiquitin-mediated circuitry. Molecular cell, 53(2), pp.235–46.

Maréchal, A. & Zou, L., 2013. DNA damage sensing by the ATM and ATR kinases. Cold Spring Harbor perspectives in biology, 5(9), p.a012716.

Matsuoka, S. et al., 2007. ATM and ATR Substrate Analysis Reveals Extensive Protein Networks Responsive to DNA Damage. Science, 316(5828), pp.1160–1166.

McVey, M. & Lee, S.E., 2008. MMEJ repair of double-strand breaks (director's cut): deleted sequences and alternative endings. Trends in genetics : TIG, 24(11), pp.529–38.

Meloni, A.R., Smith, E.J. & Nevins, J.R., 1999. A mechanism for Rb/p130-mediated transcription repression involving recruitment of the CtBP corepressor. Proceedings of the National Academy of Sciences of the United States of America, 96(17), pp.9574–9.

Mimitou, E.P. & Symington, L.S., 2009. DNA end resection: many nucleases make light work. DNA repair, 8(9), pp.983–95.

Mimitou, E.P. & Symington, L.S., 2008. Sae2, Exo1 and Sgs1 collaborate in DNA double-strand break processing. Nature, 455(7214), pp.770–4.

Mischo, H.E., Hemmerich, P., Grosse, F. & Zhang, S., 2005. Actinomycin D induces histone gamma-H2AX foci and complex formation of gamma-H2AX with Ku70 and nuclear DNA helicase II. The Journal of biological chemistry, 280(10), pp.9586–94.

Morozumi, Y., Takizawa, Y., Takaku, M. & Kurumizaka, H., 2009. Human PSF binds to RAD51 and modulates its homologous-pairing and strand-exchange activities. Nucleic Acids Research, 37(13), pp.4296–4307.

Morrical, S.W., 2015. DNA-pairing and annealing processes in homologous recombination and homology-directed repair. Cold Spring Harbor perspectives in biology, 7(2), p.a016444.

Musselman, C.A., Lalonde, M.-E., Côté, J. & Kutateladze, T.G., 2012. Perceiving the epigenetic landscape through histone readers. Nature structural & molecular biology, 19(12), pp.1218–27.

Nassif, N., Penney, J., Pal, S., Engels, W.R. & Gloor, G.B., 1994. Efficient copying of nonhomologous sequences from ectopic sites via P-element-induced gap repair. Molecular and cellular biology, 14(3), pp.1613–25.

Nick McElhinny, S.A., Snowden, C.M., McCarville, J. & Ramsden, D.A., 2000. Ku recruits the XRCC4-ligase IV complex to DNA ends. Molecular and cellular biology, 20(9), pp.2996–3003.

Nimonkar, A. V et al., 2011. BLM-DNA2-RPA-MRN and EXO1-BLM-RPA-MRN constitute two DNA end resection machineries for human DNA break repair. Genes & development, 25(4), pp.350–62.

Nimonkar, A. V., Ozsoy, A.Z., Genschel, J., Modrich, P. & Kowalczykowski, S.C., 2008. Human exonuclease 1 and BLM helicase interact to resect DNA and initiate DNA repair. Proceedings of the National Academy of Sciences, 105(44), pp.16906–16911.

Nimonkar, A. V & Kowalczykowski, S.C., 2009. Second-end DNA capture in double-strand break repair: how to catch a DNA by its tail. Cell cycle (Georgetown, Tex.), 8(12), pp.1816–7.

Orthwein, A. et al., 2015. A mechanism for the suppression of homologous

recombination in G1 cells. Nature, 528(7582), pp.422–426.

Osman, F., Dixon, J., Doe, C.L. & Whitby, M.C., 2003. Generating Crossovers by Resolution of Nicked Holliday Junctions. Molecular Cell, 12(3), pp.761–774.

Pal, S., Vishwanath, S.N., Erdjument-Bromage, H., Tempst, P. & Sif, S., 2004. Human SWI/SNF-associated PRMT5 methylates histone H3 arginine 8 and negatively regulates expression of ST7 and NM23 tumor suppressor genes. Molecular and cellular biology, 24(21), pp.9630–45.

Paull, T.T. & Gellert, M., 1999. Nbs1 potentiates ATP-driven DNA unwinding and endonuclease cleavage by the Mre11/Rad50 complex. Genes & development, 13(10), pp.1276–88.

Paulsen, R.D. et al., 2009. A Genome-wide siRNA Screen Reveals Diverse Cellular Processes and Pathways that Mediate Genome Stability. Molecular Cell, 35(2), pp.228–239.

Peterson, S.E. et al., 2013. Activation of DSB processing requires phosphorylation of CtIP by ATR. Molecular cell, 49(4), pp.657–67.

Phillips, D.H., Hewer, A., Martin, C.N., Garner, R.C. & King, M.M., 1988. Correlation of DNA adduct levels in human lung with cigarette smoking. Nature, 336(6201), pp.790–792.

Pierce, A.J., Johnson, R.D., Thompson, L.H. & Jasin, M., 1999. XRCC3 promotes homology-directed repair of DNA damage in mammalian cells. Genes & development, 13(20), pp.2633–8.

Polato, F. et al., 2014. CtIP-mediated resection is essential for viability and can operate independently of BRCA1. The Journal of experimental medicine, 211(6), pp.1027–36.

Pollack, B.P. et al., 1999. The human homologue of the yeast proteins Skb1 and Hsl7p interacts with Jak kinases and contains protein methyltransferase activity. The Journal of biological chemistry, 274(44), pp.31531–42.

Polo, S.E. et al., 2012. Regulation of DNA-End Resection by hnRNPU-like Proteins Promotes DNA Double-Strand Break Signaling and Repair. Molecular Cell, 45(4), pp.505–516.

Polo, S.E. & Jackson, S.P., 2011. Dynamics of DNA damage response proteins at DNA breaks: a focus on protein modifications. Genes & development, 25(5), pp.409–33.

Prado, F. & Aguilera, A., 2003. Control of cross-over by single-strand DNA resection.

Trends in Genetics, 19(8), pp.428–431.

Price, B.D. & D'Andrea, A.D., 2013. Chromatin Remodeling at DNA Double-Strand Breaks. Cell, 152(6), pp.1344–1354.

Qin, B. et al., 2015. DBC1 Functions as a Tumor Suppressor by Regulating p53 Stability. Cell Reports, 10(8), pp.1324–1334.

Qvist, P. et al., 2011. CtIP Mutations Cause Seckel and Jawad Syndromes. PLoS genetics, 7(10), p.e1002310.

Radhakrishnan, S.K., Jette, N. & Lees-Miller, S.P., 2014. Non-homologous end joining: emerging themes and unanswered questions. DNA repair, 17, pp.2–8.

Rajesh, C., Baker, D.K., Pierce, A.J. & Pittman, D.L., 2011. The splicing-factor related protein SFPQ/PSF interacts with RAD51D and is necessary for homology-directed repair and sister chromatid cohesion. Nucleic Acids Research, 39(1), pp.132–145.

Rajesh, C., Gruver, A.M., Basrur, V. & Pittman, D.L., 2009. The interaction profile of homologous recombination repair proteins RAD51C, RAD51D and XRCC2 as determined by proteomic analysis. PROTEOMICS, 9(16), pp.4071–4086.

Roberts, S.A. et al., 2012. Clustered mutations in yeast and in human cancers can arise from damaged long single-strand DNA regions. Molecular cell, 46(4), pp.424–35.

Rogakou, E.P., Pilch, D.R., Orr, A.H., Ivanova, V.S. & Bonner, W.M., 1998. DNA Double-stranded Breaks Induce Histone H2AX Phosphorylation on Serine 139. Journal of Biological Chemistry, 273(10), pp.5858–5868.

Rothkamm, K., Krüger, I., Thompson, L.H. & Löbrich, M., 2003. Pathways of DNA double-strand break repair during the mammalian cell cycle. Molecular and cellular biology, 23(16), pp.5706–15.

Rouse, J. & Jackson, S.P., 2002. Interfaces Between the Detection, Signaling, and Repair of DNA Damage. Science, 297(5581), pp.547–551.

Sakofsky, C.J., Ayyar, S. & Malkova, A., 2012. Break-induced replication and genome stability. Biomolecules, 2(4), pp.483–504.

San Filippo, J., Sung, P. & Klein, H., 2008. Mechanism of Eukaryotic Homologous Recombination. Annual Review of Biochemistry, 77(1), pp.229–257.

Sartori, A.A. et al., 2007. Human CtIP promotes DNA end resection. Nature, 450(7169), pp.509–14.

Savage, K.I. et al., 2014. Identification of a BRCA1-mRNA Splicing Complex Required for Efficient DNA Repair and Maintenance of Genomic Stability. Molecular Cell, 54(3),

pp.445–459.

Schaeper, U., Subramanian, T., Lim, L., Boyd, J.M. & Chinnadurai, G., 1998. Interaction between a Cellular Protein That Binds to the C-terminal Region of Adenovirus E1A (CtBP) and a Novel Cellular Protein Is Disrupted by E1A through a Conserved PLDLS Motif. Journal of Biological Chemistry, 273(15), pp.8549–8552.

Scoumanne, A., Zhang, J. & Chen, X., 2009. PRMT5 is required for cell-cycle progression and p53 tumor suppressor function. Nucleic acids research, 37(15), pp.4965–76.

Shanbhag, N.M., Rafalska-Metcalf, I.U., Balane-Bolivar, C., Janicki, S.M. & Greenberg, R.A., 2010. ATM-dependent chromatin changes silence transcription in cis to DNA double-strand breaks. Cell, 141(6), pp.970–81.

Shibata, A. et al., 2014. DNA double-strand break repair pathway choice is directed by distinct MRE11 nuclease activities. Molecular cell, 53(1), pp.7–18.

Shiloh, Y., 2006. The ATM-mediated DNA-damage response: taking shape. Trends in Biochemical Sciences, 31(7), pp.402–410.

Shiloh, Y. & Ziv, Y., 2013. The ATM protein kinase: regulating the cellular response to genotoxic stress, and more. Nature Reviews Molecular Cell Biology, 14(4), pp.197–210.

Shkreta, L. & Chabot, B., 2015. The RNA Splicing Response to DNA Damage. Biomolecules, 5(4), pp.2935–77.

Singh, V. et al., 2004. DAL-1/4.1B tumor suppressor interacts with protein arginine N-methyltransferase 3 (PRMT3) and inhibits its ability to methylate substrates in vitro and in vivo. Oncogene, 23(47), pp.7761–71.

Singleton, B.K., Torres-Arzayus, M.I., Rottinghaus, S.T., Taccioli, G.E. & Jeggo, P.A., 1999. The C terminus of Ku80 activates the DNA-dependent protein kinase catalytic subunit. Molecular and cellular biology, 19(5), pp.3267–77.

Smolka, M.B., Albuquerque, C.P., Chen, S. & Zhou, H., 2007. Proteome-wide identification of in vivo targets of DNA damage checkpoint kinases. Proceedings of the National Academy of Sciences of the United States of America, 104(25), pp.10364–9.

Soria-Bretones, I., Saez, C., Ruiz-Borrego, M., Japon, M.A. & Huertas, P., 2013. Prognostic value of CtIP/RBBP8 expression in breast cancer. Cancer Med., 2, pp.774–783.

Sprung, C.N., Li, J., Hovan, D., McKay, M.J. & Forrester, H.B., 2011. Alternative transcript initiation and splicing as a response to DNA damage. PloS one, 6(10), p.e25758.

Stark, J.M., Pierce, A.J., Oh, J., Pastink, A. & Jasin, M., 2004. Genetic steps of mammalian

homologous repair with distinct mutagenic consequences. Molecular and cellular biology, 24(21), pp.9305–16.

Steger, M. et al., 2013. Prolyl isomerase PIN1 regulates DNA double-strand break repair by counteracting DNA end resection. Molecular cell, 50(3), pp.333–43.

Stopa, N., Krebs, J.E. & Shechter, D., 2015. The PRMT5 arginine methyltransferase: many roles in development, cancer and beyond. Cellular and molecular life sciences : CMLS, 72(11), pp.2041–59.

Stracker, T.H. & Petrini, J.H.J., 2011. The MRE11 complex: starting from the ends. Nature reviews. Molecular cell biology, 12(2), pp.90–103.

Stracker, T.H., Theunissen, J.-W.F., Morales, M. & Petrini, J.H.J., 2004. The Mre11 complex and the metabolism of chromosome breaks: the importance of communicating and holding things together. DNA Repair, 3(8), pp.845–854.

Strande, N.T., Waters, C.A. & Ramsden, D.A., 2012. Resolution of complex ends by Nonhomologous end joining - better to be lucky than good? Genome integrity, 3(1), p.10.

Sturzenegger, A. et al., 2014. DNA2 cooperates with the WRN and BLM RecQ helicases to mediate long-range DNA end resection in human cells. The Journal of biological chemistry, 289(39), pp.27314–26.

Sum, E.Y.M. et al., 2002. The LIM domain protein LMO4 interacts with the cofactor CtIP and the tumor suppressor BRCA1 and inhibits BRCA1 activity. The Journal of biological chemistry, 277(10), pp.7849–56.

Sung, P. & Klein, H., 2006. Mechanism of homologous recombination: mediators and helicases take on regulatory functions. Nature Reviews Molecular Cell Biology, 7(10), pp.739–750.

Sung, P., Krejci, L., Van Komen, S. & Sehorn, M.G., 2003. Rad51 recombinase and recombination mediators. The Journal of biological chemistry, 278(44), pp.42729–32.

Symington, L.S., 2016. Mechanism and regulation of DNA end resection in eukaryotes. Critical Reviews in Biochemistry and Molecular Biology, 51(3), pp.195–212.

Symington, L.S. & Gautier, J., 2011. Double-Strand Break End Resection and Repair Pathway Choice. Annual Review of Genetics, 45(1), pp.247–271.

Takata, M. et al., 2001. Chromosome instability and defective recombinational repair in knockout mutants of the five Rad51 paralogs. Molecular and cellular biology,

21(8), pp.2858–66.

Takeda, S., Nakamura, K., Taniguchi, Y. & Paull, T.T., 2007. Ctp1/CtIP and the MRN Complex Collaborate in the Initial Steps of Homologous Recombination. Molecular Cell, 28(3), pp.351–352.

Tanikawa, M. et al., 2013. Role of multifunctional transcription factor TFII-I and putative tumour suppressor DBC1 in cell cycle and DNA double strand damage repair. British journal of cancer.

Tkáč, J. et al., 2016. HELB Is a Feedback Inhibitor of DNA End Resection. Molecular Cell, 61(3), pp.405–418.

Trujillo, K.M. et al., 2003. Yeast xrs2 binds DNA and helps target rad50 and mre11 to DNA ends. The Journal of biological chemistry, 278(49), pp.48957–64.

Truong, L.N. et al., 2013. Microhomology-mediated End Joining and Homologous Recombination share the initial end resection step to repair DNA double-strand breaks in mammalian cells. Proceedings of the National Academy of Sciences of the United States of America, 110(19), pp.7720–5.

Uematsu, N. et al., 2007. Autophosphorylation of DNA-PKCS regulates its dynamics at DNA double-strand breaks. The Journal of cell biology, 177(2), pp.219–29.

Valko, M., Rhodes, C.J., Moncol, J., Izakovic, M. & Mazur, M., 2006. Free radicals, metals and antioxidants in oxidative stress-induced cancer. Chemico-Biological Interactions, 160(1), pp.1–40.

Venkitaraman, A.R., 2002. Cancer Susceptibility and the Functions of BRCA1 and BRCA2. Cell, 108(2), pp.171–182.

Verbiest, V. et al., 2008. Protein arginine (N)-methyl transferase 7 (PRMT7) as a potential target for the sensitization of tumor cells to camptothecins. FEBS Letters, 582(10), pp.1483–1489.

Visvader, J.E. et al., 2001. The LIM domain gene LMO4 inhibits differentiation of mammary epithelial cells in vitro and is overexpressed in breast cancer. Proceedings of the National Academy of Sciences of the United States of America, 98(25), pp.14452–7.

Wang, H. et al., 2014. CtIP Maintains Stability at Common Fragile Sites and Inverted Repeats by End Resection-Independent Endonuclease Activity,

Wang, H. et al., 2012. CtIP protein dimerization is critical for its recruitment to chromosomal DNA double-stranded breaks. The Journal of biological chemistry,

287(25), pp.21471–80.

Wang, H. & Xu, X., 2017. Microhomology-mediated end joining: new players join the team. Cell & bioscience, 7, p.6.

Wang, J. et al., 2016. Loss of CtIP disturbs homologous recombination repair and sensitizes breast cancer cells to PARP inhibitors. Oncotarget, 7(7), pp.7701–14.

Wang, J. et al., 2014. PTIP associates with Artemis to dictate DNA repair pathway choice. Genes & development, 28(24), pp.2693–8.

Wang, J.-H. et al., 1996. Selective Defects in the Development of the Fetal and Adult Lymphoid System in Mice with an Ikaros Null Mutation. Immunity, 5(6), pp.537–549.

Wang, L., Pal, S. & Sif, S., 2008. Protein arginine methyltransferase 5 suppresses the transcription of the RB family of tumor suppressors in leukemia and lymphoma cells. Molecular and cellular biology, 28(20), pp.6262–77.

Ward, J.F., 1988. DNA Damage Produced by Ionizing Radiation in Mammalian Cells: Identities, Mechanisms of Formation, and Reparability. Progress in Nucleic Acid Research and Molecular Biology, 35, pp.95–125.

Waters, C.A., Strande, N.T., Wyatt, D.W., Pryor, J.M. & Ramsden, D.A., 2014. Nonhomologous end joining: a good solution for bad ends. DNA repair, 17, pp.39–51.

Weintraub, S.J., Prater, C.A. & Dean, D.C., 1992. Retinoblastoma protein switches the E2F site from positive to negative element. Nature, 358(6383), pp.259–261.

Wilson, M.D. et al., 2016. The structural basis of modified nucleosome recognition by 53BP1. Nature, 536(7614), pp.100–103.

Wong, A.K. et al., 1998. Characterization of a carboxy-terminal BRCA1 interacting protein. Oncogene, 17(18), pp.2279–2285.

Wu, G. & Lee, W.-H., 2006. CtIP, a Multivalent Adaptor Connecting Transcriptional Regulation, Checkpoint Control and Tumor Suppression. Cell Cycle, 5(15), pp.1592–1596.

Xu, G. et al., 2015. REV7 counteracts DNA double-strand break resection and affects PARP inhibition. Nature, 521(7553), pp.541–4.

Xu, J. et al., 2007. TRB3 interacts with CtIP and is overexpressed in certain cancers. Biochimica et Biophysica Acta (BBA) - General Subjects, 1770(2), pp.273–278.

Yaneva, M., Kowalewski, T. & Lieber, M.R., 1997. Interaction of DNA-dependent protein

kinase with DNA and with Ku: biochemical and atomic-force microscopy studies. The EMBO journal, 16(16), pp.5098–112.

Yang, K., Guo, R. & Xu, D., 2016. Non-homologous end joining: advances and frontiers. Acta Biochimica et Biophysica Sinica, 48(7), pp.632–640.

Yano, K. et al., 2008. Ku recruits XLF to DNA double-strand breaks. EMBO reports, 9(1), pp.91–6.

Yoo, S. & Dynan, W.S., 1999. Geometry of a complex formed by double strand break repair proteins at a single DNA end: recruitment of DNA-PKcs induces inward translocation of Ku protein. Nucleic acids research, 27(24), pp.4679–86.

You, Z. & Bailis, J.M., 2010. DNA damage and decisions: CtIP coordinates DNA repair and cell cycle checkpoints. Trends in Cell Biology, 20(7), pp.402–409.

You, Z., Chahwan, C., Bailis, J., Hunter, T. & Russell, P., 2005. ATM activation and its recruitment to damaged DNA require binding to the C terminus of Nbs1. Molecular and cellular biology, 25(13), pp.5363–79.

Yu, X. & Chen, J., 2004b. DNA damage-induced cell cycle checkpoint control requires CtIP, a phosphorylation-dependent binding partner of BRCA1 C-terminal domains. Molecular and cellular biology, 24(21), pp.9478–86.

Yu, X., Fu, S., Lai, M., Baer, R. & Chen, J., 2006. BRCA1 ubiquitinates its phosphorylation-dependent binding partner CtIP. Genes & development, 20(13), pp.1721–6.

Yu, X., Wu, L.C., Bowcock, A.M., Aronheim, A. & Baer, R., 1998. The C-terminal (BRCT) Domains of BRCA1 Interact in Vivo with CtIP, a Protein Implicated in the CtBP Pathway of Transcriptional Repression. Journal of Biological Chemistry, 273(39), pp.25388–25392.

Yuan, J. & Chen, J., 2009. N terminus of CtIP is critical for homologous recombination-mediated double-strand break repair. The Journal of biological chemistry, 284(46), pp.31746–52.

Zannini, L., Buscemi, G., Kim, J.-E., Fontanella, E. & Delia, D., 2012. DBC1 phosphorylation by ATM/ATR inhibits SIRT1 deacetylase in response to DNA damage. Journal of Molecular Cell Biology, 4(5), pp.294–303.

Zhang, F. et al., 2009. PALB2 links BRCA1 and BRCA2 in the DNA-damage response. Current biology : CB, 19(6), pp.524–9.

Zhang, S., Schlott, B., Görlach, M. & Grosse, F., 2004. DNA-dependent protein kinase (DNA-PK) phosphorylates nuclear DNA helicase II/RNA helicase A and hnRNP

proteins in an RNA-dependent manner. Nucleic acids research, 32(1), pp.1–10.

Zhao, W. et al., 2008. Negative regulation of the deacetylase SIRT1 by DBC1. Nature, 451(7178), pp.587–90.

Zhong, Q. et al., 1999. Association of BRCA1 with the hRad50-hMre11-p95 complex and the DNA damage response. Science (New York, N.Y.), 285(5428), pp.747–50.

Zhou, C. et al., 2015. Dna2 nuclease-helicase structure, mechanism and regulation by Rpa. eLife, 4, pp.267–273.

Zierhut, C. & Diffley, J.F.X., 2008. Break dosage, cell cycle stage and DNA replication influence DNA double strand break response. The EMBO journal, 27(13), pp.1875–85.

Zong, D., Chaudhuri, A.R. & Nussenzweig, A., 2016. More end resection is not merrier. Nature Structural & Molecular Biology, 23(8), pp.699–701.

Zou, L. & Elledge, S.J., 2003. Sensing DNA Damage Through ATRIP Recognition of RPA-ssDNA Complexes. Science, 300(5625), pp.1542–1548.

PUBLISHED RESULTS

nature COMMUNICATIONS

ARTICLE

Received 30 Mar 2016 | Accepted 27 Jun 2016 | Published 9 Aug 2016

DOI: 10.1038/ncomms12364 OPEN

A genome-wide screening uncovers the role of CCAR2 as an antagonist of DNA end resection

Ana López-Saavedra[1,2,*], Daniel Gómez-Cabello[2,*], María Salud Domínguez-Sánchez[2,*], Fernando Mejías-Navarro[1,2], María Jesús Fernández-Ávila[2], Christoffel Dinant[3], María Isabel Martínez-Macías[1,2,†], Jiri Bartek[3,4] & Pablo Huertas[1,2]

There are two major and alternative pathways to repair DNA double-strand breaks: non-homologous end-joining and homologous recombination. Here we identify and characterize novel factors involved in choosing between these pathways; in this study we took advantage of the SeeSaw Reporter, in which the repair of double-strand breaks by homology-independent or -dependent mechanisms is distinguished by the accumulation of green or red fluorescence, respectively. Using a genome-wide human esiRNA (endoribonuclease-prepared siRNA) library, we isolate genes that control the recombination/end-joining ratio. Here we report that two distinct sets of genes are involved in the control of the balance between NHEJ and HR: those that are required to facilitate recombination and those that favour NHEJ. This last category includes CCAR2/DBC1, which we show inhibits recombination by limiting the initiation and the extent of DNA end resection, thereby acting as an antagonist of CtIP.

[1] Departamento de Genética, Universidad de Sevilla, 41080 Sevilla, Spain. [2] Department of Regenerative Medicine, Centro Andaluz de Biología Molecular y Medicina Regenerativa, 41092 Sevilla, Spain. [3] Genome Integrity Unit, Danish Cancer Society Research Centre, Strandboulevarden 49, 2100 Copenhagen, Denmark. [4] Department of Medical Biochemistry and Biophysics, Science for Life Laboratory, Karolinska Institute, 171 76 Stockholm, Sweden. * These authors contributed equally to this work. † Present address: Genome Damage and Stability Centre, University of Sussex, Falmer, Brighton BN1 9RQ, UK. Correspondence and requests for materials should be addressed to P.H. (email: pablo.huertas@cabimer.es).

DNA double-strand breaks (DSBs) are the most dangerous form of DNA damage. Unrepaired breaks lead to cell death, while improperly repaired breaks cause an increase in genomic instability and, in humans, diseases such as cancer and premature aging[1,2]. There are two major pathways to repair DSBs: non-homologous end-joining (NHEJ) and homologous recombination (HR)[3–5]. NHEJ consists of a ligation of two DNA ends without using homology[5]. In HR, a homologous sequence is used as an information donor in a highly regulated mechanism[3]. Several recombination subpathways have been described, each one with distinct outcomes and consequences[3]. The choice between these two repair mechanisms is highly regulated, and changes in the ratio between them can increase genomic instability[4]. So far, the best-known regulated step of the DSB repair pathway choice is the so-called DNA end resection[4]. Here strands are degraded 5′–3′ at each DNA end, giving rise to ssDNA tails that are immediately coated by the replication protein A (RPA) complex for protection[4]. RPA-coated ssDNA is an obligatory substrate of HR and hampers NHEJ[4]. A major player in the choice between NHEJ and HR is CtIP (CtBP interacting protein), which licenses HR by activating DNA end resection[6]. Multiple signals converge on CtIP to initiate DNA end resection at those breaks that will be repaired by HR[4,6,7]. In order to find and characterize new factors involved in this crucial choice, we took advantage of the SeeSaw Reporter (SSR), a system designed to assess the balance between NHEJ and HR[8]. Using a genome-wide human esiRNA library, we found that downregulation of 1.35% of the genes shifts the NHEJ:HR ratio towards NHEJ, while depletion of a further 0.71% has the opposite effect. We focused on CCAR2, which we found to cause hyper-recombination when depleted. We show that it acts as an inhibitor of recombination. Specifically, we found that CCAR2 inhibits initiation and limits the extent of DNA end resection through its functional interaction with CtIP. This regulation of DNA end processing modulates the choice between NHEJ and HR.

Results

A genome-wide screening for regulators of the NHEJ:HR ratio. The SSR2.0 system (Fig. 1a) was designed to calculate the balance between NHEJ and HR as the ratio of green fluorescent protein (GFP)-positive versus red fluorescent protein (RFP)-positive cells of a lone DSB induced by the meganuclease I-SceI (ref. 8). Note that, in this reporter, mainly a specific subtype of HR termed single-strand annealing (SSA) is measured, which is Rad51-independent and does not require strand invasion[3]. SSA is very sensitive to DNA end resection but does not require additional steps; thus, our screening focused on the early steps shared by the various HR subpathways. We measured the ratio of green versus red cells using a high-throughput microscope after individually downregulating human genes using a genome-wide esiRNA library (Fig. 1b). We used 96-well plates and included esiRNA against luciferase in each plate as a control. We discarded the results of any plate in which the green versus red cell ratio of the luciferase control varied more than 10% relative to the average value from all luciferase controls. The ratio of green versus red cells was calculated for each esiRNA and normalized with the value of the internal esiRNA against luciferase. The experiment was repeated independently three times (Supplementary Data 1). Genes were ranked accordingly to average GFP:RFP cell ratio normalized with luciferase and represented graphically (Fig. 1c). We observed three categories of genes with respect to the shape of the curve. Downregulation of the majority of the genes showed a NHEJ:HR ratio similar to the control (for example, normalized GFP:RFP ratio close to 1; dashed black rectangle, Fig. 1c). Depletion of 0.71% of the genes skewed the balance towards an increase in HR (for example, normalized GFP:RFP ratio below 0.5; red ellipse, Fig. 1c). As downregulation of those genes increased HR, we categorize them as genes that naturally favour NHEJ. An additional 1.35% of the genes favoured HR, that is, NHEJ increased when downregulated (for example, normalized GFP:RFP ratio above 3; green ellipse, Fig. 1c). The thresholds of 0.5 and 3 were established with respect to the inflection points of the curve. Data analyses revealed false-positive signals for some genes because of a single experiment with extreme values. To eliminate those, we established the following criteria (Supplementary Data 2): genes for which depletion caused an average normalized GFP:RFP ratio below 0.5, with an individual GFP:RFP normalized ratio below 0.75 for all three replicas, were included in the category of genes that favour NHEJ. In contrast, genes for which depletion caused an average normalized GFP:RFP ratio above 3, with an individual GFP:RFP normalized ratio above 2 for all three replicas, were included in the category of genes that favour HR.

Cell cycle is a major regulator of DSB repair pathway choice, as DNA end resection is limited to the S and G2 phases. Thus, any genes whose downregulation has an impact on cell cycle distribution might indirectly affect the NHEJ:HR ratio. To discard those cases, we used FUCCI-U2OS cells, in which the cell cycle distribution can be visualized under the microscope because of the accumulation of cell cycle-controlled protein fragments fused to fluorescent markers[9]. We used 358 candidate esiRNAs (Supplementary Data 2) to transfect FUCCI-U2OS cells. The percentage of G1 cells was determined by the expression of orange-labelled Cdt1. Cell cycle distribution was normalized to control cells transfected with esiRNA against luciferase to obtain a cell cycle correction factor. We then adjusted the NHEJ:HR ratio according to cell cycle distribution (Supplementary Data 3). Cell cycle correction had little effect on the NHEJ:HR ratio in the majority of cases, and only 18 genes were discarded. In other cases, the corrected ratio was even more robustly shifted. Thus, after considering cell cycle, we ended up with a list of 117 genes that favour NHEJ and 223 genes that favour HR (Supplementary Data 3).

Network analysis. We next analysed these candidate genes *in silico* by evaluating whether they were over-represented in certain functional categories defined automatically using the IPA software (Ingenuity Systems). Both the genes that favour NHEJ and those that favour HR were enriched in the functional categories *Cell Cycle* and *DNA Replication, Recombination and Repair* (Fig. 1d). Moreover, and in agreement with previous results, RNA metabolism is related to the balance between HR and NHEJ[10] (Fig. 1d). We also found that Cancer-related genes were over-represented in both sets of genes (Fig. 1d), validating the relevance of balanced DSB repair for avoiding tumorigenesis. The Cell Cycle, DNA Repair and Cancer networks are shown (Fig. 1e).

CCAR2 is a bona fide regulator of DSB repair pathway choice. The gene for CCAR2 (Cell Cycle and Apoptosis Regulator 2) was ranked first among the candidates that favour NHEJ (Supplementary Data 3). CCAR2 is also known as DBC1 (Deleted in Breast Cancer 1) and KIAA1967. We thereafter focused in the role of CCAR2 in DSB repair pathway choice.

We initially validated the unbalance between HR and NHEJ using the SSR system in cells depleted of CCAR2 by using different short interfering RNA (siRNA) and short hairpin RNA (shRNAs; for CCAR2 depletion, see Supplementary Fig. 1a,b). CCAR2 downregulation increased HR at the expense of NHEJ in all cases (Fig. 2a,b). We used the DNA resection gene CtIP

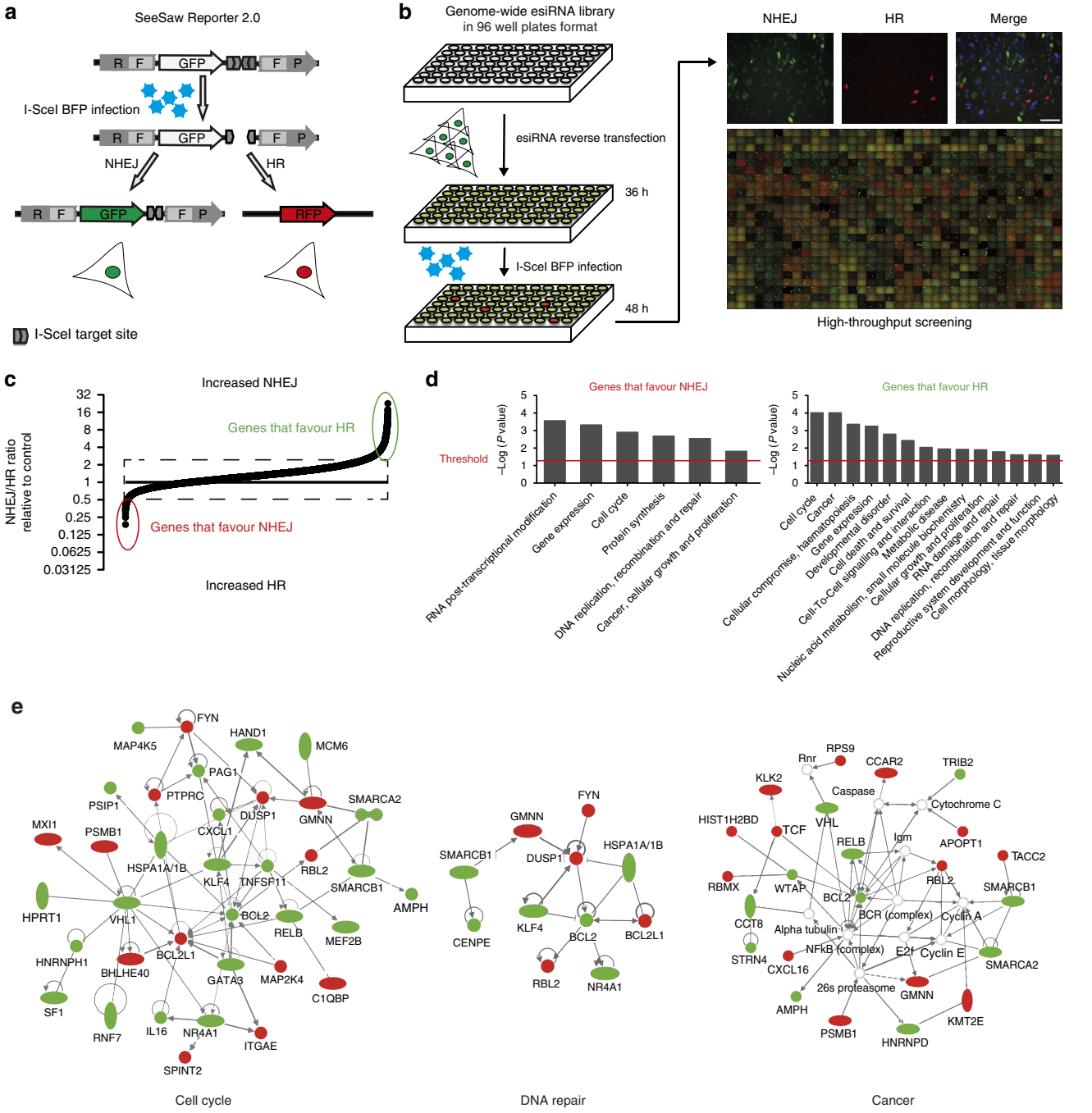

Figure 1 | A genome-wide screening for factors that control the balance between NHEJ and HR. (**a**) Schematic representation of the SSR. An I-SceI-induced DSB can be repaired by NHEJ, thus reconstructing an active GFP gene, or by homologous recombination using RFP fragments, thus creating a functional RFP gene. (**b**) Workflow of the screening method. Individual esiRNAs deposited in a 96-well plate format were used to reverse-transfect U2OS cells harbouring a single copy of the SSR system. After 36 h, lentiviral particles bearing I-SceI and the BFP genes were transduced into cells. After 2 days, cells were imaged using a high-throughput microscope for green, red and blue fluorescence. The number of green and red cells was then established for each individual esiRNA. Scale bar, 100 μm (**c**). The ratio between green and red cells was established for each individual esiRNA and normalized to an internal control (esiRNA targeted against luciferase) that was included in each plate. The individual NHEJ:HR ratio was then ordered and plotted. Cells with a normalized ratio close to one occupy the central dashed rectangle. Genes for which depletion reduced the ratio (that is, HR was increased) are marked in the red ellipse and correspond to proteins that naturally favour NHEJ. In contrast, genes that encode pro-recombination proteins (that is, NHEJ increased when they were downregulated) are included inside the green ellipse. (**d**) Functional categories enriched among candidates. The list of candidates that alter the NHEJ:HR ratio was analysed using the IPA Software and categorized into functional groups. Those categories in which genes were statistically significantly over-represented in the set of genes that favour NHEJ (left) or HR (right) are plotted. (**e**) Network of genes involved in *cell cycle, DNA repair, replication and recombination* and *cancer*, which appear in the set of candidates isolated in the screening. Genes that favour HR are labelled in green, and those that facilitate NHEJ, in red.

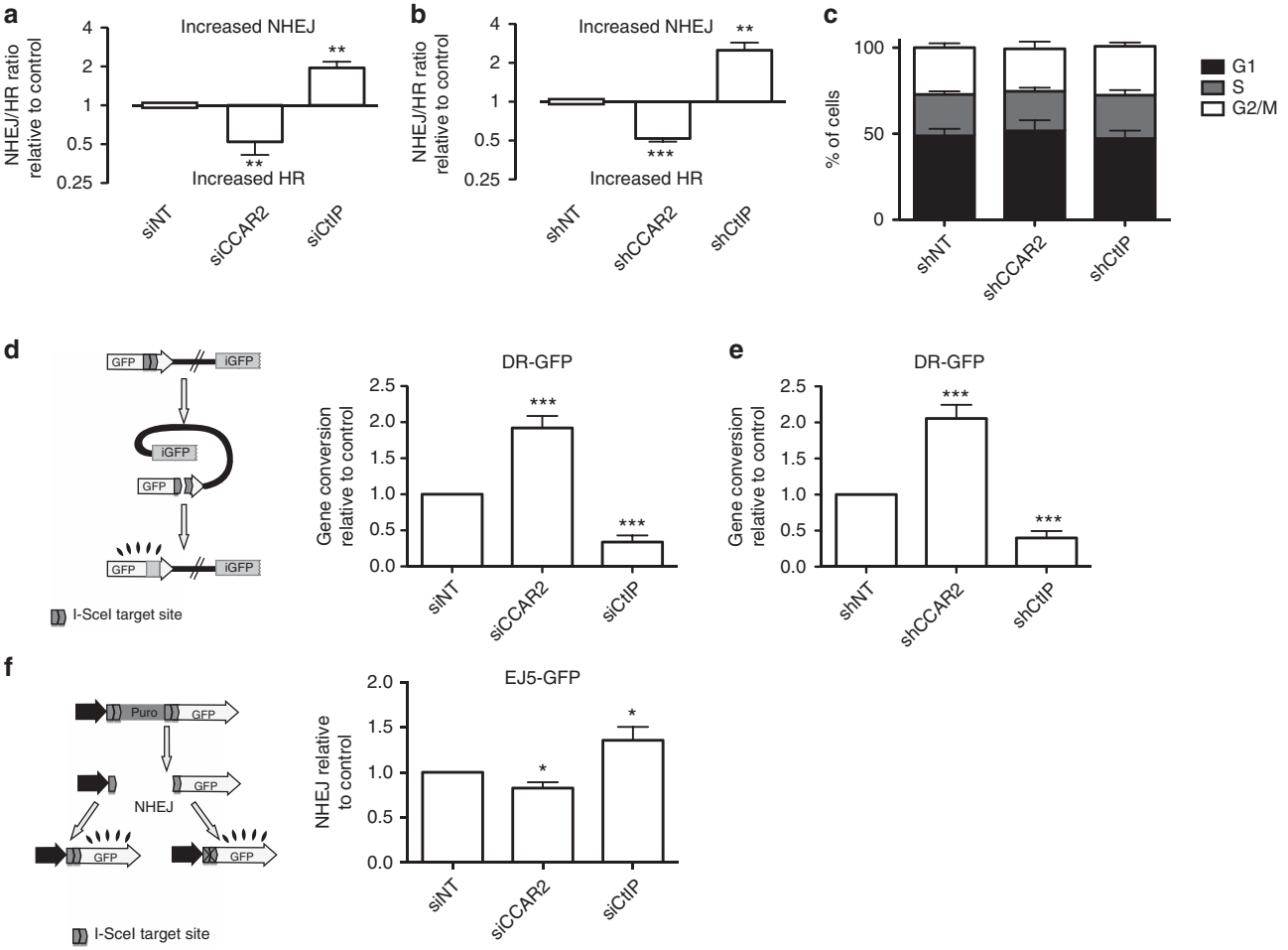

Figure 2 | CCAR2 depletion leads to hyper-recombination. (**a**) Cells harbouring a single copy of SSR were transfected with the indicated siRNAs. A non-target siRNA (siNT) and an siRNA against CtIP were used as negative and positive controls, respectively. The resultant NHEJ:HR ratio was normalized to control cells and plotted. The average and s.d. of four independent experiments performed in triplicate are shown. Statistical significance is marked with one to three asterisks, as described in the Methods section. (**b**) Same as **a**, but with cells infected with lentiviral particles harbouring the indicated shRNAs. shNT (a non-target shRNA) and shRNA against CtIP were used as negative and positive controls, respectively. (**c**) Cell cycle distribution of cells after downregulation of the indicated genes with shRNA. (**d**) A schematic representation of the HR reporter DR-GFP is shown on the left side. An intramolecular gene conversion is shown, although it is possible that such reporter engages in an intermolecular recombination event with the sister chromatid, with the same results. Cells bearing such reporters were transformed with the indicated siRNAs. Further details are as in **a**. (**e**) Same as **d**, except that cells were transduced with viral particles containing the indicated shRNAs. (**f**) A schematic representation of the NHEJ reporter EJ5-GFP is shown on the left side. Cells bearing such a reporter were transformed with the indicated siRNAs. Further details are as in **a**.

as a positive control. The shift towards HR with CCAR2 downregulation was not because of a change in cell cycle distribution (Fig. 2c). As the SSR system measures specifically the SSA type of HR[8], which does not require strand invasion[3], we tested whether the hyper-recombination observed upon CCAR2 downregulation was specific for the SSA HR subpathway or whether it is a general feature. For this, we tested the effect of its depletion on the reporter DR-GFP, which render cells GFP-positive if gene conversion has occurred after an I-SceI-induced DSB but not if the break was repaired by SSA[11] (Fig. 2d,e). CCAR2 also inhibited gene conversion. We confirmed that the main contribution of CCAR2 in DSB repair balance is to control HR, as only a mild decrease in NHEJ was observed on the NHEJ reporter EJ5-GFP[12] (Fig. 2f). Thus, CCAR2 is a bona fide general inhibitor of HR in human cells.

CCAR2 has been shown to control the response to cellular stress by reducing SIRT1 activity and p53 acetylation[13,14]. Thus, one possibility was that CCAR2 depletion caused an upregulation of SIRT1 activity, leading to an increase in HR. In that scenario, decrease in SIRT1 should have the opposite effect, that is, reduce HR. We discarded this hypothesis, as SIRT1 depletion actually increases recombination (Supplementary Fig. 2). Hence, we conclude that CCAR2 inhibits HR in a SIRT1-independent manner.

CCAR2 recruitment to sites of DNA damage. Proteins involved in DSB repair commonly act locally at the vicinity of damaged DNA. Such activity can be visualized by the local accumulation of the protein to damaged chromatin. Indeed, CCAR2 changed its localization when cells were challenged with ionizing radiation, after which it accumulated at DSBs labelled by the presence of H2AX phosphorylated at Serine 139 (γH2AX; Fig. 3a). Recruitment of DNA repair proteins to DNA damage usually depends on the activation of the DNA damage response. To understand in more detail CCAR2 retention at broken DNA, we used inhibitors targeting the two major kinases that trigger the damage response, ATM and ATR, as well as the poly

(ADP-ribose) polymerase (PARP). ATM inhibition completely abolished CCAR2 recruitment upon exposure to ionizing radiation, whereas ATR inhibitor only partially reduced CCAR2 accumulation (Fig. 3b). Note that this effect was evident even for cells that retained some γH2AX despite the ATM inhibition. In contrast, cells treated with PARP inhibitors behaved as control cells following radiation.

Only a subset of γH2AX foci colocalized with CCAR2 foci (Fig. 3a). To monitor CCAR2 recruitment at a higher resolution, we used a laser microirradiation (Fig. 3c). Using an antibody

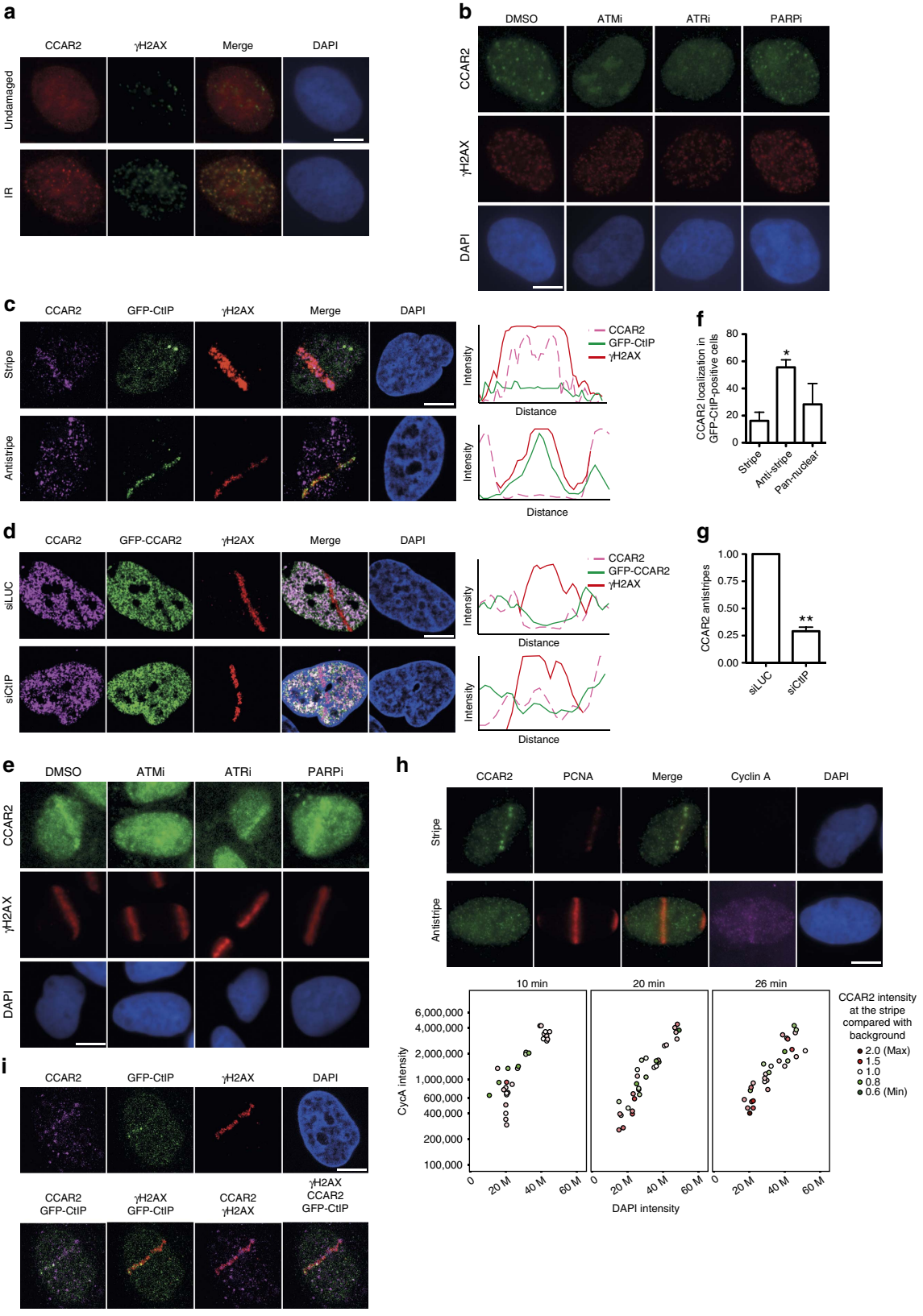

against CCAR2, we observed that indeed it accumulates at sites of DNA damage in 7% of cells (CCAR2 stripe; Fig. 3c). In contrast, we observed that damaged chromatin, labelled with γH2AX, was devoid of CCAR2 in 37% of the cells (CCAR2 antistripe; Fig. 3c). In the remaining cells (56%), we did not observe any specific recruitment pattern; however, we cannot determine for those cells whether CCAR2 was not mobilized upon DNA damage, whether the difference between its signal and background was too low to be distinguished or whether the combination of recruitment and exclusion on the same laser lines prevent its visualization. We interpreted such results as showing that CCAR2 is recruited to DNA damage in a subset of breaks but is actively excluded in another subset. Other proteins that form both stripes and so-called antistripes upon laser microirradiation have been already described[10,15,16]. We confirmed the existence of CCAR2 antistripes by repeating the experiment in cells stably expressing GFP-CCAR2 (Fig. 3d). Treatment of cells with inhibitors against ATM, ATR or PARP before laser microirradiation rendered a similar picture as for CCAR2 foci formation (Fig. 3e). Thus, CCAR2 laser stripes, but not antistripes, are completely dependent on ATM, partially dependent on ATR and independent of PARP activity (Fig. 3e).

An interesting hypothesis is that cells that use NHEJ for repair recruit CCAR2 to inhibit HR, while cells that use HR for repair exclude CCAR2 from damaged chromatin to allow recombination to take place. Indeed, CCAR2 immunostaining appeared to be mutually exclusive with accumulation of the pro-resection protein CtIP in cells harbouring a GFP-CtIP construct. Further, more than 50% of cells that accumulated CtIP showed clear CCAR2 exclusion from damaged chromatin (Fig. 3c,f). In contrast, the majority of the cells that showed CCAR2 stripes did not show GFP-CtIP accumulation (Fig. 3c). We observed colocalization in less than 20% of the cells (Fig. 3f). Moreover, the formation of CCAR2 antistripes was reduced by fourfold after CtIP depletion in GFP-CCAR2 cells (Fig. 3d,g). We conclude that CtIP was recruited and retained to DNA damage independently of CCAR2, but that CCAR2 antistripes depended on either CtIP accumulation or CtIP-mediated resection.

DNA resection is constrained to the S and G2 cell cycle phases because of, among other things, the phosphorylation of CtIP by cyclin-dependent kinases (CDKs)[4,7,17]. In order to investigate whether cell cycle position affected CCAR2 retention at, or exclusion from, damaged chromatin, we performed laser microirradiation in cells stained with proliferating cell nuclear antigen (PCNA), to visualize the DNA damage and cyclin A, to follow cell cycle progression. Cyclin A accumulates in S and G2 phases. To discriminate between them, we followed the intensity of the staining with cyclin A, which steadily increases during the cell cycle, and 4′,6-diamidino-2-phenylindole (DAPI), which also increases as a consequence of DNA replication. Thus, G1 cells (low cyclin A and low DAPI signal) evolved into G2 (high cyclin and DAPI signal) going through the S phase (intermediate cyclin and DAPI signals; Fig. 3h). At early time points, we observed higher levels of CCAR2 at damaged chromatin as compared with background (stripes) mainly in G1 and G2 phases but also in the S phase. In contrast, the average intensity at microirradiated lesions was below the background levels (antistripe) mostly in the S phase (Fig. 3h). With time, CCAR2 recruitment became more obvious in G1 and G2, and some CCAR2 exclusion was observed in G2 but never in G1 (Fig. 3h). This suggested that CCAR2 exclusion from DSBs was mainly restricted to replicating cells, with only cells in G1 or G2 able to recruit and retain CCAR2.

CtIP does not form laser stripes in G1 cells[6]. Thus, we hypothesized that cells with both CtIP and CCAR2 stripes would reflect only a proportion of G2 cells. Laser microirradiation causes hundreds of breaks in a given cell. For cells containing laser lines for both CtIP and CCAR2, we wondered whether both were recruited to the same locations. Indeed, when we looked closely at cells with recruitment of both proteins, we observed that the two signals tended not to colocalize (Fig. 3i); this probably reflects the different mechanisms and/or kinetics of repair for DSBs created on the same laser track.

Resection is inhibited by CCAR2. CtIP-mediated resection is a well-known molecular switch that controls the balance between NHEJ and HR[6,7]. As our results suggested that CCAR2 might act as an antagonist of CtIP, we next tested whether CCAR2 regulates DNA end resection. Downregulation of CCAR2 slightly increased the number of cells that were positive for RPA foci upon exposure to ionizing radiation (Fig. 4a). There are two non-exclusive ways to affect DNA end resection: increasing the number of cells that initiate resection and increasing the amount of DNA resected at each specific break. RPA foci formation is a good measurement of the former, but it is not sensitive enough to estimate the latter. Thus, as most S and G2 cells initiate resection, and hence show RPA foci, it is hard to observe an increase in the number of cells positive for RPA. To better resolve the increased resection upon CCAR2 depletion, and to test whether CCAR2 also affected the length of resection, we used a high-resolution technique to analyse DNA resection in single molecules *in vivo* (SMART; see Methods section Single-molecule analysis of resection tracks for details)[18]. In short, it is a modified DNA-combing protocol in which ssDNA length is measured on stretched DNA fibres[18]. Downregulation of CCAR2 not only affected the number of cells that resect DNA, but also allowed resection to continue deeper

Figure 3 | Opposite recruitment of CCAR2 and CtIP to damaged chromatin. (**a**) CCAR2 (red) and the phosphorylated form of H2AX (γH2AX; green) were immunodetected in cells untreated or exposed to 10 Gy of IR. (**b**) Cells pretreated with inhibitors against ATM (ATMi), ATR (ATRi), PARP (PARPi) or DMSO as a control were irradiated and used for immunofluorescence against CCAR2 and γH2AX. (**c**) Cells expressing a GFP–CtIP fusion were microirradiated. CCAR2 recruitment or exclusion from damaged chromatin was determined with an anti-CCAR2 antibody (magenta). Damaged DNA was visualized using an antibody against γH2AX (red). CtIP was observed as accumulation of GFP signal. The intensities of the signals of the CCAR2 antibody, GFP-CtIP and γH2AX were determined by an orthogonal line that crossed the damaged chromatin and plotted. (**d**) Same as in **c**, but in cells bearing a GFP-CCAR2 construct and transfected with siRNA against CtIP or luciferase, as indicated. (**e**) Same as in **c**, but cells were pretreated with the mentioned inhibitors. (**f**) Percentage of cells with GFP–CtIP recruitment that showed recruitment, exclusion or pan-nuclear staining of CCAR2. The average and s.d.'s of three independent experiments are shown. Statistical significance is marked with one to three asterisks, as described in the Methods section. (**g**) Number of CCAR2 antistripes upon depletion of CtIP. Data were normalized with an siLUC. The average and s.d. of three independent experiments are shown. (**h**) Cells were harvested at the indicated times after laser microirradiation and stained for PCNA (red), CCAR2 (green), Cyclin A (magenta) or DNA (DAPI; blue). The nuclear intensity of the DAPI and Cyclin A of individual cells (represented as coloured circles) was measured and plotted to follow cell cycle progression. The intensity of CCAR2 at damaged chromatin (automatically detected as PCNA stripes) was compared with background levels and plotted in red (intensity at the laser tracks over background; that is, CCAR2 stripes) or green (intensity at the laser tracks below background; that is, CCAR2 antistripes) according to the legend. Representative images are shown on top. (**i**) A representative cell with both CtIP (green) and CCAR2 (magenta) stripes is shown. γH2AX is shown in red. Images merging two or three colours are shown. In all panels, scale bars, 7.5 μm.

into the chromosomes (Fig. 4b,c). In addition, such hyper-resection was completely dependent on CtIP (Fig. 4b,c), genetically placing them in the same pathway. Both SMART and RPA foci were observed upon exposure to ionizing radiation. To extend our results, and to link them with the hyper-recombination phenotype observed using nuclease-induced DSBs (Fig. 2), we measured the accumulation of RPA at AsiSI-induced breaks by chromatin immunoprecipitation (ChIP; Fig. 4d). Some breaks induced by this enzyme are repaired only by NHEJ, while others are repaired by both NHEJ and HR[19].

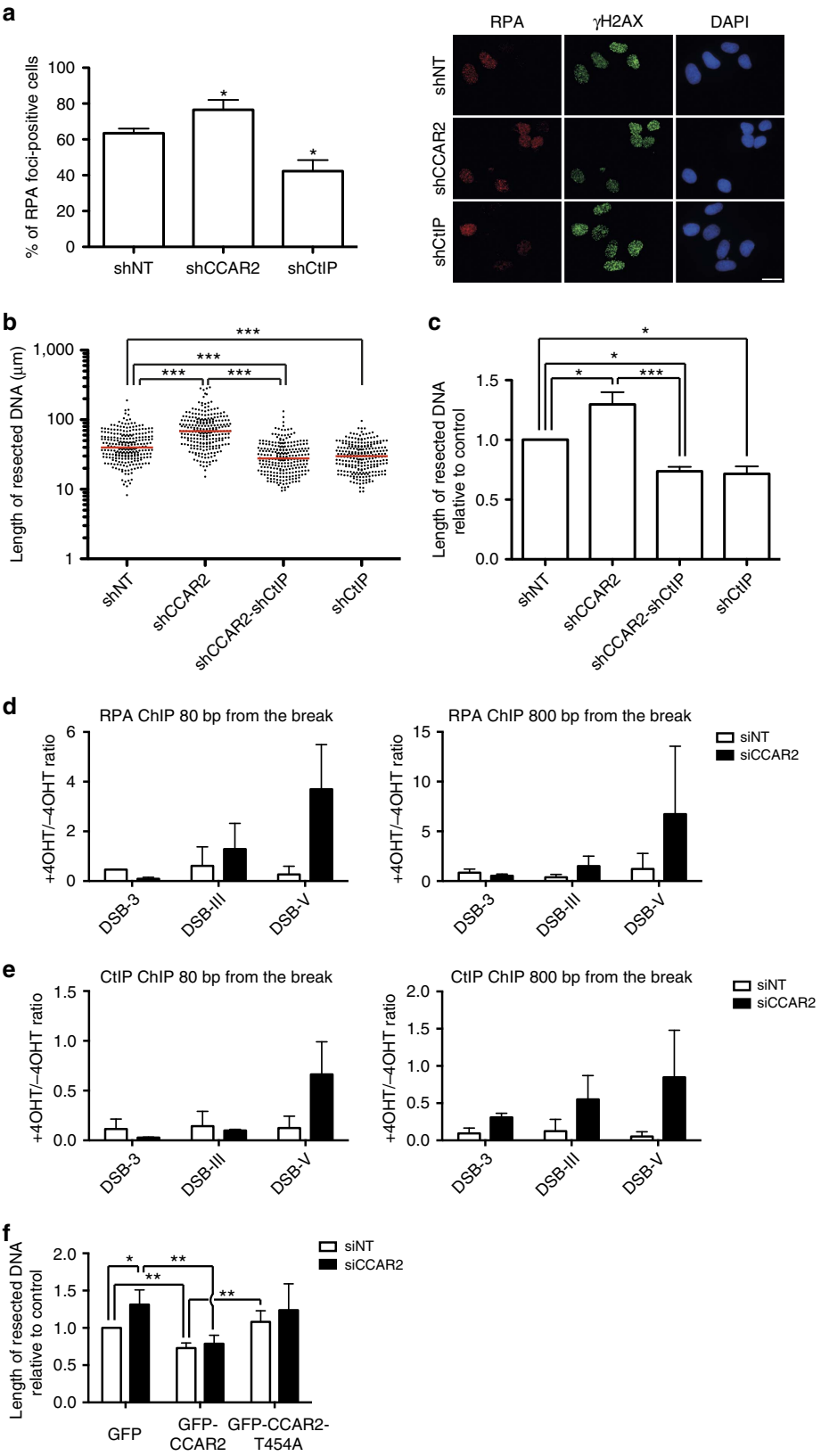

Upon CCAR2 downregulation, we saw an increased accumulation of RPA at two different AsiSI-induced breaks that are normally repaired by NHEJ and HR (Fig. 4d; DSB-III and DSB-V) but no effect when we analysed a break that is exclusively repaired by NHEJ (Fig. 4d; DSB-3). The same was observed using different distances of the cleavage site (Fig. 4d). Thus, it seems that CCAR2 limits resection at breaks that are normally resected. To better understand how this occurs, we tested CtIP recruitment at those same sites after forming DSBs by AsiSI. We observed an increase in CtIP recruitment at all the breaks, especially at distances further away from the actual cleavage site (Fig. 4e).

An interesting idea is that CCAR2 might limit resection of those breaks to which it is actively recruited in an ATM-dependent manner. As ATM itself heavily affects DNA end resection, we could not simply inhibit ATM activity. However, it has been shown previously that ATM phosphorylates CCAR2 at threonine 454 (ref. 20). Thus, we measured resection length at cells depleted of endogenous CCAR2 and complemented with either wild-type or the T454A mutant. Expression of the wild-type version of the protein completely suppressed the hyper-resection observed in cells depleted for CCAR2 (Fig. 4f). Indeed, as exogenous CCAR2 expression led to a overexpression of the protein (Supplementary Fig. 1c), the length of resected DNA in cells harbouring the wild-type gene was shorter than in control cells, reinforcing the idea that CCAR2 is antagonistic to DNA end resection (Fig. 4f). This was not observed when the non-phosphorylatable version of the protein was introduced in the cells, indicating that ATM phosphorylation is truly essential for the inhibitory role of CCAR2 on end processing (Fig. 4f). Indeed, although this mutant partially rescued the resection defect, it was not statistically significantly different from the GFP control (Fig. 4f). Thus, CCAR2 limits the extent of DNA that is resected in an ATM-dependent manner.

CCAR2 antagonizes CtIP by their physical interaction. To elucidate how CCAR2 exerts its function, we assessed whether CCAR2 and CtIP physically interact. We observed such an interaction using a proximity-ligation assay (PLA; Fig. 5a; Supplementary Fig. 3a; controls for the specificity of the technique are shown in Supplementary Fig. 3b). We wondered whether the interaction is direct or mediated by BRCA1, as both CCAR2 and CtIP have been shown to interact with BRCA1 (refs 21,22). Depleting BRCA1 did not change the interaction between CtIP and CCAR2 (Fig. 5a). In fact, the CCAR2–CtIP interaction seemed constitutive and did not depend on the presence of DNA damage (Fig. 5a). To confirm the interaction, we purified CtIP from U2OS cells using GFP- and FLAG-tagged version of the protein. Using mass spectrometry, we identified CCAR2 as an interactor of CtIP (see Supplementary Table 1). We observed such an interaction in cells arrested in G1, S and G2. Moreover, using total cell extracts, we were able to co-immunoprecipitate endogenous CCAR2 with GFP-CtIP, both in the presence and absence of DSBs (Fig. 5b and Supplementary Fig. 4a). Note that endogenous CtIP was also specifically immunoprecipitated (Fig. 5b, arrow), in agreement with the ability of CtIP to self-interact[23]. Furthermore, the reciprocal interaction was observed when GFP-CCAR2 was used to immunoprecipitate endogenous CtIP (Fig. 5c and Supplementary Fig. 4b). Remarkably, only the non-phosphorylated form of CtIP (lower band) was co-immunoprecipitated with GFP-CCAR2 from lysates of irradiated cells, in agreement with a damage-independent interaction (Fig. 5c).

In addition, by using purified, bacterial-expressed GST (glutathione *S*-transferase)-CtIP as bait, we were able to pull-down GFP-CCAR2 from whole extracts from human cells (Fig. 5d and Supplementary Fig. 4c). By expressing three truncated versions of GFP-CCAR2, we mapped the interaction region of CCAR2 and CtIP to the first two-thirds of the protein (Fig. 5d and Supplementary Fig. 4c).

We then performed *in vitro* direct binding assays using full-length His_6-CCAR2 and GST-CtIP purified from bacteria. We detected a direct interaction between the two proteins (Fig. 5e). Using a series of CtIP fragments, we mapped the interaction between CtIP and CCAR2 to the C-terminal part of CtIP (from amino acid 650 to the end of the protein), which covers the region that mediates the interaction of CtIP and the MRN complex (amino acids 790–897)[6] (Fig. 5e,f). This interaction between CtIP and CCAR2 was at odds with the lack of colocalization of both proteins at laser-induced damage. However, we reasoned that these observations could reflect a general interaction of both proteins in the bulk population in contrast to what occurs with local exclusion at damaged chromatin (Fig. 3c). Hence, we repeated the proximity-ligation assay in cells expressing GFP-MDC1, which is recruited to damaged DNA. We analysed the interaction between CCAR2 and CtIP in the vicinity of the damaged chromatin (that is, in MDC1 foci; Fig. 5g). We clearly observed that the CCAR2–CtIP PLA signal almost never colocalized with DNA damage, in agreement with the two proteins being recruited to laser microirradiation mainly in a mutually exclusive manner.

Discussion

Using a unique reporter, we identified 340 genes that have a role in maintaining the balance between NHEJ and HR in human cells. We used very stringent conditions for the selection of positive candidates. Thus, some proteins with a role in the DSB repair pathway choice may be missing from our final list (Supplementary Data 3). In fact, several proteins that we knew to affect the SSR are not present in this list, but nonetheless shifted the balance in the predicted manner (see Supplementary Data 1 for details). These include pro-recombination activities such as CtIP, BRCA1, MRE11, BLM and EXO1 as well as NHEJ proteins such as LIG4. Moreover, as our genomic approach does not guarantee

Figure 4 | CCAR2 inhibits CtIP-mediated resection. (**a**) Cells transduced with shRNAs against the indicated genes were irradiated (10 Gy). One hour after irradiation, cells were fixed and immunostained as indicated in the Methods section. The number of cells that show RPA foci was scored and represented as a percentage of the total. The graph represents the average and s.d.'s of three independent experiments. Representative images are shown at the right. Scale bar, 20 μm (**b**). The length of resected DNA was calculated using the SMART technique at individual DNA molecules. A Mann–Whitney test was performed to analyse the differences in dispersion. A representative experiment is shown. The median is shown in red. (**c**) The median of the resected DNA lengths was normalized to controls in cells depleted of the indicated proteins. The plot represents the average and s.d. of the normalized medians of four independent experiments. (**d**) DiVA cells were treated with 4-OHT to induce translocation of the nuclease AsiSI to the nucleus or were mock-treated, as described in the Methods section. Chromatin bound to RPA was immunoprecipitated and the occupancy of RPA was detected by qRT–PCR at 80 bp (left) or 800 bp (right) of three DSBs. DSB-3 represents a chromosome break that is exclusively repaired by NHEJ, whereas both NHEJ and HR can repair DSB-III and DSB-V. The same approach was performed in cells depleted for CCAR2 (black bars) or control cells (white bars). (**e**) Same as **d**, but using an antibody against CtIP for ChIP. (**f**) SMART assay with cells expressing the indicated plasmids and transfected with siRNA against CCAR2 (black bars) or a control sequence (siNT, white bars). Further details are as in **c**.

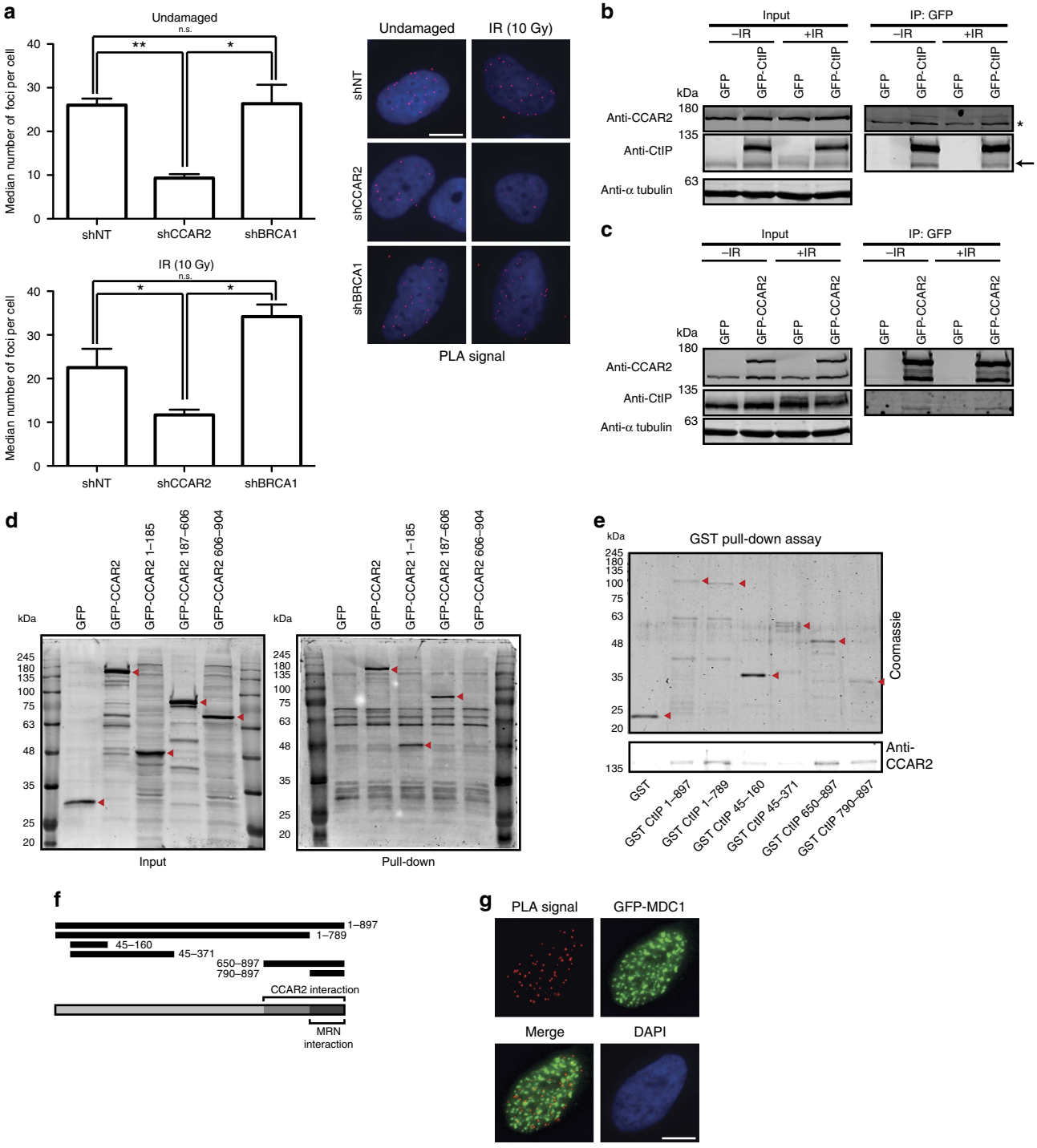

Figure 5 | CCAR2 and CtIP interacts physically in a constitutive manner. (**a**) Cells depleted of the indicated genes were analysed with a PLA using CtIP and CCAR2 antibodies. The average and s.d. of the medians of three independent experiments are plotted on the left. A representative image of each condition is shown on the right. The top graph was obtained with cells unchallenged by exogenous damage. The plots on the bottom side were calculated in cells 1 h after irradiation (10 Gy). Scale bar, 7.5 μm. (**b**) Protein samples from cells stably transfected with either GFP or GFP–CtIP in undamaged conditions or 1 h after ionizing radiation (10 Gy) were used for immunoprecipitation with anti-GFP resin. Immunoprecipitates were resolved in SDS–PAGE and blotted for the indicated antibodies. The asterisk marks an unspecific band that binds to the resin, and the arrow marks the endogenous CtIP protein. (**c**) Same as **b**, but with cells expressing GFP or GFP-CCAR2. (**d**) GST–CtIP was used as bait for pull-down experiments from whole-cell extracts using cells expressing GFP, GFP-CCAR2 full-length or three deletion mutants of CCAR2, as indicated. Western blots with an anti-GFP antibody using inputs (left) and pull-downs (right) are shown. The red arrows label the position of GFP fusions. (**e**) Bacterial-purified His_6-CCAR2 was pulled down with bacterial-purified GST-CtIP full-length and deletion constructs. Purified GST was used as a control. The red arrows represent the purified CtIP version. A western blot against CCAR2 is shown at the bottom. (**f**) A schematic representation of all the deletion constructs used in **e**. Full-length CtIP and the interaction regions with CCAR2 and the MRN complex are represented at the bottom. (**g**) PLA foci using CtIP and CCAR2 antibodies in cells expressing GFP-MDC1 that were collected 1 h after irradiation (10 Gy). Scale bar, 7.5 μm.

downregulation of all the genes in the library, we may have missed some important factors because of insufficient depletion.

Interestingly, we spotted not only genes that are required for HR prevalence over NHEJ but also a class of factors with the opposite role. Thus, we describe a sizeable set of genes whose depletion caused a hyper-recombinant phenotype in human cells. Such factors share similar functions to those required for NHEJ[24], those that decrease the stability of resection proteins, such as PIN1 (ref. 25) or CDH1 (ref. 26) and those that block resection, such as RIF1, 53BP1, REV7 and HELB[27–30]. In an approach similar to ours but using the recombination assay DR-GFP, a previous study found that several genes are required for gene conversion[10]. We compared both screenings and found little overlap between the two screenings. This might reflect the aforementioned weaknesses of genome-wide siRNA strategies and the stringent conditions applied to the selection of candidates in both screenings; however, it could also be that the distinct screening strategies targeted different steps in the recombination pathway and thus complemented each other. The DR-GFP screen readily responds to Rad51-dependent strand invasion, and indeed the majority of the isolated hits corresponded to proteins that affect Rad51 expression[10]. In contrast, the SSR system is Rad51-independent and readily reacts to changes in DNA resection[8]. Notably, Adamson *et al.*[10] did not find any genes that showed hyper-recombination phenotypes upon depletion. In contrast, we clearly isolated factors that favour homology-mediated repair when downregulated (Supplementary Data 3). Hyper-recombinant mutants have been abundantly isolated from other organisms[1] but rarely from higher eukaryotes. Thus, we present the first comprehensive list of genes that cause a hyper-recombinant phenotype when depleted in human cells.

The majority of genes that affected the SSR ratio belong to the functional categories of *DNA repair, replication and recombination, cell cycle* or *mRNA metabolism*, indicating the relevance of such processes in controlling DSB repair. In terms of pathogenesis, we also found a clear correlation between DSB repair balance and cancer.

We singled out CCAR2 to exemplify this category of genes that have a pro-NHEJ and antirecombination role in the cell. CCAR2 interacts with BRCA1 (ref. 21), a well-known tumour suppressor required for HR[31] and to modulate the speed of DNA end resection[18]. CCAR2 inhibits BRCA1's transcriptional role[21], affects cell proliferation by controlling SIRT1 and p53 (refs 13,14,20,32) and is involved in RNA metabolism[33]. In most published studies, the role of CCAR2 depends on its role as a SIRT1 inhibitor, a function that requires the phosphorylation of CCAR2 at threonine 454 (refs 13,14,20). However, here we describe an SIRT1-independent function in HR. In agreement, CCAR2 contribution to DNA repair has previously been shown to be SIRT1-independent[32,34]. Despite the lack of a direct involvement of SIRT1, this new function of CCAR2 is also dependent on ATM-mediated phosphorylation.

The physical relationship between CCAR2 and BRCA1 suggested the possibility that BRCA1 bridges an interaction between CtIP and CCAR2. However, we have excluded this possibility, as this interaction (measured by PLA) was maintained or even increased in the absence of BRCA1. Here we extend the relationship between CCAR2 and DNA repair by showing CCAR2's direct physical and functionally antagonistic relationship with CtIP. CCAR2 acts as a bona fide inhibitor of DNA end resection: it not only regulates which cells resect their DNA but also limits the length of the produced resected DNA. Indeed, depletion of CCAR2 increases the amount of CtIP recruited to AsiSI-induced DSBs, mostly at locations further away of the actual cleavage site. Hence, we postulate that CCAR2 might constrain the spreading of CtIP along the DNA, thereby spatially confining resection. Interestingly, in a proteomic screen CCAR2 was found to interact with all three subunits of the RPA complex[35]; hence, such an interaction might be required for this role-limiting resection. By doing so, it affects all HR pathways, including the most conservative gene conversion. Although it has a mild effect in inhibiting NHEJ, as is expected when breaks are hyper-resected, we conclude that the major role of CCAR2 in DSB repair balance is to antagonize resection spreading. In agreement, CCAR2 depletion does not affect the recruitment of NHEJ proteins such as 53BP1 (ref. 34). Such a role in HR could contribute to CCAR2 sensitivity to DSB-inducing agents[32,36]. Our data are in apparent contrast to a previously published report that proposes CCAR2 to be an enhancer of HR, using a recombination reporter in SW480sn3 cells[36]. However, this might reflect differences in the reporters used, and, more specifically, the length of gene conversion tracks required to render positive colonies. This hypothesis is supported by the fact that CCAR2 not only affects the number of DSBs to be resected but also mainly controls the length of DNA that will be resected, hence modulating gene conversion tracks and crossovers[37].

Mechanistically, we propose the following model (Fig. 6). CCAR2 interacts constitutively with CtIP in a DNA damage-independent manner in the nucleoplasm (Fig. 6i). Despite the proximity of the CCAR2 and MRN interaction sites in CtIP, there is no competition between the two (Supplementary Fig. 5). Thus, it is more likely that the physical presence of CCAR2 negatively regulates the activity of the CtIP–MRN complex. Upon the appearance of a broken DNA molecule, CCAR2 and CtIP recruitment depends on the cell cycle phase. In G1 cells, only CCAR2 is recruited, as resection will be inactive[4,17]. In G2 and (perhaps) S phase, however, they are probably recruited together to chromatin, accounting for the 18% of CtIP laser line-positive cells that also showed CCAR2 accumulation (Fig. 6 ii). The fact that CCAR2 downregulation does not affect CtIP recruitment but only limits its spreading along the DNA, while CtIP depletion reduces CCAR2 exclusion, reinforces the idea that CtIP inhibition by CCAR2 is because of the physical interaction between the two. While the bulk of CtIP and CCAR2 in the nucleoplasm retain their interaction upon DNA damage, the CCAR2–CtIP complex appears to be disrupted locally on damaged chromatin (Fig. 6 iii and iv). Remarkably, CCAR2 interacts only with the non-phosphorylated form of CtIP. In this scenario, either one factor or the other rapidly takes command of the situation. Which one dominates depends on several factors, such as cell cycle distribution or chromatin status. Indeed, CCAR2 affects the kinetics of repair of breaks that occur in heterochromatin but not in euchromatin[34]. Strikingly, CCAR2 has little effect on breaks that are always repaired by NHEJ, but is critical for DSB repair pathway choice for breaks that could be repaired by HR or NHEJ. When a break will be repaired by NHEJ (Fig. 6 iii)—that is, all of the breaks that occur in G1, and many of those in G2–CtIP exits the damaged chromatin, but CCAR2 stays on, constraining DNA end resection and allowing NHEJ to ensue. This retention of CCAR2 and its role as an antagonist of resection requires ATM activity and CCAR2 ATM-mediated phosphorylation at threonine 454 (ref. 20). This parallels the RIF1–53BP1 antiresection pathway, which is also triggered by 53BP1 ATM-mediated phosphorylation[27,28]. In contrast, DSBs that will be resected maintain CtIP at sites of DNA damage, and do not accumulate (G2) or even actively exclude (S phase) CCAR2 from these sites (Fig. 6 iv and v), probably thereby allowing the catalytic activity of the MRN complex. Such behaviour of CCAR2 is CtIP-dependent and allows CtIP and DNA end resection to be activated. An interesting hypothesis is that resection will be limited to this chromatin region devoid of CCAR2 (antistripe; Fig. 6v), and will stop as soon as it enters a nuclear region in

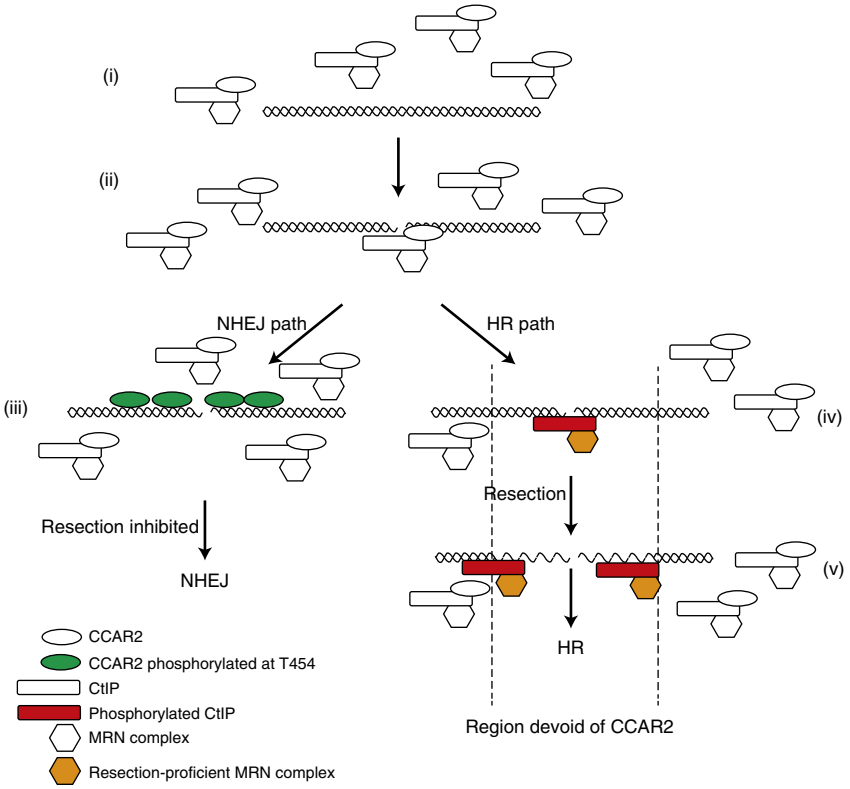

Figure 6 | Schematic depiction of the effect of CCAR2 on DNA end resection. CtIP and CCAR2 interact constitutively. Upon the appearance of DSBs, they are both recruited (ii), but soon only one of them is left remaining at the breaks (iii and iv). DSB repaired by NHEJ maintains CCAR2 in an ATM-dependent manner, facilitating repair (iii). In contrast, DSBs that require DNA end resection maintain only CtIP at the break, and, indeed, CCAR2 is completely excluded from the region in a CtIP and/or DNA end resection manner (iv). This allows resection to progress until it covers the CCAR2-free region (v).

which CCAR2 is still present. This would minimize the chance of hyper-resection of DSBs, a phenomenon that may be associated with an increase in genomic instability[37,38]. The model predicts that the extent of resection in human cells is higher in the S phase than in the G2 phase, a phenomenon that has been observed in budding yeasts[39]. This might explain the increased length of resected DNA tracks upon CCAR2 depletion, as all S- and G2-phase cells would resect their DNA as long as if they were in G2. This will also suggest that HR is probably different between S and G2 cells, as the length of resection will affect the balance between different recombination subpathways, controlling the size of gene conversion tracks and interfering with crossover formations[37].

We have observed that the CtIP–CCAR2 interaction is independent of BRCA1, suggesting that all pairwise interactions occur independently. This crosstalk between BRCA1, CtIP and CCAR2 might then regulate the fidelity of DNA repair, which could explain why all three of these are related to the appearance of breast cancer yet have opposite effects on HR[40–42]. Thus, CCAR2 is emerging as a critical protein controlling cellular response to stress, including DNA damage, and it elicits a very complex response that involves many parallel reactions.

Methods

Cell culture and manipulations. Cells were cultured in high-glucose DMEM supplemented with 10% fetal bovine serum (FBS), 2 mM glutamine, 100 μg ml^{-1} streptomycin and 100 U ml^{-1} penicillin at 37 °C in 5% CO_2. Plasmids were transfected using FugeneHD Transfection Reagent (Promega) according to the manufacturer's instructions. siRNAs against CCAR2 (5′-GCUUAUAGUUCGA AGGUAC-3′), CtIP (5′-GCUAAAACAGGAACGAAUC-3′), luciferase (5′-CGUA CGCGGAAUACUUCGA-3′), SIRT1 (Dharmacon SMARTpool L-003540-00) and a control non-target sequence (a mix of 5′-UGGUUUACAUGUCGACUAA-3′, 5′-UGGUUUACAUGUUGUGUGA-3′, 5′-UGGUUUACAUGUUUUCUGA-3′ and 5′-UGGUUUACAUGUUUUCCUA-3′) were transfected with RNAiMax Lipofectamine Reagent Mix (Life Technologies), according to the manufacturer's instructions. Lentiviruses harbouring shRNA vectors (SIGMA) targeting CtIP (TRCN0000318738), CCAR2 (TRCN0000053723), BRCA1 (TRCN0000009823) or a non-target sequence (SHC016V 01031212MN) were used to infect U2OS cells. Lentiviral particles were obtained as described[8]. Briefly, lentiviral particles were generated by calcium phosphate transfection in A293T cells. After 48 hours, lentiviruses were collected from the media by 100,000 *g* centrifugation for 2 hours at 4 °C. Cells stably expressing the shRNAs were selected by adding 1 μg ml^{-1} puromycin to the medium after infection. U2OS were a gift from Stephen P. Jackson. FUCCI-U2OS cells were obtained by stably transfecting U2OS cells with pFucci-G1 Orange (AM-V9003) and pFucci-S/G2 Green (AM-V9010) from Amalgaam.

esiRNA human whole-genome screening. All manipulations were performed using a Hamilton Microlab STAR robot (301–3,811) following a protocol designed by the Genomic Unit of CABIMER. The screening was carried out using the MISSION esiRNA library (SIGMA) targeting 16,538 human genes based on sequence annotation from the ENSEMBL database. The esiRNAs were aliquoted (30 nM) in a 96-well plate format, with each plate harbouring an esiRNA against luciferase as a control. U2OS-SSR2.0 cells were then reverse-transfected at 6,000 cells per well using RNAiMax Lipofectamine Reagent Mix (Life Technologies), according to the manufacturer's instructions. After 6 h, media was replaced to minimize cell death. At 36 h after transfection, I-SceI–BFP (blue fluorescent protein) lentivirus (multiplicity-of-infection of 10) and 6 μg ml^{-1} polybrene diluted in DMEM were added to the cells. Cells were washed the next day with new media; after another 24 h, cells were washed with PBS, fixed with 4% paraformaldehyde and washed twice with PBS. Before staining with Hoechst 33,342, a representative picture was taken to calculate the efficiency of the I-SceI–BFP infection. Plates were then imaged using an ImageXpress Micro (Molecular Devices) at ×10 magnification, and pictures were taken at nine sites (fields) per well. Nuclei, GFP and RFP signals were detected with blue, green and Texas Red filters, respectively. Images were analysed, and the amount of GFP- and RFP-positive cells were quantified automatically with the Image MetaExpress Software (Molecular Devices). The ratio of GFP:RFP cells in each well was normalized using the internal control with esiLUC (Supplementary Data 1).

Plasmids. GFP-CtIP was published elsewhere[7]. Full-length CCAR2 cDNA was inserted into the pET28a expression vector (Novagen) to add a polyhistidine (His_6)

tag at the N terminus of CCAR2 protein. The cDNA was also cloned into pEGFP-C1 to create the full-length GFP-CCAR2 construct and mutated to avoid silencing with the siRNA. The GFP-CCAR2-T454A mutant was obtained by mutagenesis. CCAR2 deletion mutants were obtained from the full-length construct by cleavage with ApaI and ligation of the obtained fragments in pEGFP-C1 linearized with ApaI (1–185 fragment) or EcoRI-ApaI (187–606 and 608–924 fragments). The full-length pGEX-CtIP construct and CtIP fragment constructs and GFP-MDC1 were a kind gift from Steve Jackson (University of Cambridge, UK).

Gene conversion:NHEJ and NHEJ:HR balance analysis. U2OS cells bearing a single-copy integration of the reporters DR-GFP (Gene conversion)[11], EJ5-GFP (NHEJ)[12] or SSR (NHEJ:HR)[8] were used to analyse the different DSB repair pathways. In all cases, 4,000 cells were plated in 96-well plates. One day after seeding, cells were transfected with the indicated siRNA or infected with lentiviral particles carrying the indicated shRNA. The medium was changed after 6–8 h. The following day, cells were infected with a lentivirus harbouring I-SceI and labelled with BFP[43] at an multiplicity-of-infection of 10. After 24 h, cells were washed with fresh medium and maintained during an additional 24 h. Cells were then fixed with 4% paraformaldehyde, stained with Hoechst 33,432 and washed with PBS before visualization with a fluorescent microscope for blue, green and, in the case of SSR, red fluorescence, as described in the previous section. The repair frequency was calculated as the percentage of blue cells expressing GFP for the DR-GFP and EJ5-GFP. For the NHEJ:HR balance, the ratio between green versus red cells in each conditions was calculated as published[8]. To facilitate the comparison between experiments, this ratio was normalized with siRNA or an shRNA control. Conditions that skewed the balance towards increased NHEJ repair resulted in a fold increase above 1. In contrast, a net decrease of this ratio (for example, values below 1) represented an imbalance of SSR towards HR. Data represent a minimum of four sets of triplicate experiments.

***In silico* analysis.** Candidate gene sets were analysed using the IPA Software (Ingenuity Systems, www.ingenuity.com) available through PAB (The Andalusian Platform of Bioinformatics, www.scbi.uma.es) from the University of Malaga. A total of 330 ID genes of 340 candidates were recognized and analysed using the Ingenuity Knowledge database. The core analysis tool was used to visualize functional categories' enrichment and associated networks. Fisher's exact test right-tailed was performed using the IPA Software to calculate *P* values using a cutoff of 0.05.

Cell cycle analysis using flow cytometer. Cells were harvested, washed with PBS and resuspended in ice-cold PBS. EtOH (70%) was added dropwise while vortexing at low speed, and cells were then fixed at 4 °C for at least 2 h. Cells were washed with PBS and treated with 250 μg ml^{-1} RNase A (SIGMA) and 10 μg ml^{-1} propidium iodide diluted in PBS (Fluka). Cells were incubated at 37 °C for 30 min and analysed using a FACSCalibur (BD).

Immunofluorescence microscopy. U2OS cells were infected with lentivirus harbouring the indicated shRNA or a control sequence. After 48 h, cells were irradiated (10 Gy) or mock-treated, incubated 1 h for foci formation and collected. For the experiment with inhibitors, ATMi (10 μM), ATRi (5 μM) or PARPi (1 μM) was added to the plates 30 min before irradiation. For RPA foci formation, coverslips were treated for 5 min on ice with pre-extraction buffer (25 mM Tris-HCl, pH 7.5, 50 mM NaCl, 1 mM EDTA, 3 mM $MgCl_2$, 300 mM sucrose and 0.2% Triton X-100), and then fixed with 4% paraformaldehyde (w/v) in PBS for 15 min. For CCAR2 foci, cells were fixed with 4% paraformaldehyde (w/v) in PBS for 15 min on ice, washed twice with PBS and permeabilized with 0.2% Triton X-100 (v/v) in PBS for 10 min on ice. Then, coverslips were washed three times with PBS and blocked for at least 1 h with 5% FBS diluted in PBS. Cells were incubated with the adequate primary antibodies (Supplementary Table 2), diluted in 5% FBS in PBS for 2 h at room temperature, washed with PBS and then incubated with secondary antibodies (Supplementary Table 3) diluted in 5% FBS in PBS for 1 h at room temperature. Cells were then washed twice with PBS, and coverslips were mounted with Vectashield mounting medium (Vector Laboratories) containing DAPI and analysed using a LEICA microscope. At least 200 cells were scored per sample. Experiments were repeated independently at least three times.

Laser microirradiation. For laser microirradiation, cells with the indicated downregulated proteins were grown in medium containing 10 μM bromodeoxyuridine (BrdU, GE Healthcare) for 24 h in glass-bottom dishes or on coverslips. Pretreatment with inhibitors was performed as described in the previous section. A Zeiss PALM Microbeam microscope was used to induce DNA damage with a UV-A (355 nm) laser. Experiments of microirradiated cells were performed in CO_2-independent, phenol red–free DMEM. Laser output was set to the lowest setting that induced DNA damage, as monitored by phosphorylation of H2AX. Confocal images were obtained with a Leica Microscope TCS 5PS, using the LAS AF Software (Leica). The MetaMorph Software was used to quantify the amount of fluorescence (stripes and antistripes) across a linear pathway transversal to the microirradiated signal, visualized as γH2AX. At least 200 cells positive for γH2AX stripes were counted per sample.

Proximity-ligation assay. PLAs were performed using the Duolink PLA Kit (Olink Bioscience, Uppsala, Sweden) according to the manufacturer's protocol. Briefly, U2OS cells were infected with lentivirus harbouring the indicated shRNA or a control sequence. After selection in medium with 1 μg ml^{-1} puromycin during 3 days, cells were treated with ionizing radiation (10 Gy) or mock-treated, incubated 1 h and then collected. Coverslips were washed with PBS, fixed on ice with methanol for 10 min followed by acetone for 30 s, washed three times with PBS and blocked with blocking solution from the Duolink PLA Kit for 30 min at 37 °C. Samples were incubated with primary antibodies against CCAR2 and CtIP (Supplementary Table 2) overnight at 4 °C, followed by MINUS and PLUS secondary PLA probes (antimouse minus and antirabbit plus) for 1 h at 37 °C. Detection was carried out with the Duolink Detection Kit Red (Olink Bioscience). At least 200 cells were analysed using a Leica Fluorescence microscope and foci counted automatically using command Granularity of the MetaMorph software.

Immunoblotting. Extracts were prepared in Laemmli buffer (4% SDS, 20% glycerol and 125 mM Tris-HCl, pH 6.8), and proteins were resolved using SDS–PAGE and transferred to PVDF-LF membranes (Millipore), followed by immunoblotting. Western blot analysis was carried out using the antibodies listed in Supplementary Tables 2 and 3. Results were visualized using an Odyssey Infrared Imaging System (Li-Cor). Uncropped images of the most important blots are shown in Supplementary Figures.

Single-molecule analysis of resection tracks. SMART was performed as described[18]. Briefly, U2OS cells downregulated for the indicated genes were grown in the presence of 10 μM BrdU for 24 h. Cultures were then irradiated (10 Gy) and harvested after 1 h. Cells were embedded in low-melting agarose (Bio-Rad), followed by DNA extraction. To stretch the DNA fibres, silanized coverslips (Genomic Vision) were dipped into the DNA solution for 15 min and pulled out at a constant speed (250 μm s^{-1}). Coverslips were baked for 2 h at 65 °C and incubated directly without denaturation with an anti-BrdU mouse monoclonal antibody (Supplementary Table 2). After washing with PBS, coverslips were incubated with the secondary antibody (Supplementary Table 3). Finally, coverslips were mounted with ProLong Gold Antifade Reagent (Molecular Probes) and stored at − 20 °C. DNA fibres were observed with a Nikon NI-E microscope and a PLAN FLOUR 40 × 0.75 PHL DLL objective. The images were recorded and processed with the NIS ELEMENTS Nikon Software. For each experiment, at least 200 DNA fibres were analysed, and the length of DNA fibres was measured with Adobe Photoshop CS4 Extended version 11.0 (Adobe Systems Incorporated).

Protein expression and purification. Recombinant proteins were expressed in *Escherichia coli* BL21 (DE3). A fresh single transformant colony was inoculated into 5 ml of LB medium containing kanamycin (30 μg ml^{-1}) for His_6-CCAR2, or ampicillin (50 μg ml^{-1}) for pGEX-CtIP constructs, and the cultures were incubated at 37 °C overnight with shaking. A 2.5 ml aliquot of the overnight culture was inoculated into 250 ml of LB medium containing the appropriate antibiotic and incubated at 23 °C (for His_6-CCAR2) or 30 °C (for GST-CtIP constructs), until A_{600} reached 0.7. Expression was induced by adding isopropyl-1-thio-D-galactopyranoside (IPTG, Duchefa Biochimie). The final concentration of IPTG was 1 mM for CCAR2 and 0.1 mM for CtIP fragments. At 3 h after induction, cells were collected by centrifugation at 13,000*g* for 30 min, and the bacterial pellets were frozen immediately at − 80 °C. For His_6-CCAR2, the stored pellet was thawed and resuspended in sonication buffer (20 mM Tris-HCl, pH 8, 500 mM NaCl, 20% glycerol, 15 mM β-mercaptoethanol and 1% Tween-20). For CtIP fragment purification, the pellets were thawed and resuspended in PBS. Cells were disrupted by sonication, and the lysate was clarified by centrifugation. For His_6-CCAR2 purification, supernatant was loaded onto a Ni^{2+}-sepharose column (His-Trap HP columns, GE Healthcare) that had been pre-equilibrated with sonication buffer (SB). The column was washed with 10 ml of SB supplemented with 60 mM imidazole, eluted with a 30 ml gradient of imidazole (at 60 mM to 1 M) in SB and then collected in 0.5 ml fractions. For CtIP purification, the supernatant was loaded on a GSTrap HP column (GE Healthcare) pre-equilibrated with PBS. The columns were washed with PBS and eluted with 50 mM Tris-HCl, pH 8 and 10 mM reduced glutathione.

An aliquot of each fraction from the purifications was analysed by SDS–PAGE, and those containing the overexpressed protein were pooled and dialysed against either dialysis buffer 1 (50 mM Tris-HCl, pH 8.0, 500 mM NaCl, 1 mM dithiothreitol and 50% glycerol) for CCAR2, or dialysis buffer 2 (PBS, 30% glycerol) for CtIP and its deletion fragments. The protein preparation was divided into aliquots and stored at − 80 °C. Protein concentrations were determined by the Bradford assay, and denatured proteins were analysed by SDS–PAGE.

Pull-down assay using purified proteins. Eighty pmol of purified GST alone, GST-CtIP or GST fused to CtIP fragments were resuspended in a final volume of

300 µl with PBS, mixed with 100 µl of pre-equilibrated glutathione sepharose 4b resin (GE Healthcare) and incubated for 1 h at 4 °C. The resin was washed twice with binding buffer (20 mM Tris, pH 7.5, 1 mM EDTA, 10 mM beta-mercaptoethanol, 0.5% Triton and 50 mM NaCl). One hundred pmol of purified His_6-CCAR2 was incubated at 4 °C for 1 h with either GST or GST-tagged proteins bound to resin. The matrix was washed twice with wash buffer (binding buffer with 3 mM reduced glutathione). Bound proteins were separated by SDS–PAGE (7.5%), transferred to polyvinylidene difluoride (PVDF) membranes and analysed by western blot analysis using antibodies against CCAR2.

Pull-down assay from whole-cell extracts. Protein extracts from cells transfected with the different versions of GFP-CCAR2 were prepared in lysis buffer (20 mM Tris, pH 7.5, 1 mM EDTA, 0.5% Triton, 50 mM NaCl, 1 × protease inhibitors (Roche) and 1 × phosphatase inhibitor cocktail 1 (Sigma)). The amount of expression of each CCAR2 fragment was calculated by western blotting. Similar amounts of each CCAR2 truncated version were used for pull-down assays. After adding beta-mercaptoethanol (final concentration 10 mM) to the samples, cell extracts were pre-cleared by incubating with 50 µl of pre-equilibrated glutathione sepharose 4B resin (GE Healthcare) for 1 h at 4 °C.

Eighty pmol of purified GST-CtIP were resuspended in a final volume of 500 µl with PBS, mixed with 100 µl of pre-equilibrated glutathione sepharose 4B resin and incubated for 1 h at 4 °C. The resin was washed twice with binding buffer (lysis buffer with 10 mM beta-mercaptoethanol but without protease and phosphatase inhibitors) and then incubated with the pre-cleared cell extracts for 2 h at 4 °C. The matrix was washed twice with wash buffer (binding buffer with 3 mM reduced glutathione), and proteins were eluted by boiling the slurry for 5 min in protein-loading buffer. Precipitated proteins were separated by SDS–PAGE, transferred to PVDF membranes and analysed by western blot analysis.

Immunoprecipitation. U2OS cells overexpressing GFP, GFP-CtIP or GFP-CCAR2 were irradiated (10 Gy) or mock-treated and harvested 1 h later in lysis buffer (50 mM Tris-HCl pH 7.5, 50 mM NaCl, 0.2% Triton X-100, 1 × protease inhibitors (Roche) and 1 × phosphatase inhibitor cocktail 1 (Sigma)). Protein extract (900 µg) was mixed with 30 µl of pre-equilibrated magnetic anti-GFP resin (GFP-Trap_M, Chromotek) and incubated overnight at 4 °C by gently rocking. Beads were then washed three times with lysis buffer, and the precipitate was eluted in 40 µl of Laemmli buffer.

Chromatin immunoprecipitation. ChIP assays were carried out essentially as described[44]. Briefly, DiVA cells harbouring the nuclease AsiSI fused to the oestrogen receptor were incubated for 4 h with 300 nM of tamoxifen (4-OHT) to induce the translocation of the nuclease to the nucleus and the induction of DSBs. Cells expressing shRNA against CCAR2 or shRNA non-target were used as a control. Chromatin (300 µg) was immunoprecipitated with 2 µg of anti-RPA, anti-CtIP and anti-IgG (mock; Supplementary Table 2). The enrichment of specific DNA loci was analysed in immunoprecipitated chromatin and the input in triplicates by quantitative reverse transcriptase PCR (qRT–PCR). Primers are listed in Supplementary Table 4.

Statistical analysis. Statistical significance was determined with a paired Student's *t*-test using the PRISM software (Graphpad Software Inc.). Statistically significant differences were labelled with one, two or three asterisks if $P<0.05$, $P<0.01$ or $P<0.001$, respectively. A Mann–Whitney test was used to detect statistically significant differences between the populations of resected DNA ends detected by SMART.

Data availability. The authors declare that all data supporting the findings of this study are available within the article (and its Supplementary Information files) and upon request.

References

1. Aguilera, A. & Gomez-Gonzalez, B. Genome instability: a mechanistic view of its causes and consequences. *Nat. Rev. Genet.* **9,** 204–217 (2008).
2. Jackson, S. P. & Bartek, J. The DNA-damage response in human biology and disease. *Nature* **461,** 1071–1078 (2009).
3. Heyer, W. D., Ehmsen, K. T. & Liu, J. Regulation of homologous recombination in eukaryotes. *Annu. Rev. Genet.* **44,** 113–139 (2010).
4. Huertas, P. DNA resection in eukaryotes: deciding how to fix the break. *Nat. Struct. Mol. Biol.* **17,** 11–16 (2010).
5. Lieber, M. R. The mechanism of human nonhomologous DNA end joining. *J. Biol. Chem.* **283,** 1–5 (2008).
6. Sartori, A. A. *et al.* Human CtIP promotes DNA end resection. *Nature* **450,** 509–514 (2007).
7. Huertas, P. & Jackson, S. P. Human CtIP mediates cell cycle control of DNA end resection and double strand break repair. *J. Biol. Chem.* **284,** 9558–9565 (2009).
8. Gomez-Cabello, D., Jimeno, S., Fernandez-Avila, M. J. & Huertas, P. New tools to study DNA double-strand break repair pathway choice. *PLoS ONE* **8,** e77206 (2013).
9. Sakaue-Sawano, A. *et al.* Visualizing spatiotemporal dynamics of multicellular cell-cycle progression. *Cell* **132,** 487–498 (2008).
10. Adamson, B., Smogorzewska, A., Sigoillot, F. D., King, R. W. & Elledge, S. J. A genome-wide homologous recombination screen identifies the RNA-binding protein RBMX as a component of the DNA-damage response. *Nat. Cell Biol.* **14,** 318–328 (2012).
11. Pierce, A. J., Johnson, R. D., Thompson, L. H. & Jasin, M. XRCC3 promotes homology-directed repair of DNA damage in mammalian cells. *Genes Dev.* **13,** 2633–2638 (1999).
12. Bennardo, N., Cheng, A., Huang, N. & Stark, J. M. Alternative-NHEJ is a mechanistically distinct pathway of mammalian chromosome break repair. *PLoS Genet.* **4,** e1000110 (2008).
13. Kim, J. E., Chen, J. & Lou, Z. DBC1 is a negative regulator of SIRT1. *Nature* **451,** 583–586 (2008).
14. Zhao, W. *et al.* Negative regulation of the deacetylase SIRT1 by DBC1. *Nature* **451,** 587–590 (2008).
15. Altmeyer, M. *et al.* The chromatin scaffold protein SAFB1 renders chromatin permissive for DNA damage signaling. *Mol. Cell* **52,** 206–220 (2013).
16. Polo, S. E. *et al.* Regulation of DNA-end resection by hnRNPU-like proteins promotes DNA double-strand break signaling and repair. *Mol. Cell* **45,** 505–516 (2012).
17. Ferretti, L. P., Lafranchi, L. & Sartori, A. A. Controlling DNA-end resection: a new task for CDKs. *Front. Genet.* **4,** 99 (2013).
18. Cruz-Garcia, A., Lopez-Saavedra, A. & Huertas, P. BRCA1 accelerates CtIP-mediated DNA-end resection. *Cell Rep.* **23,** 451–459 (2014).
19. Aymard, F. *et al.* Transcriptionally active chromatin recruits homologous recombination at DNA double-strand breaks. *Nat. Struct. Mol. Biol.* **21,** 366–374 (2014).
20. Zannini, L., Buscemi, G., Kim, J. E., Fontanella, E. & Delia, D. DBC1 phosphorylation by ATM/ATR inhibits SIRT1 deacetylase in response to DNA damage. *J. Mol. Cell Biol.* **4,** 294–303 (2012).
21. Hiraike, H. *et al.* Identification of DBC1 as a transcriptional repressor for BRCA1. *Br. J. Cancer* **102,** 1061–1067 (2010).
22. Yu, X. & Chen, J. DNA damage-induced cell cycle checkpoint control requires CtIP, a phosphorylation-dependent binding partner of BRCA1 C-terminal domains. *Mol. Cell Biol.* **24,** 9478–9486 (2004).
23. Davies, O. R. *et al.* CtIP tetramer assembly is required for DNA-end resection and repair. *Nat. Struct. Mol. Biol.* **22,** 150–157 (2015).
24. Munoz-Galvan, S. *et al.* Competing roles of DNA end resection and non-homologous end joining functions in the repair of replication-born double-strand breaks by sister-chromatid recombination. *Nucleic Acids Res.* **41,** 1669–1683 (2013).
25. Steger, M. *et al.* Prolyl isomerase PIN1 regulates DNA double-strand break repair by counteracting DNA end resection. *Mol. Cell* **50,** 333–343 (2013).
26. Lafranchi, L. *et al.* APC/C(Cdh1) controls CtIP stability during the cell cycle and in response to DNA damage. *EMBO J.* **33,** 2860–2879 (2014).
27. Chapman, J. R. *et al.* RIF1 is essential for 53BP1-dependent nonhomologous end joining and suppression of DNA double-strand break resection. *Mol. Cell* **49,** 858–871 (2013).
28. Escribano-Diaz, C. *et al.* A cell cycle-dependent regulatory circuit composed of 53BP1-RIF1 and BRCA1-CtIP controls DNA repair pathway choice. *Mol. Cell* **49,** 872–883 (2013).
29. Xu, G. *et al.* REV7 counteracts DNA double-strand break resection and affects PARP inhibition. *Nature* **521,** 541–544 (2015).
30. Tkac, J. *et al.* HELB is a feedback inhibitor of DNA end resection. *Mol. Cell* **61,** 405–418 (2016).
31. Huen, M. S., Sy, S. M. & Chen, J. BRCA1 and its toolbox for the maintenance of genome integrity. *Nat. Rev. Mol. Cell Biol.* **11,** 138–148 (2010).
32. Kim, W. & Kim, J. E. Deleted in breast cancer 1 (DBC1) deficiency results in apoptosis of breast cancer cells through impaired responses to UV-induced DNA damage. *Cancer Lett.* **333,** 180–186 (2013).
33. Close, P. *et al.* DBIRD complex integrates alternative mRNA splicing with RNA polymerase II transcript elongation. *Nature* **484,** 386–389 (2012).
34. Magni, M. *et al.* CCAR2/DBC1 is required for Chk2-dependent KAP1 phosphorylation and repair of DNA damage. *Oncotarget* **6,** 17817–17831 (2015).
35. Marechal, A. *et al.* PRP19 transforms into a sensor of RPA-ssDNA after DNA damage and drives ATR activation via a ubiquitin-mediated circuitry. *Mol. Cell* **53,** 235–246 (2014).
36. Tanikawa, M. *et al.* Role of multifunctional transcription factor TFII-I and putative tumour suppressor DBC1 in cell cycle and DNA double strand damage repair. *Br. J. Cancer* **109,** 3042–3048 (2013).
37. Prado, F. & Aguilera, A. Control of cross-over by single-strand DNA resection. *Trends Genet.* **19,** 428–431 (2003).
38. Jimeno, S. *et al.* Neddylation inhibits CtIP-mediated resection and regulates DNA double strand break repair pathway choice. *Nucleic Acids Res.* **43,** 987–999 (2015).

39. Zierhut, C. & Diffley, J. F. Break dosage, cell cycle stage and DNA replication influence DNA double strand break response. *EMBO J.* **27,** 1875–1885 (2008).
40. Chini, E. N., Chini, C. C., Nin, V. & Escande, C. Deleted in breast cancer-1 (DBC-1) in the interface between metabolism, aging and cancer. *Biosci. Rep.* **33,** e00058 (2013).
41. Paul, A. & Paul, S. The breast cancer susceptibility genes (BRCA) in breast and ovarian cancers. *Front. Biosci.* **19,** 605–618 (2014).
42. Soria-Bretones, I., Saez, C., Ruiz-Borrego, M., Japon, M. A. & Huertas, P. Prognostic value of CtIP/RBBP8 expression in breast cancer. *Cancer Med.* **2,** 774–783 (2013).
43. Certo, M. T. *et al.* Tracking genome engineering outcome at individual DNA breakpoints. *Nat. Methods* **8,** 671–676 (2011).
44. Iacovoni, J. S. *et al.* High-resolution profiling of gammaH2AX around DNA double strand breaks in the mammalian genome. *EMBO J.* **29,** 1446–1457 (2010).

Acknowledgements

DiVA cells were kindly provided by Gaëlle Legube. We thank the scientists in the Genomic and Microscopy units of CABIMER for technical support, Felix Prado and Felipe Cortes-Ledesma for critical reading of the manuscript, J. L. Sánchez-Ramos for help with the statistical analysis and Veronica Raker for style corrections. This work was funded by a R + D + I grant from the Spanish Ministry of Economy and Competitivity (SAF2010-14877) and an ERC Starting Grant (DSBRECA). A.L.-S. is the recipient of a FPI fellowship from the Spanish Ministry of Economy and Competitivity, and F.M.-N. is funded with an FPU fellowship from the Spanish Ministry of Education. M.I.M.-M. was the recipient of a Juan de la Cierva Postdoctoral Grant. M.S.D.-S. received a EMBO short-term fellowship for this project. J.B. and C.D. were supported by grants from the Danish National Research Foundation (CARD; DNRF125), the Danish Council for Independent Research (DFF-1331-00262) and the Novo Nordisk Foundation (NNF16584).

Author contributions

D.G.-C., M.S.D.-S., F.M.-N. and M.J.F.-A. performed the esiRNA screening. The experiments related to CCAR2 were performed mainly by A.L.-S., with the help of M.S.D.-S., D.G.-C. and F.M.-N., with the exception of the *in vitro* interaction of CtIP and CCAR2 (performed by M.I.M.-M.) and the laser microirradiation (performed by M.S.D.-S. in collaboration with C.D. in J.B. laboratory). P.H. supervised the work and wrote the paper. All authors read and commented on the paper.

Additional information

Supplementary Information accompanies this paper at http://www.nature.com/naturecommunications

Competing financial interests: The authors declare no competing financial interests.

Reprints and permission information is available online at http://npg.nature.com/reprintsandpermissions/

How to cite this article: López-Saavedra, A. *et al.* A genome-wide screening uncovers the role of CCAR2 as an antagonist of DNA end resection. *Nat. Commun.* 7:12364 doi: 10.1038/ncomms12364 (2016).